Northwestern University

Aberrant Acetylation of Mitochondrial Proteins, due to Loss of SIRT3, Results in Tumor Permissive Phenotypes and Increases Breast Cancer Malignancy Risk

A DISSERTATION

SUBMITTED TO THE GRADUATE SCHOOL IN PARTIAL FULFILLMENT OF THE REQUIREMENTS

For the degree

DOCTOR OF PHILOSOPHY

Field of Driskill Graduate Program in the Life Sciences

By

Xianghui Zou

EVANSTON, ILLINOIS

June 2017

ABSTRACT

SIRT3 is a mitochondrial-localized, NAD^+-dependent deacetylase, tumor suppressor protein that functions to direct mitochondrial energy sensing and antioxidant proteins, increasing the efficiency of energy utilization, providing a redox balanced environment, and preventing aging-related diseases. One SIRT3 deacetylation target is $NADP^+$-dependent isocitrate dehydrogenase 2 (IDH2), a key Krebs Cycle enzyme that produces α-ketoglutarate by oxidizing isocitrate, linking glucose metabolism to oxidative phosphorylation. In addition, IDH2 catalyzes the production of NADPH, a reducing reagent to maintain cellular redox balance. It has been shown that acetylation of IDH2 at lysine 413 decreases IDH2-dependent enzymatic activity. However, the mechanism by which acetylation of IDH2 inhibits activity, as well as the phenotypes due to its aberrant acetylation, remain unknown. In my thesis, we report that loss of *SIRT3* increases IDH2 acetylation at lysine 413 (IDH2-K413-Ac) decreases IDH2 enzymatic activity via a mechanism that decreased IDH2 dimer formation. Native-PAGE analysis of eluted mutant IDH2 proteins (acetylation mimetic mutant, $IDH2^{K413Q}$) showed a decreased IDH2 dimerization. Metabolically, expression of $IDH2^{K413Q}$ in cancer cells significantly decreased oxygen consumption, ATP turnover, mitochondrial respiration, and glutathione levels, and increased cellular reactive oxygen species (ROS) and glycolysis, suggesting a shift in mitochondrial metabolism to an environment promoting oxidative stress. In addition, enforced expression of $IDH2^{K413Q}$ promoted *in vitro* transformation of NIH3T3 cells and tumorigenesis in nude mice. Finally, immunohistochemistry (IHC) staining showed that IDH2 acetylation was higher in high-risk Luminal B patients than low-risk Luminal A patients. Overall, these results

suggest a potential relationship between SIRT3 enzymatic activity, IDH2-K413-Ac and dimerization, and a transformation and/or carcinogenic permissive phenotype.

ACKNOWLEDGEMENT

First and foremost, it is an honor for me to show my gratitude to Dr. David Gius for his tremendous assistance during my four years in his laboratory. The initial period of my Ph.D. training was very difficult, as I kept switching to different thesis projects. Fortunately, David helped me with his support and we decided on my final thesis project. He kept providing scientific feedback and encouraging me in my journey to the finishing line of my Ph.D. training. More importantly, David was very supportive when I told him that I would like to apply for medical school in the winter of 2015. He allowed me to shadow him in his clinic to gain more clinical exposure and offered his help during my medical school application processes. Now that I will be going to medical school in the fall of 2017, I owe my greatest gratitude to you, my advisor—David Gius. Without your support, proofreading and editing, this thesis may not be possible and my career switch in medicine would be much more difficult and challenging.

In addition, I would like to thank my lab mate and friend, Dr. Yueming Zhu, for his technical assistance. Starting from the fall of 2014, we started collaborating on our projects, as our field of study was very similar. There are certain techniques that require his expertise, and without a doubt he either helps me with my experiment or teaches me the techniques. I feel very happy that we are co-first authors in many of our papers, including one review paper published in *ARS*, one research paper published in *Cancer Research* and another research paper about to publish in *Molecular Cell* or *JEM*. I will never forget how I learned science and experimental techniques under your guidance and I will also never forget the conversations we hold in the cell

culture room. I wish you the best in your future career and I certainly hope that we will collaborate more often in the future. Enjoy more time with your parents, your wife and your son.

Furthermore, I would like to thank another two post-doctoral scholars who have provided tremendous technical support, Dr. Guoxiang Liu and Dr. Seong-Hoon Park. No matter when I have questions regarding to my experiments, they both devote their personal time to help me trouble shoot my experiments or walk me through new techniques. I wish both of you guys great success and I wish your family well.

I would like to thank my friends for their support during my Ph.D. training as well, Mr. Zhe Li, Mr. Wei Luo, Mr. Linchang Tan, Ms. Xiaodan Tang (Ms. 9.5/10), Ms. Siwen Yang (Ms. 9.5/10) and Ms. Hao Chen (Ms. 9.5/10), as we spend countless of weekends playing together. I can talk with the guys about anything and the ladies are truly eye beauties.

Finally, I would like to thank my parents for providing the best they can to me for a life-long time, especially their support during my Ph.D. training and my future medical training. While you guys do not know much about science, I appreciate it every time when I called you guys and complained about my failures and challenged. Without your support, I am and never will be who I am in my future career. Thank you for tolerating another four years of me being in school. I love you and I hope you still love me, despite that you guys will spend some money for my medical education. Just be patient and wait another four years before I contribute financially to the family again.

Table of Contents

ABSTRACT…….2-3

ACKNOWLEDGEMENT…….……...4-5

TABLE OF CONTENTS……..…….…….….6

LIST OF FIGURES AND TABLES……..……..7-9

CHAPTER 1: INTRODUCTION……..…….…..10-28

CHAPTER 2: MATERIALS AND METHODS……..29-39

CHAPTER 3: RESULTS RELATED TO IDH2 ACETYLATION AT LYSINE 413……..40-100

CHAPTER 4: RESULTS RELATED TO MNSOD ACETYLATION AT LYSINE 68 …101-121

CHAPTER 5: DISCUSSION…….……..122-136

REFERENCE……...……137-148

List of Figures and Tables

Figure 1: Loss of SIRT3 increases IDH2 acetylation at lysine 413, decreases IDH2 dimerization, and activity in mice……..…..……42

Figure 2: Loss of SIRT3 increases IDH2 acetylation at lysine 413, decreases IDH2 dimerization, and its activity in cancer cells.……...……44

Figure 3: Expression of $IDH2^{K413Q}$ in MCF7 breast cancer cells and HEK-293T cells decreases IHD2 dimerization.…….……..…….……..……..….46

Figure 4: Acetyl mimetic of IDH2 at lysine 413 affects mitochondrial energy metabolism…..…50

Figure 5: MCF7 breast cancer cells expressing the acetylation mimic mutants exhibit altered glycolytic metabolism..……..52

Figure 6: Addition of metabolites that mimics IDH2 activity switch affects cancer cell metabolism…….54

Figure 7: Acetyl IDH2 mimetic increases mitochondrial ROS levels and decreases detoxification in vitro and in vivo……..58

Figure 8: Decreased production of ROS by mitoTEMPO decreased clonogenic survival of MCF7-shIDH2-$IDH2^{K413Q}$ cells in vitro……60

Table 1: Summary of tumorigenesis in nude mice……65

Figure 9: Expression of $IDH2^{K413Q}$ promotes a transformation permissive phenotype in MCF7 cells……66

Figure 10: Expression of $IDH2^{K413Q}$ promotes a transformation permissive phenotype in NIH3T3 cells……..……..68

Figure 11: Expression of IDH2^{K413R} partially reverses a transformation permissive phenotype in MCF7 cells…….70

Figure 12: Expression of *IDH2*^{K413R} partially reverses a transformation permissive phenotype in *Sirt3*$^{-/-}$ MMT cells……..72

Figure 13: Expression of *IDH2*^{K413R} decreases the Ki67 proliferative index in *Sirt3*$^{-/-}$ MMT cells……74

Figure 14: Co-expression of *IDH2*^{K413Q} with *Myc* or oncogenic *Ras*^{G12D} increases the invasiveness of NIH3T3 cells in soft agar colony formation assay……...76

Figure 15: Exogenous alpha-ketoglutarate alters clonogenic growth and switches cancer cell metabolism *in vitro*……78

Figure 16: Exogenous alpha-ketoglutarate or isocitrate alters clonogenic growth and switches cancer cell metabolism *in vitro*……..80

Figure 17: Expression of IDH2 acetyl mimetics results in larger tumors in nude mice……82

Figure 18: Expression of acetyl mimetics of IDH2 results in heavier tumor formation in nude mice……84

Figure 19: Expression of acetyl mimetics of IDH2 results in faster tumor growth in nude mice……86

Figure 20: Luminal B breast cancer patient samples have a higher IDH2^{K413} staining…….89

Figure 21: Luminal B breast cancer patient samples have a lower SIRT3 staining……..91

Figure 22: Representative images of Luminal A vs Luminal B breast cancer staining…….93

Figure 23: The breast cancer samples with lower SIRT3 levels have a higher IDH2^{K413} staining……...95

Figure 24: Acetylation of IDH2 negatively correlate with SIRT3 protein levels in breast cancer patient samples……...97

Figure 25: Summarized mechanism……...99

Figure 26: MnSOD-K68-Ac leads to Tam resistance in human breast cancer cells……...103

Figure 27: Resistance to tamoxifen in human breast cancer cells leads to a loss of SIRT3-MnSOD-Ac signature……..105

Figure 28: MnSOD-K68-Ac leads to increased oxidative stress in human breast cells……..108

Figure 29: Tamoxifen exposure increases oxidative stress in cancer cells……..110

Figure 30: Luminal B breast cancer exhibited a higher MnSOD-K68-Ac staining by IHC……113

Figure 31: Luminal B breast cancer exhibited a lower SIRT3 staining by IHC……..115

Figure 32: Representative images of Luminal A vs Luminal B breast cancer staining……...117

Figure 33: Acetylation of IDH2 at lysine 413 might affect MnSOD tetramerization…….120

CHAPTER I

INTRODUCTION

Aging, human illness and carcinogenesis

Over the last 20 years, it has become increasingly clear that the incidence of solid tumors in human is strongly correlated with aging. In fact, the increase of age is significantly associated for solid tumor carcinogenesis from somatic cells (Ershler and Longo, 1997a). As the age of an organism increases, the incidence of cancer increases. Therefore, cancer has been regarded as an aging-related disease. The curve for cancer incidence starts with an initial flat shape, followed by an inflection point around the age of fifty, from which the incidence of cancer begins to rise exponentially. Based on these observations, it seems reasonable to suggest that there might be possible alterations in certain biological processes and/or cellular reparative pathways that occur at this inflection point, resulting in tumor permissive phenotypes or phenotypes that favor carcinogenesis (Tao et al., 2014).

Aging is a universal process that can be summarized as a decrease in fertility and survival probability. However, the quantification of aging remains relatively undetermined and elusive. To investigate aging-related processes, measuring patterns of longevity seems necessary. The curve of longevity measures how an organism survives over time statistically and illustrates the survival probability across different lifespans. Although the maximum lifespan between species varies enormously, a common pattern emerges from longevity curves across various species ranging from *C. elegans* to humans (Guarente, 2007; Tao et al., 2014; Zhu et al., 2014). The shape of the *C. elegans* longevity curve is very similar to the curve of human cancer incidence. It starts with a relatively flat initial slope, representing the initial high survival probability, and followed by an inflection point at roughly two to three weeks, after which the slope of the curve

changes rapidly, representing a steep decline in the probability of survival before the maximal longevity of *C. elegans*. The overall pattern of an inflection point that occurs before the steep slope appears seems to be present in the survival curve of most species. Even though the curves for survival and the incidence of human cancers are inverted, the same pattern is evident: both starts with a flat slope followed by a sharp transition to a steep slope marked by an inflection point (Tao et al., 2014). This raises rather interesting questions: 1) Do the inherent cellular reparative biological processes or genes that are directly related to longevity play a role in the observed increased incidence of solid tumors? 2) For these processes and/or genes, are there alterations of enzymatic activities/gene expressions at the inflection point?

Sirtuins as an aging related protein family that directs the cellular acetylome

Sirtuins (homolog of yeast Sir2) were initially discovered in yeast and *C. elegans*, and these genes play a critical role in extending the life cycle by suppressing toxic rDNA formation, suggesting a potential role of sirtuins in anti-aging (Guarente, 2007). In addition, it has been shown that the interaction between Sir2 and Ku is required for DNA double-stranded break repair (Boulton and Jackson, 1998). Therefore, loss of sirtuins may play a significant role in the control of the life cycle. Furthermore, analysis of the *C. elegans* longevity data has suggested that the survival rate of *C. elegans* has an inflection point that indicates a steep decrease in *C. elegans* survival (Guarente and Kenyon, 2000; Zhu et al., 2014). Overexpression of sirtuins in *C. elegans* can shift the inflection point to the right, prolonging their life span; whereas knocking out sirtuins in *C. elegans* can shift the inflection point to the left, reducing their life span (Guarente and Kenyon, 2000).

Mammalian sirtuins, the class III histone deacetylase family, are different from conventional class I and II histone deacetylases (HDACs) (Donmez and Guarente, 2010; Saunders and Verdin, 2009). Mammalian sirtuins share homology with yeast silent information regulator 2 (Sir2) and use nicotinamide adenine dinucleotide (NAD^+) as a cofactor. Seven sirtuins (SIRT1–SIRT7) have been found in humans and localized in different cellular compartments. SIRT1, SIRT6 and SIRT7 are nuclear sirtuins, which function as a regulator of several important transcription factors related to cellular metabolism (Finkel et al., 2009; Guarente, 2008), with SIRT1 being the most intensively studied sirtuin in the nucleus. Studies have investigated whether the loss of a specific sirtuin gene can affect mice life span. Mice, lacking one of the seven sirtuin genes (except *Sirt6*), do exhibit murine physiological phenotypes similar to that observed in humans for several age-related illnesses, including insulin resistance, cardiovascular disease, neurodegeneration, and most importantly tumorigenesis permissive phenotypes (Donmez and Guarente, 2010; Saunders and Verdin, 2009).

It was first discovered in 2001 that SIRT1 can deacetylate p53 (Vaziri et al., 2001). During DNA damage, SIRT1 is overexpressed and interacts with p53. This results in the deacetylation of p53 at lysine 382, inactivating p53 as a transcription factor. This discovery suggests that during DNA damage response, SIRT1 can inhibit p53 function through deacetylation, therefore reversing damage-induced transcription and reducing the possibility of apoptosis (Vaziri et al., 2001). Later, many other publications have shown that SIRT1 functions to repress the activation of different transcription factors. For example, SIRT1 binds to Hairy-related proteins (bHLH) and represses transcription (Takata and Ishikawa, 2003). Under stress conditions, SIRT1 regulates FOXO transcription factor by increasing its ability of cell cycle

arrest and decreasing FOXO3-induced cell death, suggesting that SIRT1 functions to increase longevity by inhibiting apoptosis and increasing stress resistance (Brunet et al., 2004). SIRT1 also binds to forkhead transcription factor and inhibits forkhead-dependent apoptosis, suggesting that SIRT1 can down-regulate different damage-responsive proteins. All these are initial discoveries show SIRT1 increases lifespan through repression of regulation of transcription factors and/or activation of transcription repressors.

Sirtuin proteins dysregulation and their roles in carcinogenesis

More recent discoveries have suggested that SIRT1 may function as a double-sided coin in carcinogenesis, either by suppressing tumor growth or promoting carcinogenesis and resistance to chemo/radiotherapy. There are many publications suggesting that SIRT1 functions as a tumor suppressor protein. SIRT1 fucntions as a tumor suppressor protein in human papillomaviruses (HPV) by regulation E1-E2 mediated DNA replication. Knocking out SIRT1 results in an increase of replication through acetylation and increased stabilization of E2 protein (Das et al., 2017). As a metabolic protein, SIRT1 can regulate glutamine metabolism (Ren et al., 2017). Haploinsufficiency of SIRT1 elevates c-Myc expression, promoting utilization of glutamine, proliferation and tumor cell growth (Ren et al., 2017). In mesenchymal stem cells, overexpression of SIRT1 inhibits breast cancer and prostate cancer cell growth by recruiting nature killer cells and macrophages, suggesting the potential role of SIRT1 in regulating the tumor inflammatory microenvironment (Yu et al., 2016b; Yu et al., 2016c).

On the contrary, there are also many publications indicating SIRT1 as a protein that promotes oncogenesis. For example, hypermethylated in cancer 1 (HIC1) is a transcription factor

that functions with p53 and suppresses cancer growth in mice (Chen et al., 2005). However, inactivation of HIC1 results in SIRT1 upregulation and allows cancer cells to bypass DNA damage-induced apoptosis (Chen et al., 2005). Therefore, it is hypothesized that upregulation of SIRT1 may result in an increase of tumor incidence in mammalians cells. Treatment of oxaliplatin, a chemotherapy reagent, functions to inhibit SIRT1-induced p53 deacetylation, activating apoptosis and reducing cyclin D expression. This results in an elongation of the cell cycle and decreases tumor cell proliferation (Chen et al., 2017). SIRT1 has also been shown as a potential indicator of advanced pathological parameter in gastric cancer, and high Beclin-1 and SIRT1 expression correlates with a worse clinical outcome and shorter overall survival (Qiu et al., 2016). In addition, another study in gastric cancer has shown that overexpression of SIRT1 and phosphorylated STAT3 (p-STAT3) is associated with a worse clinical outcome in gastric cancer patients, as advanced stage gastric cancer patients have a higher SIRT1 and p-STAT3 staining. While almost every single protein has dual functions related to carcinogenesis/pathogenesis, it is hypothesized that depending on the type of cancer, SIRT1 may have different functions either as a tumor suppressor protein or as a protein that potentially promotes tumorigenesis.

The only cytoplasmic sirtuin, SIRT2, has similar functions as SIRT1, as it can also provide control over cell cycle progression and genomic stability. For example, loss of SIRT2 results in mammary tumors in female mice and hepatocellular carcinoma (HCC) in male mice. SIRT2 regulates the activity of the anaphase-promoting complex/cyclosome (APC/C) through deacetylation of the APC/C coactivators. Therefore, loss of SIRT2 results in increased mitosis, increased genomic instability, and aneuploidy (Kim et al., 2011). These are all phenotypes

observed in different types of cancer, and staining of breast and HCC patient samples suggest that compared with normal tissues, SIRT2 is reduced in tumor samples (Kim et al., 2011). In addition, SIRT2 deacetylates and inactivates the peroxidase activity of peroxiredoxin (Prdx-1), therefore sensitizing cancer cells to DNA damage and cytotoxicity (Fiskus et al., 2016). Furthermore, SIRT2 was downregulated in serous ovarian carcinoma (SOC). Inhibition of SIRT2 in SOC cells results in an increase in tumor cell migration and invasion (Du et al., 2017). Metabolically, loss of SIRT2 results in increased acetylation of PKM2, inhibiting active, tetrameric PKM2 formation and promoting tumorigenesis in *Sirt2*$^{-/-}$ mammary tumor cells and HeLa cancer cells by inhibiting oxidative phosphorylation and promoting glycolysis (Park et al., 2016b).

However, there are other discoveries suggesting potential roles of SIRT2 in promoting different types of cancer. For example, a study in melanoma suggests that SIRT2 was upregulated in samples with lymph node metastasis (Wilking-Busch et al., 2017). In addition, SIRT2 was found to be upregulated in non-small cell lung cancer cell (NSCLC), and degradation of SIRT2 results in an inhibition of NSCLC growth (Luo et al., 2017). Moreover, overexpression of SIRT2 was found in basal-like breast cancer, as well as deactylating Slug protein at lysine 116 and preventing Slug degradation, and overexpression of Slug protein is associated with basal-like breast cancer aggressiveness (Zhou et al., 2016).

While initial discoveries have suggested that SIRT2 localizes in the cytoplasm and is mainly involved in the regulation of cellular mitosis (Kim et al., 2011; Park et al., 2012), a recent discovery from our laboratory has provided a potentially novel localization of SIRT2, as it can

localize in the mitochondria and control autophagy, energy utilization and redox homeostasis (Liu et al., 2016). Specifically, loss of *Sirt2* results in an increase of pan-acetylation in mice mitochondrial extracts, suggesting its potential role in regulating mitochondrial acetylation/deacetylation process (Liu et al., 2016). Loss of *Sirt2* results in an increase of GSSG:GSH ratio and mitochondrial ROS, suggesting that loss of *Sirt2* could create an environment that leads to redox imbalance. Furthermore, loss of *Sirt2* decreases cellular respiration capacity, ATP turnover and cellular detoxification, suggesting that SIRT2 may affect metabolic properties as well (Liu et al., 2016). In addition, SIRT2 interacts with many mitochondrial proteins, including SIRT3, suggesting that a potential crosstalk between different sirtuins localized in different cellular compartments may potentially exist.

SIRT3 dysregulation, aberrant intracellular acetylation, and carcinogenesis

Among the sirtuins that are localized in the mitochondria (SIRT3, SIRT4 and SIRT5), SIRT3 is the primary mitochondrial deacetylase (Lombard et al., 2007) and has been demonstrated to be a legitimate tumor suppressor by regulating mitochondrial energy metabolism (Hirschey et al., 2010), limiting the accumulation of mitochondrial ROS (Ahn et al., 2008; Kim et al., 2010). Admittedly, there are discoveries suggesting SIRT3 as a protein that promotes tumorigenesis in gastric cancer and non-small cell lung cancer (Cui et al., 2015; Xiong et al., 2017); however, most discoveries related to SIRT3 suggest that SIRT3 functions as tumor suppressor protein. Because of the mitochondrial localization of SIRT3, one possible explanation why loss of SIRT3 enzymatic activity results in tumor permissive phenotypes can be explained through the aberrant metabolic properties due to loss of SIRT3.

Many additional studies have suggested that SIRT3 plays a critical role in maintaining mitochondrial metabolism homeostasis through its deacetylation activity. It is has been suggested that SIRT3 can regulate mitochondrial energy homeostasis proteins including acetyl-coenzyme A synthetase, long-chain acyl-coenzyme A dehydrogenase, and 3-hydroxy-3-methylglutaryl coenzyme A synthase 2 to respond to nutrient stress (Fritz et al., 2012; Hirschey et al., 2010; Jing et al., 2011; Zhu et al., 2012). SIRT3 also deacetylates ATP synthase F1 complex specifically at lysine 139 of Oligomycin sensitivity-conferring protein (OSCP), and deacetylation of OSCP lysine 139 increases ATP production and mitochondrial energy homeostasis efficiency.

Sixty years ago, Otto Warburg described that tumor cells tend to have aberrant mitochondrial metabolism with a dysregulation of ATP production and mitochondrial energy homeostasis, where cancer cells exhibit higher levels of glucose consumption as compared to their normal counterparts (Warburg, 1956). In this regard, Finley et al have shown that cells lacking *Sirt3* exhibit increased glucose consumption (Finley et al., 2011). Loss of *Sirt3* increased the stabilization of HIF-1α protein, which functions as a transcription factor that activates multiple cellular pathways including metabolic reprogramming and cancer cell proliferation (Haigis et al., 2012). Loss of *Sirt3* increased glucose uptake and lactate production, whereas overexpression of SIRT3 proteins decreased lactate production and suppressed the Warburg effects in cancer cells (Finley et al., 2011). In addition, it has been shown that loss of *Sirt3* increased mitochondrial ROS levels, which increases genomic instability, activates HIF-1α and promotes carcinogenesis (Bell et al., 2011; Haigis et al., 2012; Kim et al., 2010; Tao et al., 2010). Similarly, Ozden et al also suggested that loss of SIRT3 enzymatic activity could affect the pyruvate dehydrogenase enzymatic activity and thus promote the cell to a more transformed

phenotype and prefer glycolysis (Ozden et al., 2014). These results provide a potential mechanistic link between mitochondrial acetylome, aging, carcinogenesis.

SIRT3 regulation of cellular oxidation / reduction status and/or reactive oxygen species

It is well known that ROS production is closely linked to the mitochondrial energy metabolism and carcinogenesis. As a result of using oxygen to generate ATP, mitochondria produce ROS as a byproduct. Electrons transfer through oxidative phosphorylation (OXPHOS) constitutes a major way of ROS production, since electrons can leak out of complexes I and III, resulting in one-electron reductions of oxygen to produce the superoxide radical (Spitz et al., 2004). Loss of *Sirt3* induced increased acetylation of electron transport chain proteins induced higher steady-state levels of ROS (Finley et al., 2011; Vassilopoulos et al., 2014). Not only is SIRT3 involved in ROS production process, it is recently recognized that SIRT3 could also directly regulate the ROS detoxification enzymatic activity through deacetylation of (Manganese superoxide dismutase) (MnSOD) and NADPH production through deacetylation of Isocitrate dehydrogenase 2 (IDH2). On this topic, several studies have demonstrated that MnSOD and IDH2 contain several reversible acetyl lysines and that acetylation alters its enzymatic function (Chen et al., 2011; Qiu et al., 2010; Someya et al., 2010; Tao et al., 2010; Yu et al., 2012).Two mitochondrial target proteins, MnSOD and IDH2, both of which are SIRT3 deacetylation targets, become the main focus of my thesis research, as both are critical regulators for cellular redox balance and detoxification processes.

MnSOD was previously regarded as a simple ROS scavenging enzyme with its activity thought to be only stoichiometrically dependent on the levels of mitochondrial superoxide.

However, recent studies have been suggested that MnSOD activity could be regulated by several cellular mechanisms including, transcriptional, translational, and perhaps most importantly, post-translational regulation, depending on the intracellular signals or environmental triggers (Dhar and St Clair, 2012; Hitchler et al., 2008; Huang et al., 1999; Li et al., 2006). Furthermore, intracellular sensing proteins recognizing specific intracellular physiological conditions and initiating post-translational signaling cascades has been known as a fundamental paradigm in biology (Bisht et al., 2003; Gius et al., 1999a; Gius et al., 1999b; Hallahan et al., 1993). Lysine acetylation has recently been regarded as an important post-translational modification mechanism that regulates mitochondrial proteins (Choudhary et al., 2009; Kim et al., 2006; Kouzarides, 2000; Lombard et al., 2007). In this regard, it is logical to hypothesize that MnSOD may contain specific lysine residues, which can be deacetylated by SIRT3.

On this topic, three seminal papers have been published to illustrate how *Sirt3* could directly affect MnSOD activity through site-specific deacetylation (Chen et al., 2011; Qiu et al., 2010; Tao et al., 2010). Tao *et al*. showed that lysine 122 of MnSOD can be targeted for deacetylation by Sirt3. When examining the 3D protein structure of MnSOD, lysine 122 is located near the entrance to the MnSOD inner catalytic core. The data presented in this paper provide significant experimental data to validate the electrostatic facilitation model proposed by Dr. Fridovich (Benovic et al., 1983; Tao et al., 2010; Zhu et al., 2012). Using site-directed mutagenesis, lysine 122 was mutated to an arginine (positive charge mimicking a deacetylated state, $MnSOD^{K122R}$). This mutation induced higher level of MnSOD activity and decreased mitochondrial superoxide level. In contrast, when lysine 122 was mutated to a glutamine (neutral charge mimicking an acetylated state, $MnSOD^{K122Q}$), MnSOD activity was decreased and

mitochondrial superoxide level increased. Given the positively charged lysine residue 122 is located close to the entrance of the catalytic core and ideally oriented to provide superoxide anion attraction. Thus it is reasonable to propose the mechanism of increased MnSOD enzymatic activity is due to the attraction of the negatively charged superoxide anion toward the positively charged lysine residues. However, when lysine 122 is acetylated, the electrostatic funnel shows a neutral to negative charge, which repels superoxide anion, therefore, decreasing the possibility of superoxide entering the active site to H_2O_2 conversion. In addition, the role of MnSOD lysine 122 acetylation in carcinogenesis was confirmed by experiments that infection of *Sirt3*$^{-/-}$ MEFs with lenti-MnSOD^{K122R} but not lenti-MnSOD^{K122Q} inhibited *in vitro* immortalization by an oncogene Ras, or exposure to irradiation (Tao et al., 2010).

Similarly, MnSOD lysine 68 was also suggested to be a potential deacetylation site guided by SIRT3 (Chen et al., 2011). Results showed that SIRT3 was able to deacetylate MnSOD at lysine 68 and further increase the enzymatic activity of MnSOD. It is also shown that when cells challenged with DMNQ, a reagent that is known to increase mitochondria ROS level, Sirt3 can be stimulated and further lead to MnSOD activation by deacetylation and protect cells from increased intracellular mitochondrial ROS. All these studies showed that SIRT3 could physically interact with MnSOD and deacetylate MnSOD in cell-free, *in vitro*, and *in vivo* (murine) model systems. In addition, loss of *SIRT3* in different cell lines resulted in increased intracellular and mitochondrial superoxide levels, whereas overexpression of WT SIRT3 but not the deacetylation-null, decreased cellular ROS and mitochondrial superoxide levels (Kim et al., 2010; Tao et al., 2010). The deacetylation of lysine 68 and 122 significantly increases the MnSOD enzymatic activity and thus protecting cells from ROS induced genomic instability and

other deleterious effects (Chen et al., 2011; Jing et al., 2011; Tao et al., 2010). In addition, it is now well documented that MnSOD activity is decreased in early breast cancer and several sources have demonstrated that MnSOD plays a critical role in breast cancer cell proliferation, as well as metastasis through controlling the superoxide and hydrogen peroxide production to activate several redox-sensitive survival and proliferation related cell signaling pathways (Becuwe et al., 2014; Kaewpila et al., 2008; Kattan et al., 2008; Li et al., 1995; Sarsour et al., 2012; Vera-Ramirez et al., 2011; Wang et al., 2005)

IDH2, another mitochondrial protein, has been shown to be a SIRT3 deacetylation target. IDH2 was regarded as an enzyme that functions in the TCA cycle. Its primary role is to oxidize isocitrate into alpha-ketoglutarate (α-KG). The active form of IDH2 is a homodimer that binds to isocitrate and $NADP^+$ and catalyzes the production of α-KG and NADPH. NADPH is long regarded as a reducing reagent that functions to remove ROS and reproduce GSH for cellular detoxification (Rush et al., 1985). Therefore, IDH2 is regarded as a critical metabolic and detoxification enzyme in the TCA cycle that supports mitochondrial integrity and energy homeostasis. On the other hand, genetic loss of *IDH2* in mice has been associated with mitochondrial dysfunction, neurotoxicity, and potentially cardiac hypertrophy and Parkinson's disease (Kim et al., 2016; Ku et al., 2015; Park et al., 2016a), suggesting the role of IDH2 in mitochondrial metabolism and pathogenesis due to dysregulated mitochondrial energy homeostasis and/or detoxification.

Loss of SIRT3 enzymatic activity results in an increase of IDH2 acetylation at lysine 413. Loss of IDH2 enzymatic activity due to acetylation of IDH2 at lysine 413 increases GSSG / GSH

ratio, increases mitochondrial ROS levels, and is associated with B cell malignancy (Yu et al., 2016a; Yu et al., 2012). Furthermore, studies also suggested that the induction of deacetylation activity also appears to protect against the development of age-related human pathology, including carcinogensis (Kim et al., 2010; Someya et al., 2010). Thus, with these results, it is logical to propose that SIRT3 functions as a sensing or fidelity protein which can regulate downstream targets through post-translational modifications involving protein acetylation to modify cellular metabolism and redox balance and may be involved in aging-related diseases like cancer.

Three seminal papers have been published to illustrate how SIRT3 could directly affect IDH2 activity through site-specific deacetylation (Yu et al., 2012). It was first shown that caloric restriction (CR) extends the lifespan of mice by activating SIRT3 and IDH2. Activation of IDH2 and SIRT3 by CR reduced oxidative stresses in mice and prevented acute hearing loss. In addition, overexpression of *SIRT3* increased NADPH levels and protects cells from oxidative stress (Someya et al., 2010). Later, Yu *et al*. showed that lysine 413 of IDH2 can be targeted for deacetylation by SIRT3. When examining the 3D protein structure of IDH2, lysine 413 is located near the catalytic $NADP^+$ binding site of IDH2. Using site-directed mutagenesis, lysine 413 was mutated to an arginine (positive charge mimicking a deacetylated state, $IDH2^{K413R}$). This mutation induced higher levels of IDH2 activity and decreased mitochondrial superoxide levels. In contrast, when lysine 413 was mutated to a glutamine (neutral charge mimicking an acetylated state, $IDH2^{K413Q}$), IDH2 activity significantly decreased, the Km value for isocitrate and $NADP^+$ binding significantly increased, the V_{max} decreased, and the GSSG / GSH ratio significantly increased (Yu et al., 2012). Thus, it is reasonable to propose that the mechanism of decreased

IDH2 enzymatic activity is that when lysine 413 is acetylated, the inability to bind to $NADP^+$ and isocitrate decreases the association of IDH2 monomeric proteins, and therefore decreases the formation of IDH2 homodimers.

Several years later, Yu *et al*. published another manuscript suggesting that loss of SIRT3 enzymatic activity provides a growth advantage for malignant B cells (Yu et al., 2016a). They discovered that in malignant B cells, SIRT3 protein levels and *SIRT3* mRNA levels were lower compared to normal B cells, resulting in a higher IDH2 acetylation levels and a higher Ki67 percentage. In addition, these cells possess higher mitochondrial ROS levels. All these pathological and biochemical phenotypes provide a growth advantage for B cell malignancy. Overall, all these properties associated with loss of SIRT3 enzymatic activity and IDH2 acetylation at lysine 413 suggest that dysregulated IDH2 acetylation, due to loss of SIRT3 enzymatic activity, can provide at least partial explanations of tumor permissive phenotypes and/or tumorigenesis related to *Sirt3* loss.

Overall, cells lacking Sirt3 may have dysfunctional coordination of both mitochondrial energy metabolism and detoxification enzymes, which can ultimately result in aberrant and potentially damaging ROS production that may have deleterious biological effects. All these results related to SIRT3, mitochondrial energy homeostasis, ROS production and detoxification also raise several important questions regarding the role of SIRT3 in carcinogenesis that include: (1) what are the roles of sirtuins, specifically SIRT3, in tumorigenesis? (2) how are sirtuins, specifically SIRT3, involved in regulation of cancer cell metabolism, proliferation and metastasis through site-specific acetylation/deacetylation?

SIRT3 is a breast cancer tumor suppressor protein

While mice lacking one of the seven sirtuin genes do not exhibit changes in life span, these mice exhibit physiological phenotypes for several age-related illness, including insulin resistance, cardiovascular disease, neurodegeneration, and most importantly a tumorigenesis permissive phenotype (Desouki et al., 2014). Recently, the Gius laboratory created a *Sirt3* knock-out mouse model, and these mice not only exhibit dysregulated mitochondrial detoxification pathways but also contain increased cellular and mitochondrial reactive oxygen species (ROS). In addition, the mice lacking *Sirt3* develop estrogen receptor positive (ER+) mammary tumors that display high Ki-67 and are poorly differentiated with poor prognosis, and this histopathology is similar to that observed in women with luminal B breast malignancies (Desouki et al., 2014; Kim et al., 2010; Tao et al., 2010).

Breast cancer is the most common and frequent cancer among women in the US, and it is the second cause of cancer death in women worldwide (Fadoukhair et al., 2015; Lumachi et al., 2015). The expected number of new breast cancer cases in the US is approximately 231800 in 2015, which accounts for 29% of all cancers (Lumachi et al., 2015). Breast cancers are categorized into four different subtypes with different molecular characteristics: luminal A, luminal B, HER2 and triple negative breast cancer (Perou et al., 2000). The luminal A and luminal B breast cancer are hormone-receptor positive breast cancers (Fadoukhair et al., 2015). Specifically, the estrogen receptor (ER) and/or progesterone receptor (PR) are expressed in both luminal A and luminal B breast cancer, the latter showing high (more than 14% positive using IHC staining) proliferation signature gene expression (Ki67) and/or oncogenic human epidermal growth factor receptor 2 (HER2) expression (Goldhirsch et al., 2011; Mitri et al., 2012; Perez et

al., 2015). HER2 and triple-negative breast cancer are hormone-receptor negative breast cancers, with the former showing HER2 overexpression, and triple negative regarded as the most aggressive breast cancer (Goldhirsch et al., 2011).

Receptor positive breast cancer (luminal A and luminal B) accounts for approximately 80% of all breast cancers (Lumachi et al., 2015). Endocrine therapy has been mainly used in receptor positive breast cancer treatment (Lumachi et al., 2015). There are several endocrine therapy methods, including ovarian function suppression (OFS), selective estrogen receptor modulators or down-regulators (SERMs or SERDs) and aromatase inhibitors (AIs) (Lumachi et al., 2015). OFS is used to suppress ovarian function, which secretes estrogen and progesterone (Love et al., 2015). Surgical removal of ovaries and gonadotropin-releasing hormone agonists (GnRHa) has been used to obtain OFS (Lumachi et al., 2015; Vitek et al., 2014). The most well-known SERM is tamoxifen (TAM), which blocks ER signaling in the breast and brain selectively (Lumachi et al., 2013; Lumachi et al., 2015). TAM mainly benefits ER+ breast cancer patients by reducing the recurrence and mortality rate (Early Breast Cancer Trialists' Collaborative et al., 2011; Lumachi et al., 2015). Fulvestrant is the only SERD approved by the FDA (Lumachi et al., 2015). It functions as an ER antagonist with no estrogen agonist activity, binding to ER and preventing ER dimerization and relocalization (Croxtall and McKeage, 2011; Dauvois et al., 1993). AIs inhibit the cytochrome P450 component of the aromatase enzyme complex to prevent estrogen biosynthesis (Mokbel, 2002).

Despite the similarity in the treatment between luminal A and luminal B breast cancer, given the impact of proliferative and oncogenic genes in luminal B breast cancer, luminal B

patients have a worse clinical outcome than luminal A patients (Goldhirsch et al., 2011; Perou et al., 2000). Pathologically, luminal B patients have a worse tumor grade and a larger tumor size than luminal A patients (Carey et al., 2006; Haque et al., 2012). Genetically, luminal B patients have a higher p53 mutation rate compared to luminal A patients, resulting in poor prognosis (Carey et al., 2006; Haque et al., 2012). Statistically, luminal B patients have a lower probability of five-year relapse-free survival rate, disease specific survival rate, overall survival rate and distant metastasis-free survival rate compared to luminal A breast cancer patients (Creighton, 2012; Jenkins et al., 2014; Parker et al., 2009). In addition, higher Ki67 expression found in luminal B breast cancer patients is correlated with higher relapse rate (Ellis et al., 2008). Because of its proliferative characteristics, luminal B breast cancer has become less responsive to chemotherapy and endocrine therapy, and approximately 30% of receptor positive breast cancer did not benefit from endocrine therapy at all (Allred et al., 2004; Creighton, 2012).

Receptor negative breast cancers, including HER2 and triple negative breast cancers, typically have a worse clinical outcome. Metastasis to brain is higher in these two breast cancer subtypes, and patients with HER2 or triple negative breast cancer have a lower survival rate (Martin et al., 2017). Despite the differences of breast cancer subtypes, all four types of breast cancer share a similarity with many other types of cancer, as cancer is an aging-related disease. The data for solid tumors in human suggest that as the age increases, an inflection point that indicates an exponential increase in human cancer incidence occurs after 50 years old (Zhu et al., 2014). Approximately half of the newly diagnosed breast cancer patients are older than 65 years (Barginear et al., 2014; Siegel et al., 2012). Furthermore, luminal B breast cancer patients older than 60 years have a two-fold increase in luminal B incidence compared to patients between 40

and 59 years old, whereas the incidence of luminal A breast cancer remains relatively constant among different age groups (Creighton, 2012). Therefore, the incidence of luminal B breast cancer is linked with aging and aging related genes. One evolutionally preserved aging-related gene that can result in luminal B breast cancer incidence is sirtuins.

To further understand the role of SIRT3 in breast carcinogenesis, our laboratory has shown that *Sirt3* knock out mouse embryonic fibroblasts (MEFs) exhibited significantly higher levels of genomic instability and could be immortalized by infection with a single oncogene, either Myc or Ras. In addition, these immortalized MEFs were able to grow in low density, soft agar and become tumorigenic in nude mice (Kim et al., 2010). These results strongly suggest that loss of *Sirt3* results in a tumor-permissive phenotype in mice. More importantly, $Sirt3^{-/-}$ mice developed mammary gland tumors over 24 months, while no $Sirt3^{+/+}$ mice developed mammary tumors during the same period. Interestingly, Histological H&E and immunohistochemistry (IHC) staining identified these tumors as estrogen receptor and progesterone receptor (ER/PR) positive. These results further suggested that $Sirt3^{-/-}$ mice developed mammary gland tumors parallel a well-differentiated, receptor-positive histological characteristic that is commonly observed in breast malignancies in older women (Kim et al., 2010). Finally, using human breast cancer sample sets including SIRT3 expression and *Sirt3* RNA levels also showed that SIRT3 expression was significantly lower in breast cancer samples as compared to normal control and negatively correlates breast cancer malignancy (Kim et al., 2010). Together, results from *in vitro*, *in vivo* and human studies strongly support the hypothesis that SIRT3 is a genomic expressed, mitochondrial localized tumor suppressor protein.

More importantly, sirtuins have been suggested to play a role in anti-aging and receptor positive breast cancer are most common in post-menopausal women, which incidence increases slowly until the mid 60's when a significant increase in incidence is observed (Ershler and Longo, 1997a, b). In this regard, results of *Sirt3* knockout mice developing ER-positive breast cancer provide a convincing argument that SIRT3 may function as critical regulators at the crossroads between metabolic regulations, aging and aging related human diseases like breast cancer, and loss of Sirt3 would contribute to creating a tumor permissive environment. Therefore, in my thesis, the overarching goal is to study how does the aberrant acetylation of mitochondrial proteins (IDH2 and MnSOD), due to loss of SIRT3 enzymatic activity, can result in an inbalanced redox environment and energy homeostasis, therefore promoting tumorigenesis and tumor permissive phenotypes.

Chapter 2: Materials and Methods

Cell culture

HEK-293T, MCF7 and NIH3T3 cells were obtained from ATCC in 2012, authenticated using CellCheck 9 Plus by IDEXX Bioresearch, and tested for mycoplasma using PlasmoTest™ - Mycoplasma Detection Kit (InvivoGen, Inc) in 2016. Early passages of cells were frozen in liquid nitrogen and cells were not passaged after six months. Cells were cultured in Dulbecco's Modified Eagle's Medium (DMEM, Gibco) supplemented with 10% fetal bovine serum (FBS, Sigma) and Antibiotic Antimycotic solution (Sigma) and incubated in a 37°C chamber with 5% CO_2. $Sirt3^{-/-}$ mammary tumor cells were generated from $Sirt3^{+/-}$ mammary tumor cells and Sirt3 was genetically deleted using Sirt3 CRISPR plasmids (System Biosciences). $Sirt3^{+/+}$ and $Sirt3^{-/-}$ mouse embryonic fibroblasts were obtained from C57BL/6 female mice embryos. Pregnant mice were sacrificed before embryos were collected, minced using a razor blade and trypsinized. Trypsinized embryos were plated on cell culture plates covered by DMEM medium supplemented with 15% FBS, 1X non-essential amino acid (Sigma) and 1X antibiotic-antimycotic solutions. MCF7 cells were grown for three months in 1 μM Tam to create MCF7-4-hydroxyl-tamoxifen-resistant (HTR) permanent cell lines and several different subclones were frozen. MCF7-HTR cells were not used for more than 5 passages, and new cell lines were subsequently thawed and expanded.

Mitochondrial fractionation

Sirt3 wild-type and knockout livers were collected from C57BL/6 mice that were between five and eight months old. Samples were cut into small pieces, washed with 1X PBS before resuspended in hypotonic buffer (10 mM HEPES, pH = 7.9, 10 mM KCl, 1.5 mM $MgCl_2$,

and 250 mM sucrose) with 1X protease inhibitor (Biotool), 1X phosphatase inhibitor (Biotool) and trichostasin A (TSA, Sigma). Samples were homogenized using a glass dounce and centrifuged at 700 x *g* at 4 ^{o}C twice. The supernatant was then transferred to a new tube and centrifuged at 5,000 x *g* for 10 min at 4 ^{o}C before the mitochondrial pellet was collected and washed with hypotonic buffer twice at 10,000 x *g* for 5 min at 4 ^{o}C.

IDH2 activity assay

IDH2 activity was measured using an IDH activity kit following the manufacturer's procedure (Sigma). Specifically, 1µg of lysed mitochondrial samples or eluted IDH2 samples resuspended in 38µL of assay buffer were added to the reaction well containing 8µL developer, 2µL IDH substrate and 2µL $NADP^+$. Since IDH2 is an $NADP^+$-dependent enzyme, whereas IDH3 is an NAD+-dependent isocitrate dehydrogenase, for the experiments in this study, only $NADP^+$ is added to the reactions and therefore, only $NADP^+$-dependent IDH2 activity is measured. The plate was incubated at 37 ^{o}C for 3 min before the absorbance (A_{450}) was measured for the first time. The absorbance was measured every 5 min for 30 min to calculate the enzymatic activity. The rate of absorbance change is used to determine IDH2 enzymatic activity.

Cloning

To clone *IDH2* genes into PCDH vectors for viral production, pcDNA3-IDH2 plasmid was used as the template for the PCR reaction. Forward (5'-CCGGAATTCCGGATGGCCGGCTACCTGCGGG-3') and reverse (5'-CGCGGATCCGCGCTACTTGTCGTCATCGTC-3') primers (IDT) were used. QIAGEN fast

cycling PCR kit (QIAGEN) was used to PCR amplify *IDH2* gene. Specifically, 10µL QIAGEN fast cycling PCR mix was mixed with 0.5µM forward primer, 0.5µM reverse primer, 300ng template plasmid, and RNAse-free water (Corning) to bring the volume to 20µL. In the amplifications, the first 5 min denaturation step at 95 °C was followed by 30 PCR cycles with each consisting of: 5 seconds at 96 °C (denaturation), 5 minute at 60 °C (annealing) and 1 minutes at 68 °C (extension). A final extension step was performed at 72 °C for 1 minutes. The PCDH plasmid was digested by BamHI and EcoRI. Specifically, 6µg of PCDH vector was mixed with 5µL NEB buffer cutsmart, 1µL BamHI-HF, 1µL EcoRI-HF and RNAse-free water to bring the volume to 50µL. The reaction mixture was incubated at 37 °C overnight.

PCR products and digested plasmids were purified using the gel extraction kit (Qiagen). Specifically, the PCR products were loaded to a 0.8% agarose gel and electrophoresed for 30 min before the gels containing the PCR product were visualized under UV light, cut using a new razor blade, weighed and collected in a microcentrifuge tube. Three volumes of QG buffer were added to 1 volume of gel and the mixture was incubated at 50 °C until the gels were completely dissolved. The samples were added to the QIAquick column and centrifuged at 14,000 rpm for one minute before the flow through was discarded. The PCR product was washed using 0.75 mL buffer PE and centrifuged at 14,000 rpm for one minute before the flow through was discarded. An additional one-minute centrifugation was performed to remove residual ethanol before the purified PCR product was eluted using 30µL RNAse-free water.

For cloning of IDH2 shRNAs, human IDH2 shRNA forward (5’-CCGGCCTCTCTGGAGGCCTTTCTAGCTCGAGCTAGAAAGGCCTCCAGAGAGGTTTTT

G-3') and reverse (5'-AATTCAAAACCTCTCTGGAGGCCTTTCTAGCTCGAGCTAGAAAGGCCTCCAGAGAGG-3') oligos were purchased and cloned into pLKO.1 vector. Specifically, 5μL of forward oligo and 5μL of reverse oligo were mixed with 5μL 10X NEB Buffer 2 (New England Biolab) and 35μL RNAse free water. To anneal the oligos, the 50μL mixture was incubated in a PCR machine for 5 min at 95 °C, 5 min at 90 °C, 5 min at 85 °C, 5 min at 80 °C, 5 min at 75 °C, 5 min at 70 °C, 5 min at 65 °C, 5 min at 60 °C, 5 min at 55 °C, 5 min at 50 °C, 5 min at 45 °C, 5 min at 40 °C, 5 min at 35 °C, 5 min at 30 °C and 5 min at 25 °C. The pLKO.1 plasmid was digested by AgeI and EcoRI. Specifically, 6μg of pLKO.1 vector was mixed with 5μL NEB buffer cutsmart, 1μL AgeI-HF, 1μL EcoRI-HF and RNAse-free water to bring the volume to 50μL. The reaction mixture was incubated at 37 °C overnight before separated by DNA electrophoresis. The 7kb band was collected and gel purified.

Purified PCR products or annealed oligos were directly ligated into the digested vector in 10 μL ligation reactions containing 1μL T4 DNA ligase (Thermo), 2μL 5X rapid ligation buffer and 7μL PCR products or annealed oligos. All ligation reactions were incubated at room temperature for 4 hours before 2 μL of each ligation reaction were transformed into 40 μL DH5α E. coli cells (Invitrogen) using heat-shock transformation. Specifically, the ligation reaction was mixed with E. coli cells and incubated on ice for 5 min before heat-shocked at 42 °C for 30s. The mixture was recovered on ice for 5 min before plated on an LB-Amp plate (100 mg/L ampicillin) and incubated overnight at 37 °C.

Recombinant colonies were picked and cultured overnight at 37 °C in 250 mL of LB-Amp media (100 mg/L ampicillin). Plasmids were then extracted from the cultured cells and purified using the Macherey-Nagel Midiprep kit (Macherey-Nagel) according to manufacturer's directions. Specifically, cultured cells were centrifuged at 6,000 rpm for 5 min before resuspended in 8mL buffer RES. Resuspended cells were lysed in 8mL blue buffer LYS for 5 min before neutralized in 8mL buffer NEU to make sure the reaction mixture is colorless. The column was equilibrated using 12mL buffer EQU before the lysates were loaded to the column. Lysates were washed using 5mL buffer EQU before the filter of the column was discarded. The plasmid bound to the column was washed using 8mL buffer WASH before eluted into 5mL isopropanol (Sigma) by 7mL buffer ELU. Eluted solutions containing the recombinant plasmids were centrifuged at 2,000 x *g* for 20 min before the supernatants were discarded. Pellets were washed using 1mL 70% ethanol before air-dried and dissolved using 200µL RNAse-free water. The concentration of plasmids was measured using Nano-drop machine and recombinant plasmids containing inserts were sequenced at the Northwestern Core Sequencing Facility using the 5' M13-For 21 and 3' M13-Rev 24 primers.

Virus production, plasmids, short hairpin RNA constructs, and site direct mutagenesis

To generate lenti-virus for *in vitro* infection, HEK-293T cells were transfected with 5µg DNA, 5µg psPAX2 packaging plasmid, and 500ng VSV.G envelope plasmid. Viral supernatant was collected 48 hrs later after filtered through a 0.45µm filter (Corning). pLKO.1 human SIRT3 shRNA was purchased from OpenBiosystem, and mice SIRT3 CRISPR plasmids were purchased from System Biosciences. pLKO.1 human IDH2 shRNA oligos were cloned into the pLKO.1 vector (Addgene). pLKO.1-Luc was used as a control. The human IDH2 expression vector,

pCDNA3-Flag-IDH2, was used as the IDH2 wild-type (WT) plasmid and for mutagenesis. Lysine 413 in wild-type IDH2 was converted to Arginine (R: deacetyl mimic) or Glutamine (Q: acetyl mimic) by site-directed mutagenesis (Bioinnovatise). The lenti-viral IDH2 expression vector was generated by standard PCR amplification into two PCDH-CMV vectors (Lentiviral vector, System Biosciences). MCF7 and NIH3T3 cells were infected with 5 MOI of lenti-virus and selected with DMEM containing 2 μg/mL puromycin (Invitrogen) for 14 days or 100 μg/mL G418 sulfate (Invitrogen). After a two-week selection period, cells were grown in normal DMEM with 10% FBS.

To concentrate viral supernatant, a final concentration of 8.5% PEG-6000 (Sigma) and 150mM NaCl solution were added to the viral supernatant and incubated at 4 °C for 48 hr before the mixture was centrifuged at 3,000 x g for 20 min. The supernatant was discarded before the pellets were resuspended using 1mL DMEM medium containing 10% FBS.

Immunoblotting

Cells and tissues were washed with cold 1X PBS, harvested and lysed for 30 min on ice in IP buffer (25 mM Tris-HCl pH 7.4, 150 mM NaCl, 1 mM EDTA, 0.1% NP-40, 5% glycerol) with protease inhibitors (BioTool) and TSA (Trichostatin A, Sigma). Protein lysates were quantified with Bradford assay (BioRad) and immunoblotted using the following antibodies: SIRT3 (Cell signaling), IDH2 (Proteintech), IDH2-K413-Ac (Tao et al., 2010), actin (Sigma) and GAPDH (Millipore). For IDH2 dimerization assay, cells were lysed on ice in IP buffer for 30 minutes and treated with 0.05% glutaldehyde for 10 min at room temperature and immunoblotted with IDH2 antibody. For Native-PAGE immunoblotting, different isoforms of

IDH2 were first transfected into HEK-293T cells. Proteins were collected 48 hr later and lysed protein samples were incubated with flag-tagged beads (Sigma) on a rotary overnight before washed three times with IP buffer and one time with PBS. Washed samples were incubated with 1X flag peptide (Sigma) on a rotary for 1 hr before the lysates were concentrated using a centrifugal unit (Millipore).

Total glutathione level measurement

One million cells were counted before lysed in 1.34mM Diethylenetriaminepenta-acetic acid (DETAPAC, Sigma) dissolved in 143 mM sodium phosphate (Sigma) and 6.3 mM EDTA (Sigma), and 5% 5-sulfosalicylic acid (SSA, Sigma) were added to the sample lysate. 50 μL of lysate were mixed with 700 μL 0.298 mM NADPH (Sigma) dissolved in sodium phosphate buffer, 100 μL 6mM 5,5'-dithio-bis-2-nitrobenzoic acid (DTNB, Sigma) dissolved in sodium phosphate buffer, 100 μL water (Corning) and 50 μL 0.023 U/μL glutathione reductase (GR) dissolved in water (Sigma). The kinetic absorbance was read at 412 nm every 15 s for 2.5 min using xMark™ Microplate Absorbance Spectrophotometer (BioRad), and the rates were compared to a standard curve. For tumor samples, tumors were chopped and lysed in DETAPAC buffer before assays were conducted. Protein concentrations of tumor samples were measured for standardization of total glutathione levels.

Determination of intracellular superoxide levels using MitoSox oxidation

Steady-state levels of mitochondrial $O_2^{\bullet-}$ were estimated using the oxidation of a fluorescent dye, dihydroethidium (DHE), purchased from Life Technologies. Cells were trypsinized, washed and then labeled in 5 mM pyruvate containing 1X PBS with MitoSox Red (2

μM, in 0.1% DMSO) for 20 min at 37°C. After labeling, cells were kept on ice. Samples were analyzed using a Fortessa flow cytometer (Becton Dickinson Immunocytometry System, Inc., Mountain View, California; excitation 488 nm, emission 585, 25 nm band-pass filter). The mean fluorescence intensity (MFI) of 10,000 cells was analyzed in each sample and corrected for autofluorescence from unlabeled cells. The MFI data were normalized to control levels.

Clonogenic cell proliferation and survival colony assay analysis

For the clonogenic proliferation analysis, 50 MCF7-shIDH2-IDH2^{WT}, MCF7-shIDH2-IDH2^{K413R}, or MCF7-shIDH2-IDH2^{K413Q}, 50 NIH3T3-PCDH, NIH3T3-Ras^{G12D}, NIH3T3-IDH2^{K413R}, NIH3T3-IDH2^{K413Q}, 100 *Sirt3*$^{-/-}$ mammary tumor cells (MMT)-PCDH, *Sirt3*$^{-/-}$ MMT-IDH2^{K413R}, or *Sirt3*$^{-/-}$ MMT-IDH2^{K413Q}, and 250 MCF7-shSIRT3-PCDH, MCF7-shSIRT3-IDH2^{K413R}, or MCF7-shSIRT3-IDH2^{K413Q} cells were seeded onto a 6-well plate. In addition, 250 MCF7 cells were incubated with solvent control (water), 1mM isocitrate (Sigma) or 2mM isocitrate and seeded onto a 6-well plate. For clonogenic survival analysis, 250 MCF7-shIDH2-IDH2^{K413Q} cells were incubated with solvent control (DMSO), 5mM dimethyl-alpha-ketoglutarate (DKG, Sigma) or 10mM DKG and seeded onto a 6-well plate. After 14 days, colonies were stained with crystal violet and counted with a Zeiss Stemi dissecting microscope.

Soft agar colony formation assay analysis

Ten thousand NIH3T3 cells permanently infected with different virus combinations were plated on 0.3% agar in growth medium over 0.6% base agar foundation layer in growth medium. After 21 days, the colonies were visualized under a 20X microscope (Zeiss) and images were acquired.

Immunofluorescence sample preparation and image acquisition

Sirt3$^{-/-}$ MMT cells seeded on glass coverslips were fixed in 4% paraformaldehyde and then blocked with 1% bovine serum albumin (BSA) and 10% normal goat serum in 1x PBS. Cells were incubated with anti-Ki67 (c-bioscience) antibody in 1X PBS followed by incubation with goat-rabbit IgG conjugated with Alexa Fluor 647 (Invitrogen) in 1X PBS with 5% goat serum. Cells were washed in 1X PBS, mounted, and imaged with a fluorescence microscope. Fluorescence images were captured using a laser scanning confocal microscope (Nikon A1R). The paired images in all the figures were collected at the same gain and offset settings. Post-collection processing was applied uniformly to all paired images. The images were either presented as a single optic layer after acquisition in z-series stack scans from individual fields or displayed as maximum intensity projections to represent confocal stacks.

Oxygen consumption rate (OCR) and extracellular acidification rate analysis (ECAR)

For OCR analysis, 25,000 MCF7 cells were seeded on a XF-24 microplate (Seahorse Biosciences) and incubated with DMEM containing 10% FBS overnight. 2.5 μM oligomycin A (ATP synthase inhibitor, Sigma), 10 μM carbonyl cyanide m-chlorophenyl hydrazone (CCCP, mitochondrial uncoupler, Sigma), and 2 μM antimycin/rotenone (complex I/III inhibitors, Sigma) were sequentially added into different ports of the same Seahorse cartridge. Each analysis was replicated seven times, and the results were corrected for antimycin and rotenone. For ECAR analysis, 25,000 MCF7 cells were seeded on a XF-24 microplate (Seahorse Biosciences) and incubated with DMEM containing 10% FBS. Thirty minutes before ECAR measurement, the medium was switched to DMEM without bicarbonate containing 0.5% FBS (pH=7.5). Twenty-

five mM glucose (Corning), 2.5 μM oligomycin A and 50 mM 2-deoxyglucose (2-DG, Sigma) were sequentially added into different ports of the same Seahorse cartridge. Each analysis was replicated seven times, and the results were corrected for 2DG.

Xenograft in vivo tumorigenesis analysis

Five million MCF7 cells expressing WT, $IDH2^{K413R}$ and $IDH2^{K413Q}$ were injected into *Foxn1*^{nu} athymic nude mice (The Jackson Laboratory) that were six weeks old. The sizes of tumors were examined using a Vernier caliper every two to three days, and the volumes were calculated using $V=1/2*W^2*L$ (Tomayko and Reynolds, 1989). When the sizes of tumors reached an average of 1000 mm^3, the mice were sacrificed, the tumors were collected, weighed and the levels of total glutathione were measured.

Immunohistochemistry staining and analysis

Breast cancer tissue array slides (Biomax) were immersed twice with 100% xylene (Sigma) for five minutes and 100% ethanol (Sigma) for five minutes each. Then the slides were sequentially immersed with 95%, 80% and 50% ethanol for five minutes each before immersed in H_2O and fixed in a mixture of 95 mL 95% ethanol and 5 mL 37% formaldehyde for 2 minutes. Slides were then treated in 1% Triton X-100 in 1X PBS (Corning) for 20 minutes, washed three times with 1X PBS for five minutes, and quenched in 0.3% H_2O_2 in 1X PBS for 20 minutes. Slides were blocked with 10% donkey serum (Sigma), 1% BSA (Sigma) and 0.3% Triton X-100 (Sigma) in 1X PBS for two hours before treatment with IDH2-K413-Ac (Tao et al., 2010) and SIRT3 (Avias System Biology) antibodies diluted in 1% donkey serum, 1% BSA and 0.3% Triton X-100 in 1X PBS (antibody solution) for 48 hours at 4 °C. After treatment of the primary

antibody, the slides were incubated at room temperature for one hour before being washed three times with 1X PBS for five minutes each. Rabbit secondary antibody (Sigma) in antibody solution was diluted 200X in antibody solution for one hour before being washed three times with 1X PBS for five minutes each. The slides were treated with VECTASTAIN ABC kit (Vector Laboratories) to detect avidin/biotinylated enzyme complexes for 45 minutes following manufacture's protocol. Slides were treated with DAB peroxidase substrate kit (Vector Laboratories) for approximately 15 minutes following manufacturer's protocol and stained in hematoxylin (Sigma) for 10 minutes and destained using acid ethanol (100 mL 70% ethanol and 1 mL 37% hydrochloric acid) before dehydration, a reverse protocol of dewaxing. The intensities were quantified using HistoQuest software (Tissuegnostics).

Statistical analysis

Ordinary one-way ANOVAs, two-tailed unpaired t-tests and correlation analysis were conducted using Prism 6. The statistical significance was reported when $p < 0.05$.

Chapter 3: Results related to IDH2 acetylation at lysine 413

Ch 3.1: Acetylation of IDH2 at lysine 413 affects IDH2 dimerization *in vitro* and *in vivo*

Loss of Sirt3 affects IDH2 acetylation at lysine 413 and IDH2 activity in mice

It has been previously shown that loss of *Sirt3* results in IDH2-K413-Ac and decreases IDH2 activity (Yu et al., 2012). To confirm that SIRT3 plays a role in IDH2 enzymatic activity through IDH2 deacetylation in mice, liver samples from *Sirt3* wild-type ($Sirt3^{+/+}$) and *Sirt3* knock-out ($Sirt3^{-/-}$) mice were collected and the levels of total IDH2, IHD2-K413-Ac, and IDH2 dimerization were determined. While no significant difference in the total amount of IDH2 was observed, loss of *Sirt3* increases *in vivo* IHD2-K413-Ac (**Fig. 1a, b**). In addition, after the liver lysates were cross-linked with glutaldehyde and run on an SDS-PAGE gel, we found that loss of *Sirt3* decreased the levels of dimerized IDH2 (**Fig. 1a, c**). To test mitochondrial $NADP^+$-dependent IDH2 activity in mice, five wild-type and $Sirt3^{-/-}$ mice livers were fractionated, and IDH2 activity was measured. A significant decrease in IDH2 activity was detected (**Fig. 1d**) in the mitochondria extracts from the livers of mice lacking *Sirt3,* suggesting that loss of *Sirt3* decreases IDH2 activity *in vivo*. The results of these experiments suggest that loss of *Sirt3* increased IDH2-K413-Ac, decreased IDH2 dimerization, as well as decreased IDH2 enzymatic activity.

Loss of SIRT3 directs IDH2 acetylation at lysine 413 and IDH2 dimerization in cancer cells

To extend these results to an *in vitro* model system, MCF7 breast cancer cells infected with a lenti-shRNA vector targeting the human *SIRT3* transcript were used. These experiments showed that MCF7 cells infected with lenti-shSIRT3 (MCF7-shSIRT3 cells) to knock-down *SIRT3*, as compared with control, MCF7-shctrl cells, exhibited an increase in IDH2-K413-Ac as

well as a decrease in the levels of the IDH2 dimerization complex (**Fig. 2a**). We also collected the mitochondrial lysates from both control and MCF7-shSIRT3 cells, and a significant two-fold decrease of IDH2 activity was observed (**Fig. 2b**).

IDH2 lysine 413 acetyl mimetic decreases IDH2 dimerization and activity in cancer cells

To examine if IDH2-K413-Ac status directs enzymatic activity and dimerization, a series of IDH2-K413 site-directed mutants were constructed. In this regard, it has previously been shown that substitution of a lysine with a glutamine (K413Q) mimics the acetylated lysine state, while substitution with an arginine (K413R) mimics deacetylation. Thus, mutating lysine IHD2-K413 to arginine would be predicted to mimic a deacetylated lysine, while substitution with a glutamine would be expected to mimic an acetylated lysine. We transfected flag-tagged wild-type IDH2, $IDH2^{K413R}$ and $IDH2^{K413Q}$ into MCF7 cells. After elution of flag-tagged IDH2 proteins, we ran these samples on a native gel. We found that eluted $IDH2^{K413Q}$ proteins displayed a decreased IDH2 dimerization **(Fig. 3a)**. We confirmed our result using HEK-293T cells, as expression of $IDH2^{K413Q}$ showed decreased IDH2 dimerization as well **(Fig. 3b)**. Furthermore, expression of $IDH2^{K413Q}$ significantly decreased mitochondrial IDH2 activity compared to cells expressing wild-type or $IDH2^{K413R}$ **(Fig. 3c)**. These experiments suggest that the acetylation status of IDH2, as well as the ability of IDH2 to form a dimerization complex, directs enzymatic activity in MCF7 cancer cells and HEK-293T cells.

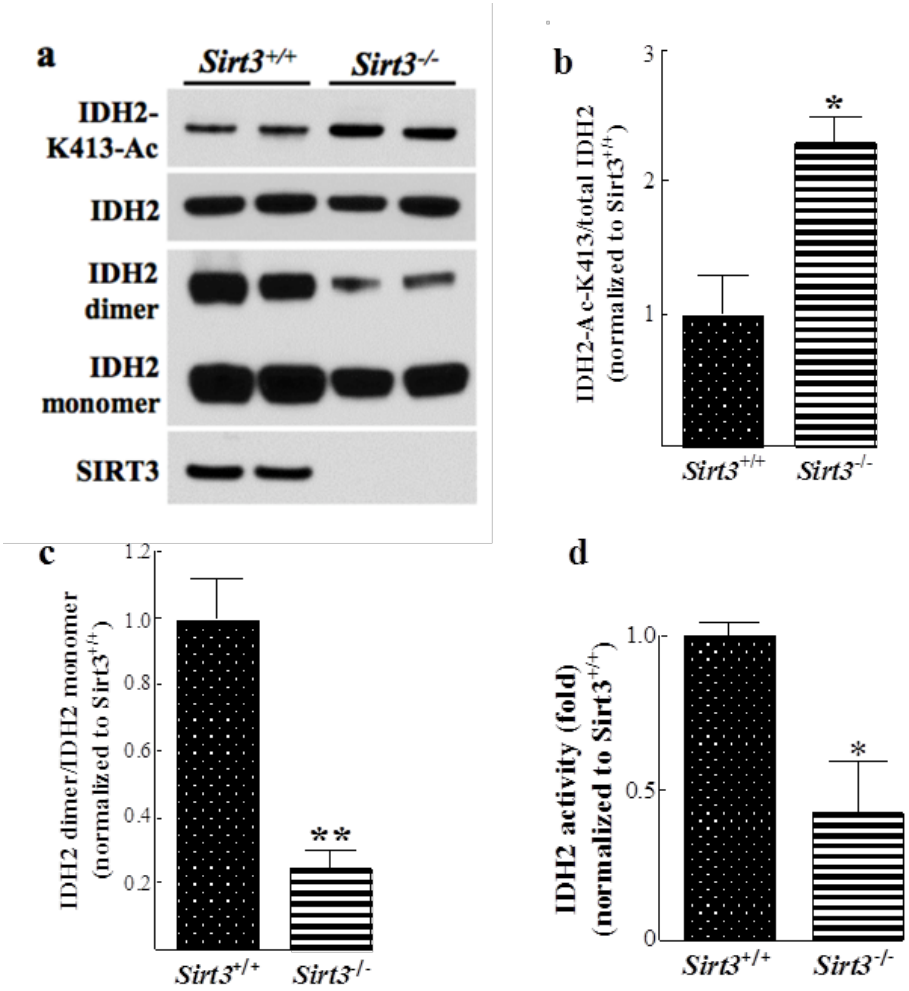
a
Sirt3+/+
Sirt3-/-
IDH2-K413-Ac
IDH2
IDH2 dimer
IDH2 monomer
SIRT3
b
IDH2-Ac-K413/total IDH2 (normalized to Sirt3+/+)
3
2
1
*
Sirt3+/+
Sirt3-/-
c
IDH2 dimer/IDH2 monomer (normalized to Sirt3+/+)
1.2
1.0
0.8
0.6
0.4
0.2
**
Sirt3+/+
Sirt3-/-
d
IDH2 activity (fold) (normalized to Sirt3+/+)
1.0
0.5
0
*
Sirt3+/+
Sirt3-/-

Figure 1. Loss of SIRT3 increases IDH2 acetylation at lysine 413, decreases IDH2 dimerization, and its activity in mice. (a) Wild-type and Sirt3-/- mice livers were harvested and lysates were SDS-PAGE gel separated and subsequently immunoblotted with anti-acetyl IDH2K413 and anti-IDH2 antibodies. For IDH2 dimerization immunoblots, liver lysates were treated with 0.05% glutaldehyde for 10 min before lysates were separated on an SDS-PAGE gel, and immunoblotted with anti-IDH2 antibody. **(b-c)** The intensity of IDH2 acetylation and IDH2 dimerization were quantified using ImageJ software, and the results were normalized to $Sirt3^{+/+}$ liver samples (n=5). **(d)** Wild-type and $Sirt3^{-/-}$ livers were harvested, the mitochondrial extracts (n=5) were collected, and mitochondrial NADP+-dependent IDH2 activity was measured (as described in the methods section). Representative images are shown. Results of this figure come from at least three separate experiments, and error bars represent one standard error mean. * indicates $p<0.05$ and ** indicates $p<0.01$ by two-tailed unpaired t test using Prism 6.0.

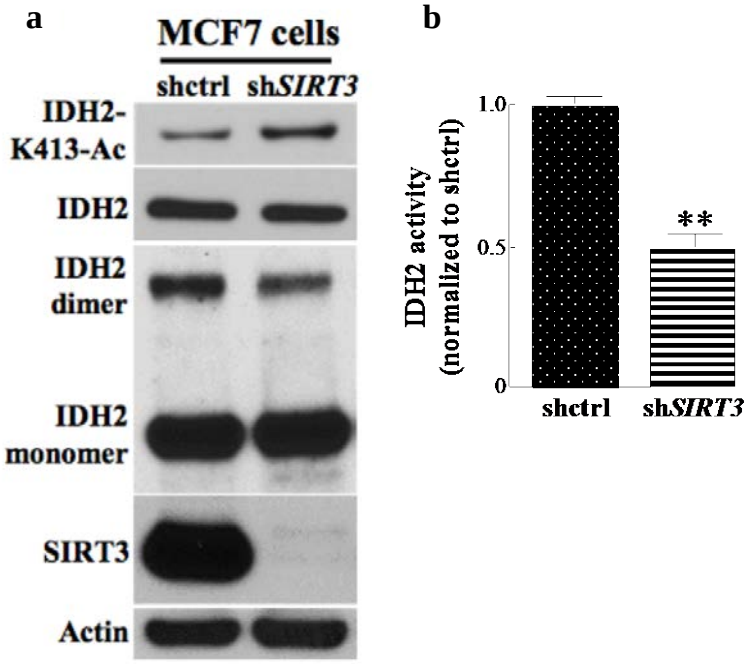
a
MCF7 cells
shctrl
shSIRT3
IDH2-K413-Ac
IDH2
IDH2 dimer
IDH2 monomer
SIRT3
Actin
b
IDH2 activity (normalized to shctrl)
1.0
0.5
0
**
shctrl
shSIRT3

Figure 2. Loss of SIRT3 increases IDH2 acetylation at lysine 413, decreases IDH2 dimerization, and its activity in cancer cells. (a) MCF7 human breast cancer cells were infected with either a control lentivirus (shctrl) or a short hairpin *SIRT3* knockdown virus (*shSIRT3*) to create MCF7-shctrl or MCF7-shSIRT3 cells. Cell lysates were immunoblotted with anti-IHD2-K413-Ac, IDH2, SIRT3 and actin antibodies. IDH2 dimerization gels were performed as described above. **(b)** MCF7-shSIRT3 or MCF7-shctrl cell mitochondrial extracts (n=3) were collected and $NADP^+$-dependent IDH2 activity was measured. Representative images are shown. Results of this figure come from at least three separate experiments, and error bars represent one standard error mean. * indicates $p<0.05$ and ** indicates $p<0.01$ by two-tailed unpaired t test using Prism 6.0.

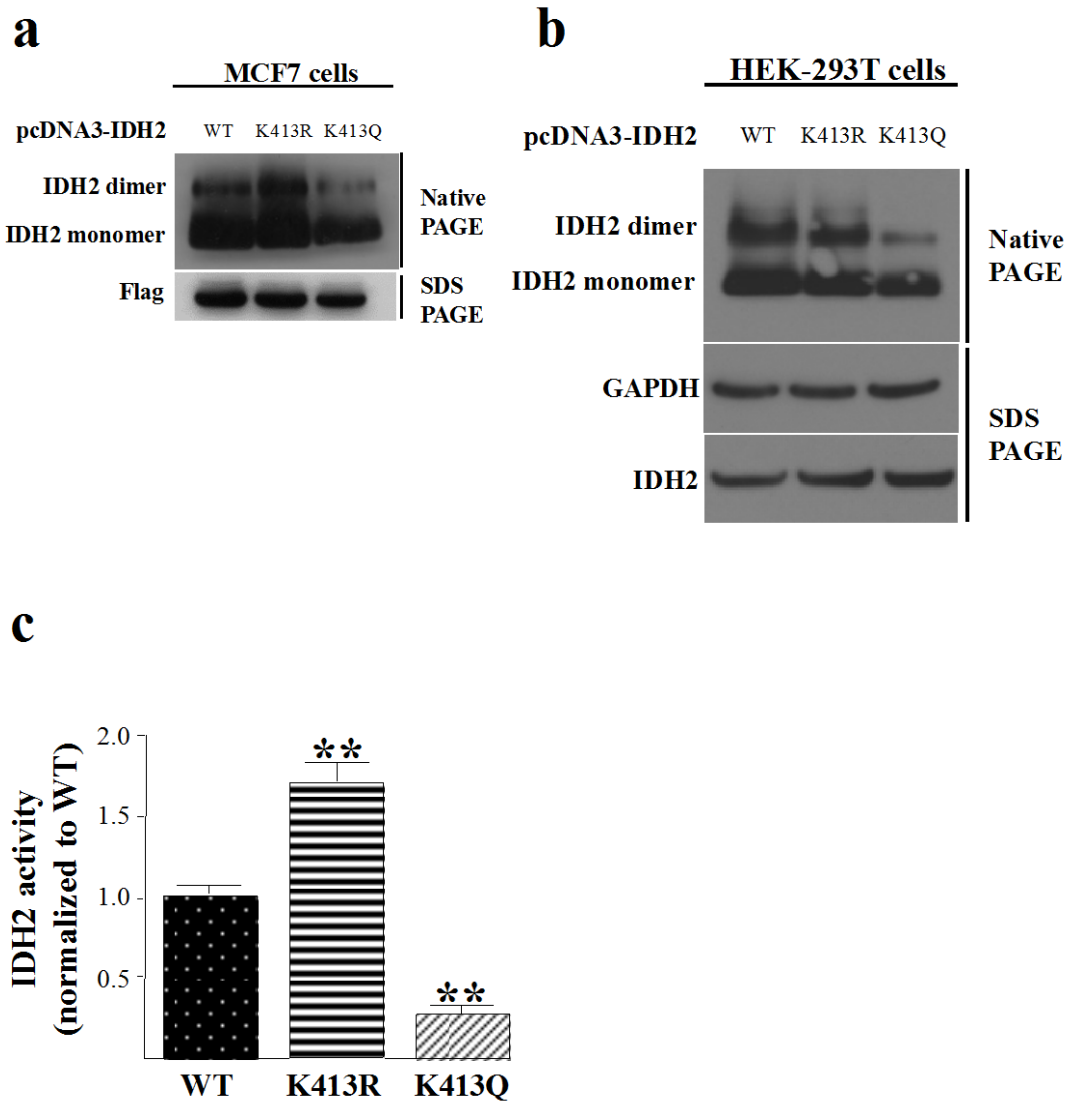
a
MCF7 cells
pcDNA3-IDH2
WT
K413R
K413Q
IDH2 dimer
IDH2 monomer
Native PAGE
Flag
SDS PAGE
b
HEK-293T cells
pcDNA3-IDH2
WT
K413R
K413Q
IDH2 dimer
IDH2 monomer
Native PAGE
GAPDH
IDH2
SDS PAGE
c
IDH2 activity (normalized to WT)
2.0
1.5
1.0
0.5
**
**
WT
K413R
K413Q

Figure 3. Expression of IDH2^{K413Q} in MCF7 breast cancer cells and HEK-293T cells decreases IHD2 dimerization.

(a-b) MCF7 and HEK-293T cells were transfected with flag-tagged IDH2^{WT}, IDH2^{K413R} (de-acetyl mimetic), or IDH2^{K413Q} (acetyl mimetic). Forty-eight hours after transfection, cells were lysed using lysis buffer before flag-tagged proteins were eluted and separated on a native-PAGE gel with G-250 additive and immunoblotted with anti-IDH2 antibody. (c) MCF7-shIDH2-IDH2^{WT}, MCF7-shIDH2-IDH2^{K413R}, or MCF7-shIDH2-IDH2^{K413Q} cells (n=3) were measured for NADP+-dependent IDH2 activity. Representative images are shown. Results of this figure come from at least three separate experiments, and error bars represent one standard error mean. * indicates $p<0.05$ and ** indicates $p<0.01$ by two-tailed unpaired t test using Prism 6.0.

Ch 3.2: Acetylation of IDH2 at lysine 413 affects mitochondrial metabolism

The IDH2^{K413} acetylation mimetic impairs mitochondrial respiration and cancer cell metabolism

Our results clearly show that the acetylation status of IDH2 changes IDH2 enzymatic activity, and the dysregulation of this key enzyme in the Krebs Cycle likely disrupts metabolic pathways as well as results in a metabolite imbalance. Thus, cells expressing the IDH2 acetyl mimetic should disrupt Krebs Cycle, oxidative phosphorylation, as well as mitochondrial metabolism. To examine how expression of the IDH2-K413 site directed mutant alters cellular metabolism, the cell lines used above were measured for mitochondrial function. In this regard, it is shown that MCF7-shIDH2 cells expressing *IDH2^{K413Q}* (MCF7-shIDH2-IDH2^{K413Q}) exhibited a significant decrease in ATP turnover **(Fig. 4a)**, basal respiration **(Fig. 4b)**, mitochondrial respiration capacity **(Fig. 4c)**, and proton leak **(Fig. 4d)**, as compared with MCF7-shIDH2-IDH2^{WT} and MCF7-shIDH2-IDH2^{K413R} cells, suggesting that the acetylation status IDH2-K413 alters breast cancer cell mitochondrial metabolism.

IDH2^{K413} acetylation mimetic directs glycolysis

In contrast to cells with active IDH2, cells with inactive IDH2 should rely on specific compensatory mechanisms responding to the dysregulation of dysregulated Krebs Cycle and oxidative phosphorylation. Thus, it is proposed that the accumulation of metabolites upstream of IDH2 and Krebs Cycle in cancer cells expressing IDH2 acetyl mimetic may preferentially reprogram to preferentially use glucose for glycolytic metabolism. Since the enforced expression of the IHD2-K413-Ac mutant alters metabolism, it seemed reasonable to determine any potential changes in glycolysis and/or mitochondrial redox balance (Tao et al., 2014). In this regard, we

found that MCF7-shIDH2-IDH2^{K413Q} cells displayed an increase in glycolysis (**Fig. 5a)**, while MCF7-shIDH2-IDH2^{K413R} cells showed a decrease in glycolytic capacity (**Fig. 5b)**, suggesting that acetyl mimetic of IDH2^{K413} directs glycolysis activity.

Metabolic mimetics of IDH2 activity affects tumor cell metabolism

To analyze if the addition of α-KG and/or isocitrate, mimicking IDH2 activity increase/decrease, alters cancer cell metabolism, mitochondrial respiration and cellular glycolytic rate was measured. In this regard, the addition of α-KG increased mitochondrial respiration capacity (**Fig. 6a**); in contrast, the addition of isocitrate increased glycolysis (**Fig. 6b**). These data suggest that metabolites that mimics IDH2 activity switch could affect tumor cell metabolism.

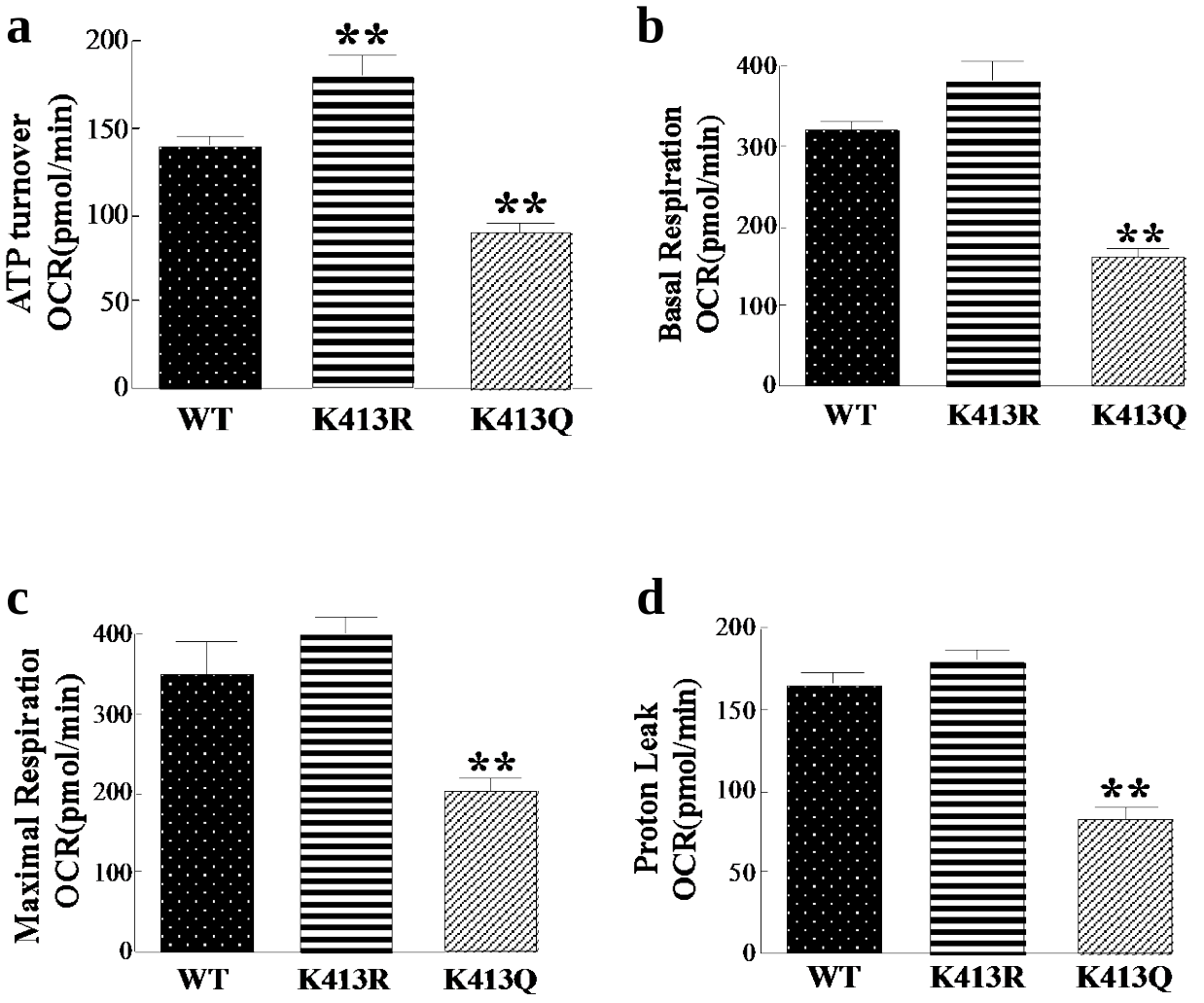
a
ATP turnover OCR(pmol/min)
200
150
100
50
0
**
**
WT
K413R
K413Q
b
Basal Respiration OCR(pmol/min)
400
300
200
100
0
**
WT
K413R
K413Q
c
Maximal Respiration OCR(pmol/min)
400
300
200
100
0
**
WT
K413R
K413Q
d
Proton Leak OCR(pmol/min)
200
150
100
50
0
**
WT
K413R
K413Q

Figure. 4 Acetyl mimetic of IDH2 at lysine 413 affects mitochondrial energy metabolism. MCF7-shIDH2-IDH2^{WT}, MCF7-shIDH2-IDH2^{K413R}, or MCF7-shIDH2-IDH2^{K413Q} cells (n=7) were measured for **(a)** ATP turnover, **(b)** mitochondrial basal respiration, **(c)** mitochondrial respiration capacity, and **(d)** proton leak. Fifty thousand cells were plated on a 24-well XF24 cell culture microplate overnight. Oligomycin, carbony cyanide m-chlorophenyl hydrazine (CCCP), and antimycin/rotenone mixture were sequentially added to measure oxygen consumption rates (OCR) in the XF24 analyzer from Seahorse Bioscience (n=7). The ATP turnover rate was determined by the difference between the starting OCR and the OCR after adding oligomycin. The basal respiration rate was determined by the difference between the starting OCR and the OCR after adding antimycin /rotenone mixture. The maximal respiration rate was determined by the difference between the OCR after adding CCCP and the OCR after adding antimycin/rotenone. The proton leak rate was determined by the difference between the OCR after adding oligomycin and the OCR after adding antimycin/rotenone mixture. Results of this figure come from seven separate experiments, and error bars represent one standard error mean. * indicates $p<0.05$ and ** indicates $p<0.01$ comparing to WT by two-tailed unpaired t-test using Prism 6.0.

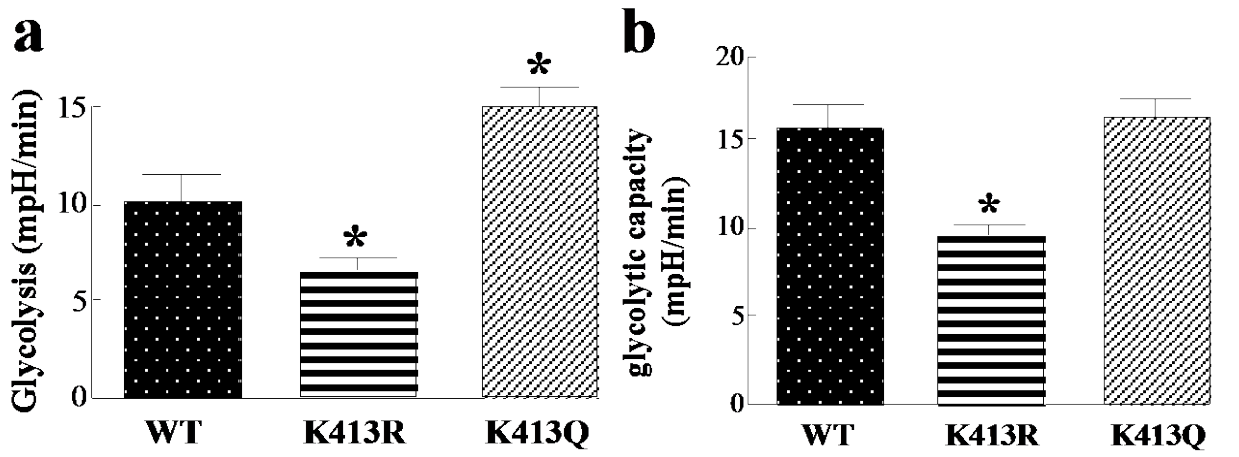
a
Glycolysis (mpH/min)
15
10
5
0
*
*
WT
K413R
K413Q
b
glycolytic capacity (mpH/mln)
20
15
10
5
0
*
WT
K413R
K413Q

Figure. 5 MCF7 breast cancer cells expressing the acetylation mimic mutants exhibit altered glycolytic metabolism.

MCF7-shIDH2-IDH2^{WT}, MCF7-shIDH2-IDH2^{K413R}, or MCF7-shIDH2-IDH2^{K413Q} cells (50,000 cells) were plated on a 24-well XF24 cell culture microplate overnight. **(a-b)** Glucose, oligomycin and 2-deoxyglucose (2-DG) were sequentially added to measure extracellular acidification rates (ECAR) in the XF24 analyzer from Seahorse Bioscience (n=7). Glycolysis ECAR rate was determined by the difference between the ECAR after adding glucose and the ECAR after adding 2-DG. Glycolytic capacity was determined by the difference between the ECAR after adding oligomycin and the ECAR after adding 2-DG.

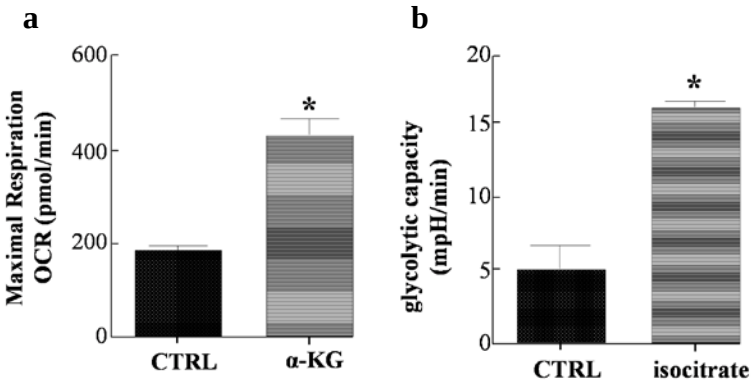
a
Maximal Respiration
OCR (pmol/min)
600
400
200
0
*
CTRL
α-KG
b
glycolytic capacity
(mpH/min)
20
15
10
5
0
*
CTRL
isocitrate

Figure 6. Addition of metabolites that mimics IDH2 activity switch affects cancer cell metabolism.

(A) MCF7-shIDH2-IDH2^{K413Q} cells grown with solvent control or with 1mM α-KG were plated on a 24-well XF24 cell culture microplate overnight. Oligomycin, carbony cyanide m-chlorophenyl hydrazine (CCCP), and antimycin/rotenone mixture were sequentially added to measure oxygen consumption rates (OCR) in the XF24 analyzer from Seahorse Bioscience (n=5). The basal respiration rate was determined by the difference between the starting OCR and the OCR after adding antimycin /rotenone mixture. The ATP turnover rate was determined by the difference between the starting OCR and the OCR after adding oligomycin. The maximal respiration rate was determined by the difference between the OCR after adding CCCP and the OCR after adding antimycin/rotenone. The proton leak rate was determined by the difference between the OCR after adding oligomycin and the OCR after adding antimycin/rotenone mixture. **(B)** MCF7 cells grown with solvent control or with 2mM isocitrate (50,000 cells) were plated on a 24-well XF24 cell culture microplate overnight. Glucose, oligomycin and 2-deoxyglucose (2-DG) were sequentially added to measure extracellular acidification rates (ECAR) in the XF24 analyzer from Seahorse Bioscience (n=5). Glycolysis ECAR rate was determined by the difference between the ECAR after adding glucose and the ECAR after adding 2-DG. Glycolytic capacity was determined by the difference between the ECAR after adding oligomycin and the ECAR after adding 2-DG. Results of this figure come from at least three separate experiments, and error bars represent one standard error mean. * indicates $p<0.05$, and ** indicates $p<0.01$ comparing to CTRL by two-tailed unpaired t-test using Prism 6.0.

Ch 3.3 IDH2 acetyl mimetic results in dysregulation of mitochondrial detoxification

IDH2^{K413} acetylation mimetic impairs mitochondrial detoxification and increases ROS levels in vitro

To directly examine whether the IHD2-K413-Ac directs mitochondrial redox balance *in vitro*, MCF7-shIDH2 cells were used to determine the levels of glutathione, a critical reducing equivalent of regulating redox balance in MCF7 cells. MCF7-shIDH2-IDH2^{K413Q} cells displayed a decrease in total glutathione levels while in contrast; MCF7-shIDH2-IDH2^{K413R} cells showed an increase in total glutathione, as compared with wild-type MCF7-shIDH2-IDH2^{WT} cells (**Fig. 7a**). In addition, MCF7-shIDH2-IDH2^{K413Q} cells have increased ROS levels, as compared with control cells, as determined by MitoSOX^{TM} fluorescence (**Fig. 7b**).

IDH2^{K413} acetylation mimetic decreased total glutathione production in vivo

To examine if the acetylation status of IDH2-K413 altered mitochondrial detoxification of ROS *in vivo*, MCF7-shIDH2-IDH2^{WT}, MCF7-shIDH2-IDH2^{K413R}, and MCF7-shIDH2-IDH2^{K413Q} cells were injected into immunodeficient mice. The examination of the total glutathione levels showed that the expression of *IDH2^{K413Q}* in xenograft tumors displayed significantly decreased total glutathione levels, as compared with tumors expressing either the wild-type *IDH2* or *IDH2^{K413R}* (**Fig. 7c**).

MitoTEMPO partially reversed the tumor permissive phenotypes in cells expressing IDH2 acetyl mimetic

To study how the chemical inhibition of ROS production will potentially reverse the tumor permissive phenotypes, we added mitoTEMPO to the MCF7-shIDH2-IDH2^{K413Q} cells,

and we found a significant decrease of clonogenic survival when grown with 25μM or 50μM mitoTEMPO (**Fig. 8a, b**). These results suggest that the chemical removal of mitochondrial ROS in these cells decreased colony formation, similar to cells expressing lenti- $IDH2^{K413R}$.

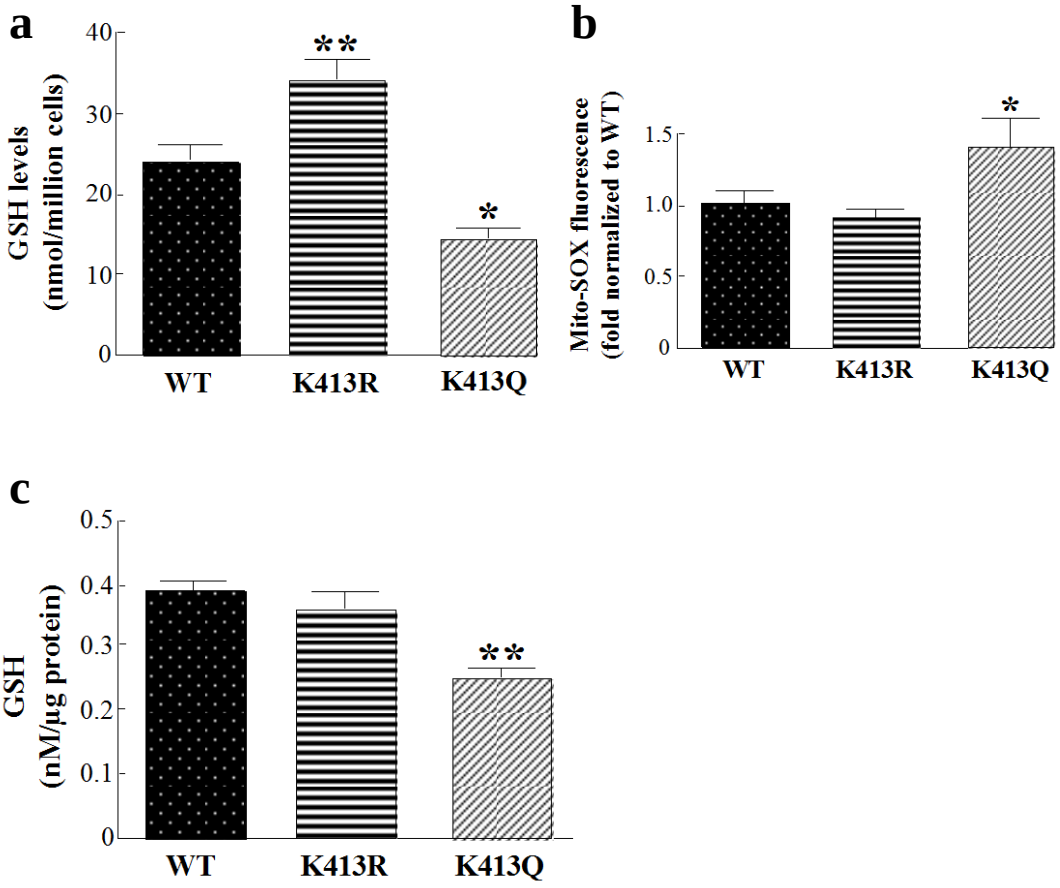
a
GSH levels
(nmol/million cells)
40
30
20
10
0
**
*
WT
K413R
K413Q
b
Mito-SOX fluorescence
(fold normalized to WT)
1.5
1.0
0.5
0
*
WT
K413R
K413Q
c
GSH
(nM/µg protein)
0.5
0.4
0.3
0.2
0.1
0
**
WT
K413R
K413Q

Figure 7. Acetyl IDH2 mimetic increases mitochondrial ROS levels and decreases detoxification in vitro and in vivo

(a) One million MCF7-shIDH2-IDH2^{WT}, MCF7-shIDH2-IDH2^{K413R}, or MCF7-shIDH2-IDH2^{K413Q} cells were collected and lysed before their GSH levels were measured (n=4). **(b)** These three cell lines were measured for mitochondrial superoxide levels in MCF7 cells as determined by MitoSOX^{TM} fluorescence. MCF7 cells were transfected with *IDH2*^{WT}, *IDH2*^{K413R} and *IDH2*^{K413Q} plasmids for 48 hrs. Transfected cells were trypsinized and resuspended before MitoSOX^{TM} (2 µM) was added to the cells and incubated for 30 min at 37 ºC. The fluorescence was measured via flow cytometry (n=3). **(c)** Tumors from the immunodeficient mice injected with MCF7-shIDH2-IDH2^{WT}, MCF7-shIDH2-IDH2^{K413R}, or MCF7-shIDH2-IDH2^{K413Q} cells were collected and lysed, and GSH levels were measured (n=4). *In vitro* results are from at least three experiments, and *in vivo* from four mice per group. Error bars represent one standard error mean. * indicates $p<0.05$ and ** indicates $p<0.01$ comparing to WT by two-tailed unpaired t-test using Prism 6.0.

a

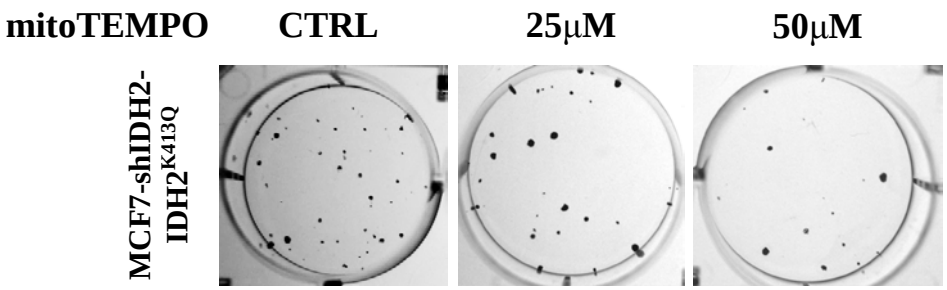
mitoTEMPO
CTRL
25μM
50μM
MCF7-shIDH2-IDH2K413Q

b

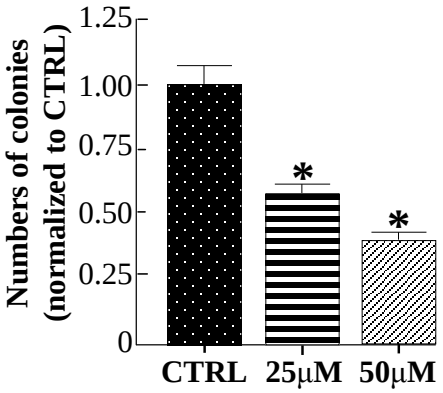
Numbers of colonies (normalized to CTRL)
1.25
1.00
0.75
0.50
0.25
0
*
*
CTRL
25μM
50μM

Figure 8. Decreased production of ROS by mitoTEMPO decreased clonogenic survival of MCF7-shIDH2-IDH2^{K413Q} cells *in vitro*.

(A) MCF7-shIDH2-IDH2^{K413Q} cells were grown with control solvent, 25μM or 50μM mitoTEMPO. Forty-eight hours later, 250 MCF7-shIDH2-IDH2^{K413Q} cells were seeded on a 6-well plate with or without mitoTEMPO in the medium, and 14 days later, the colonies were stained with crystal violet, and the colonies were counted under a Zeiss Stemi DV4 dissecting microscope. **(B)** Quantification of colony numbers under a stereoscope (n=3).

Ch 3.4 IDH2 acetyl mimetic results in tumor permissive phenotypes *in vitro* and *in vivo*

Expression of IDH2 mimetic increases clonogenic growth

We have previously shown that loss of *Sirt3* promotes tumor permissive phenotypes, *in vitro* and *in vivo*, suggesting that SIRT3 can function as a tumor suppressor (TS) protein. Therefore, we hypothesized that acetylation of IDH2 at lysine 413, which would be observed with either deletion of *Sirt3* or due to a decrease in enzymatic activity that should occur with increased age, might play a role, at least in some part, in this tumor permissive phenotype. In this regard, MCF7-shIDH2-IDH2^{K413Q} cells formed more colonies when grown at low density, as compared with MCF7 cells expressing wild-type *IDH2* (MCF7-shIDH2-IDH2^{WT}) (**Fig. 9a, b**). In addition, when IDH2^{K413Q} was expressed in NIH3T3 cells, a type of cells that have already been transformed, the clonogenic proliferation looked very similar to cells expressing oncogenic Ras^{G12D} **(Fig. 10)**, suggesting that expression of IDH2^{K413Q} increases clonogenic growth and proliferation *in vitro*.

Expression of IDH2 deacetyl mimetic partially reverses clonogenic growth and proliferation properties

To observe whether IDH2 deacetyl mimetic (IDH2^{K413R}) would partially reverse the tumor permissive phenotypes in vitro, IDH2^{K413R} and IDH2^{K413Q} were infected in MCF7-shSIRT3 cells. Fewer colonies were observed in the MCF7-shSIRT3-IDH2^{K413R} cells compared to MCF7-shSIRT3-CTRL and MCF7-shSIRT3-IDH2^{K413Q} cells (**Fig. 11a, b**). In addition, *Sirt3*$^{-/-}$ MMTs were used to examine whether expression of IDH2^{K413R} would partially reverse the tumor proliferation and proliferative properties *in vitro*. Expression of IDH2^{K413R} not only decreased clonogenic growth in vitro **(Fig. 12)**, but also decreased the Ki67 ratio **(Fig. 13a, b)**, a

proliferative index that is used to measure tumor cell proliferative properties in pathological studies. Together, these data suggest that re-expression of active, de-acetylated *IDH2* mimetic gene can, at least in some part, reverse the *in vitro* tumor permissive phenotypes.

Expression of IDH2^{K413Q} functions similarly as an oncogene

Based on the results above, it seemed reasonable to determine if enforced expression of *IDH2*^{K413R} (de-Ac-mimic) and/or *IDH2*^{K413Q} (Ac-mimic) would alter the transformative properties of immortalized NIH3T3 cells infected with virus expressing *Myc* or oncogenic *Ras* (*Ras*^{G12D}) (Land et al., 1986; Land et al., 1983). When we examined NIH3T3 cell growth in soft agar, we found that cells expressing *Myc* and/or oncogenic *Ras*^{G12D} were transformed, as they were able to form colonies in soft agar. Surprisingly, simultaneous expression of *IDH2*^{K413R} with *Myc* or *Ras*^{G12D} significantly decreased the sizes of colonies, or even abolished colony formation in soft agar. In contrast, simultaneous expression of *IDH2*^{K413Q} with *Myc* or *Ras*^{G12D} significantly increased the size of colonies that grew in soft agar, suggesting the invasiveness and transformative properties of NIH3T3 cells expressing *IDH2*^{K413Q} and *Myc*/*Ras*^{G12D} (**Fig. 14a, b**).

Metabolic mimetics of IDH2 activity affects clonogenic survival and growth

To determine if adding dimethyl-alpha-KG, mimicing an increase in IDH2 activity, and adding isocitrate, mimicing a decrease in IDH2 activity, may affect *in vitro* phenotypes, we analyzed clonogenic survival and growth of MCF7-shIDH2-IDH2^{K413Q} and MCF7 cells when treated with cell-permeable dimethyl-alpha-ketoglutarate (α-KG), a metabolite that mimics an increase of IDH2 activity and isocitrate, a metabolic that mimics a decrease of IDH2 activity. These experiments showed that MCF7-shIDH2-IDH2^{K413Q} cells grown in α-KG exhibited a

significant decrease in clonogenic survival, as compared to controls (**Fig. 15a, b**). In contrast, MCF7 cells grown in isocitrate exhibited an increase in clonogenic growth (**Fig. 16a, b**). These results suggest that low IDH2 activity promotes tumor aggressiveness, whereas high IDH2 activity partially reverses the proliferative phenotypes.

Injection of MCF7 cells expressing acetyl mimetic of IDH2 increases tumor growth in vivo

MCF7-shIDH2-IDH2^{K413Q}, MCF7-shIDH2-IDH2^{K413R}, and MCF7-shIDH2-IDH2^{WT} cells were subsequently injected into immunodeficient mice and examined for tumor growth / proliferation, as measured by tumor size and weight (**Table 1**). When the tumors were harvested, the sizes and the weight of the tumors expressing *IDH2*^{K413Q} were significantly larger and heavier than the tumors expressing wild-type *IDH2* and *IDH2*^{K413R} (**Fig. 17, 18**). Finally, the tumors expressing *IDH2*^{K413Q} grew faster than the tumors expressing wild-type *IDH2* and *IDH2*^{K413R} when the tumor volumes were examined (**Fig. 19**).

Table 1. Xenograft tumor number, weight, and size

Group i.e., gene	Number of mice	Mice with tumors	Ave tumor weight (g)	Ave tumor size (mm^3)
Wild-type	5	4	0.14	243
K413R	5	4	0.16	263
K413Q	5	5	0.52	908

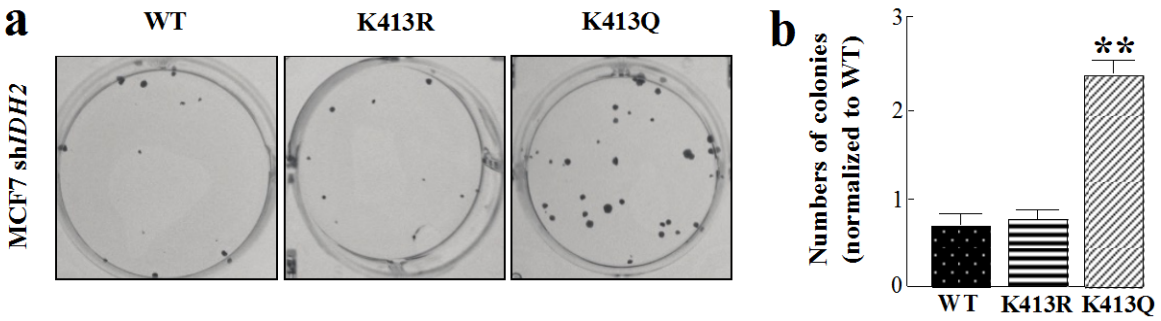
a
WT
K413R
K413Q
MCF7 shIDH2
b
Numbers of colonies
(normalized to WT)
3
2
1
0
**
WT
K413R
K413Q

Figure 9. Expression of *IDH2*^{K413Q} promotes a transformation permissive phenotype in MCF7 cells.

(a) Fifty MCF7-shIDH2-IDH2^{WT}, MCF7-shIDH2-IDH2^{K413R}, or MCF7-shIDH2-IDH2^{K413Q} cells were plated on a 6-well cell culture plate for 14 days before the colonies formed were stained using crystal violet. **(b)** Quantification of colony numbers under a stereoscope (n=4). Results of this figure come from three separate experiments, and error bars represent one standard error mean. * indicates $p<0.05$ and ** indicates $p<0.01$ comparing to WT by two-tailed unpaired t-test using Prism 6.0.

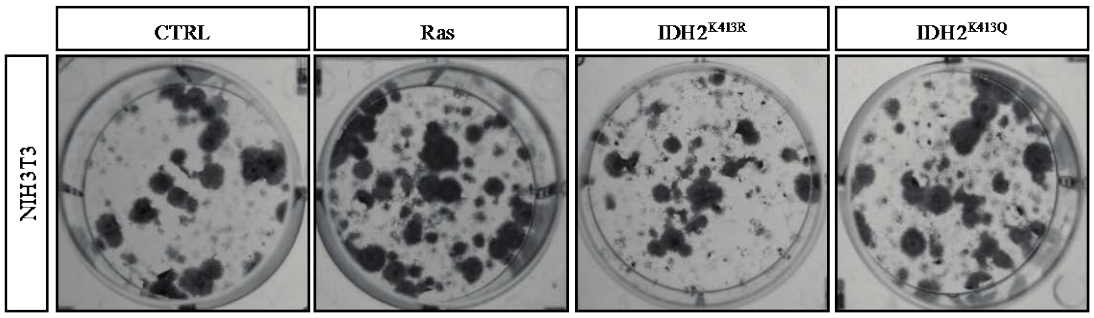
CTRL
Ras
IDH2K413R
IDH2K413Q
NIH3T3

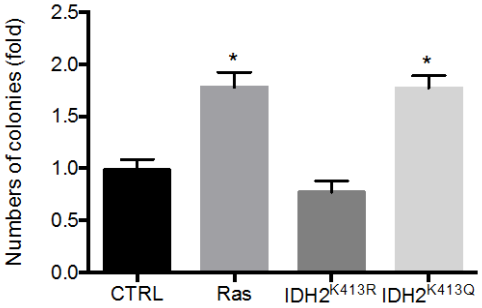
Numbers of colonies (fold)
2.5
2.0
1.5
1.0
0.5
0.0
*
*
CTRL
Ras
IDH2K413R
IDH2K413Q

Figure 10. Expression of *IDH2*^{K413Q} promotes a transformation permissive phenotype in NIH3T3 cells.

One hundred NIH3T3, NIH3T3-IDH2^{K413R}, or NIH3T3-IDH2^{K413Q} cells were plated on a 6-well cell culture plate for 14 days before the colonies formed were stained using crystal violet (n=4). Results of this figure come from three separate experiments, and error bars represent one standard error mean. * indicates $p<0.05$ and ** indicates $p<0.01$ comparing to CTRL by two-tailed unpaired t-test using Prism 6.0.

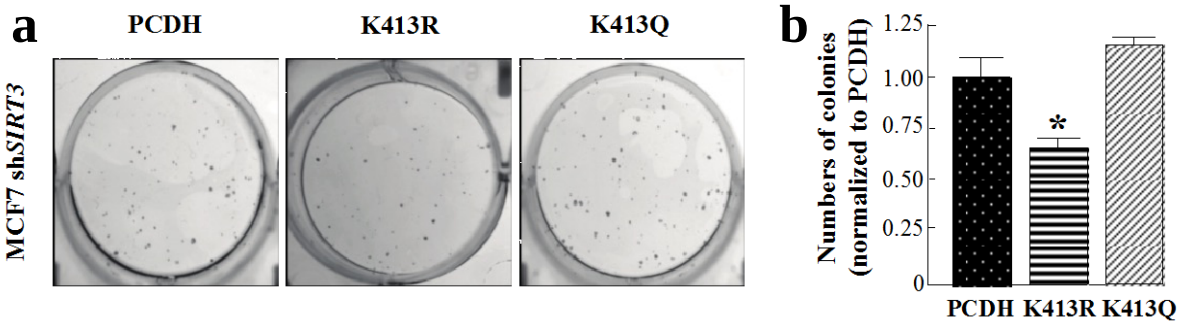
a
PCDH
K413R
K413Q
MCF7 shSIRT3
b
Numbers of colonies
(normalized to PCDH)
1.25
1.00
0.75
0.50
0.25
0
*
PCDH K413R K413Q

Figure 11. Expression of *IDH2*^{K413R} partially reverses a transformation permissive phenotype in MCF7 cells.

(A) Two hundred and fifty MCF7-shSIRT3-PCDH, MCF7-shSIRT3-IDH2^{K413R} and MCF7-shSIRT3-IDH2^{K413Q} cells were plated on a 6-well cell culture plate for 14 days before the colonies formed and were stained using crystal violet. **(B)** Quantification of colony numbers under a stereoscope (n=4). Results of this figure come from three separate experiments, and error bars represent one standard error mean. * indicates $p<0.05$ and ** indicates $p<0.01$ comparing to PCDH control by two-tailed unpaired t-test using Prism 6.0.

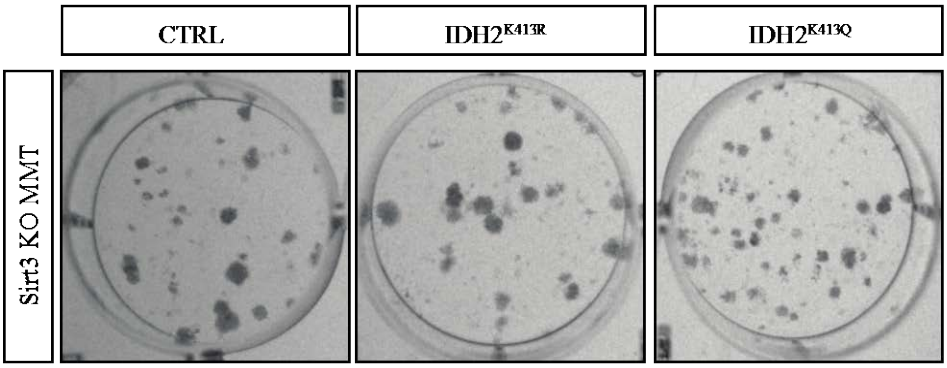
CTRL
IDH2K413R
IDH2K413Q
Sirt3 KO MMT

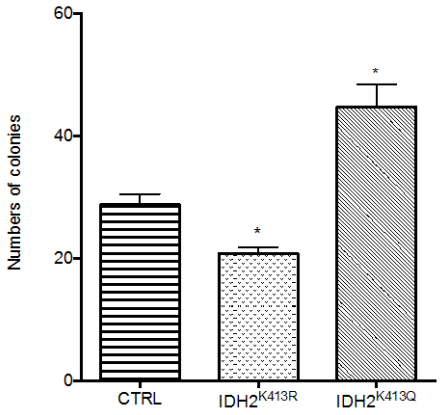
Numbers of colonies
60
40
20
0
*
*
CTRL
IDH2K413R
IDH2K413Q

Figure 12. Expression of *IDH2*^{K413R} partially reverses a transformation permissive phenotype in *Sirt3*$^{-/-}$ MMT cells.

One hundred *Sirt3*$^{-/-}$ MMT, *Sirt3*$^{-/-}$ MMT-IDH2^{K413R} and *Sirt3*$^{-/-}$ MMT-IDH2^{K413Q} cells were plated on a 6-well cell culture plate for 14 days before the colonies formed and were stained using crystal violet (n=4). Results of this figure come from three separate experiments, and error bars represent one standard error mean. * indicates $p<0.05$ and ** indicates $p<0.01$ comparing to PCDH control by two-tailed unpaired t-test using Prism 6.0.

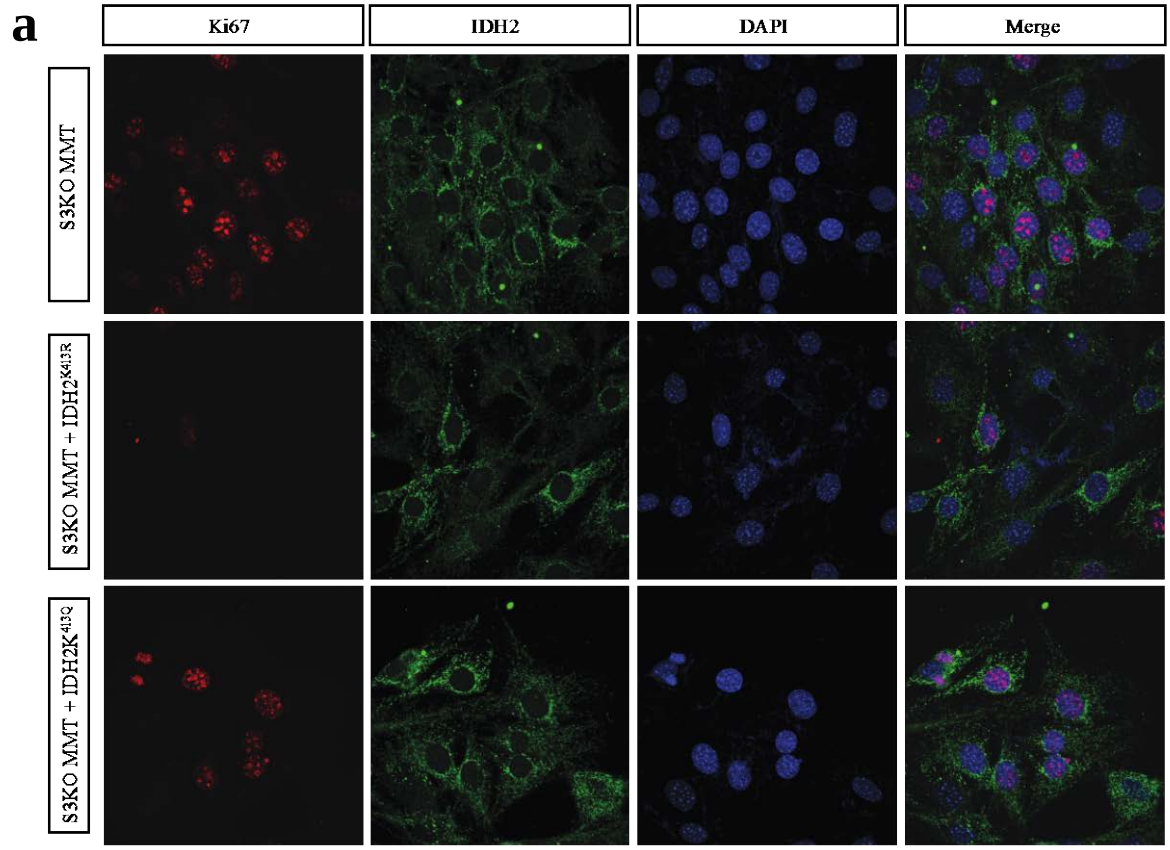
a
Ki67
IDH2
DAPI
Merge
S3KO MMT
S3KO MMT + IDH2K413R
S3KO MMT + IDH2K413Q

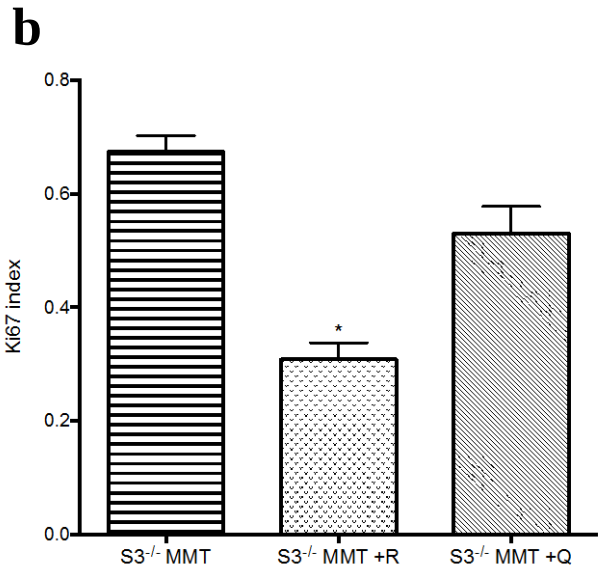
b
Ki67 index
0.0
0.2
0.4
0.6
0.8
*
S3-/- MMT
S3-/- MMT +R
S3-/- MMT +Q

Figure 13. Expression of *IDH2*^{K413R} decreases the Ki67 proliferative index in *Sirt3*$^{-/-}$ MMT cells.

(A) *Sirt3*$^{-/-}$ MMT, *Sirt3*$^{-/-}$ MMT-IDH2^{K413R} and *Sirt3*$^{-/-}$ MMT-IDH2^{K413Q} cells were plated on a 12-well cell culture plate covered with a glass slide and grown overnight. The next day, cells were fixed before stained by IDH2, Ki67 antibodies and DAPI control. Images were obtained using confocal microscopy and representative images were shown. **(B)** Quantification of Ki67 positive ration in three different images using ImageJ software. Results of this figure come from three separate experiments, and error bars represent one standard error mean. * indicates $p<0.05$ and ** indicates $p<0.01$ comparing to *Sirt3*$^{-/-}$ MMT cells by two-tailed unpaired t-test using Prism 6.0.

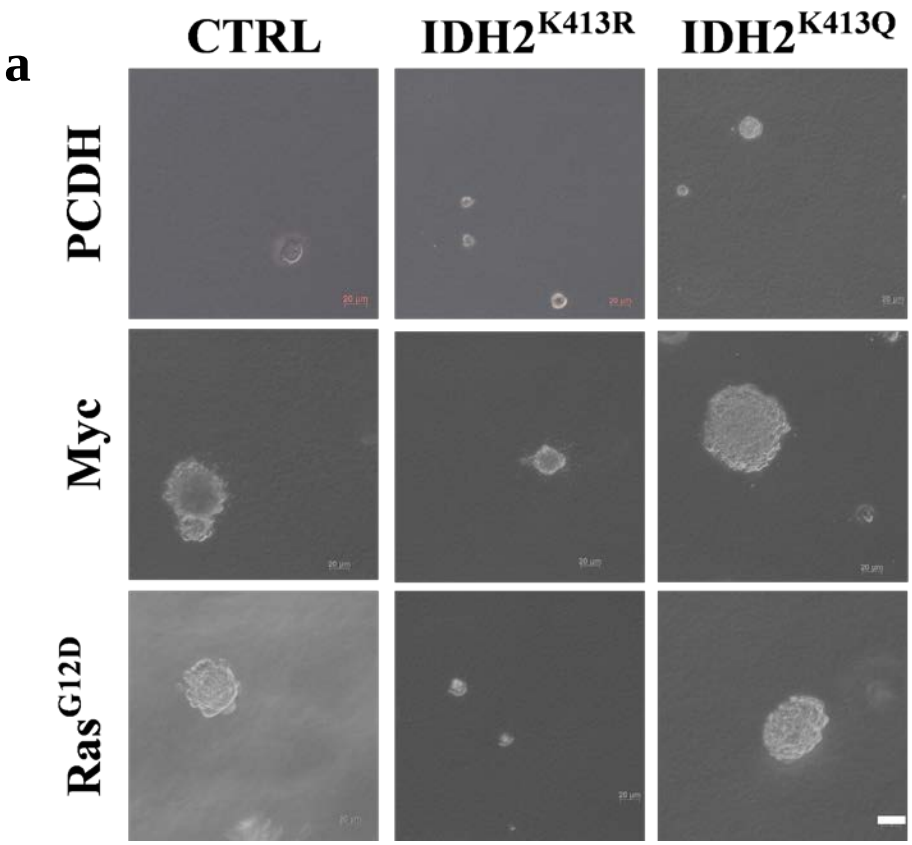
a
CTRL
IDH2K413R
IDH2K413Q
PCDH
Myc
RasG12D

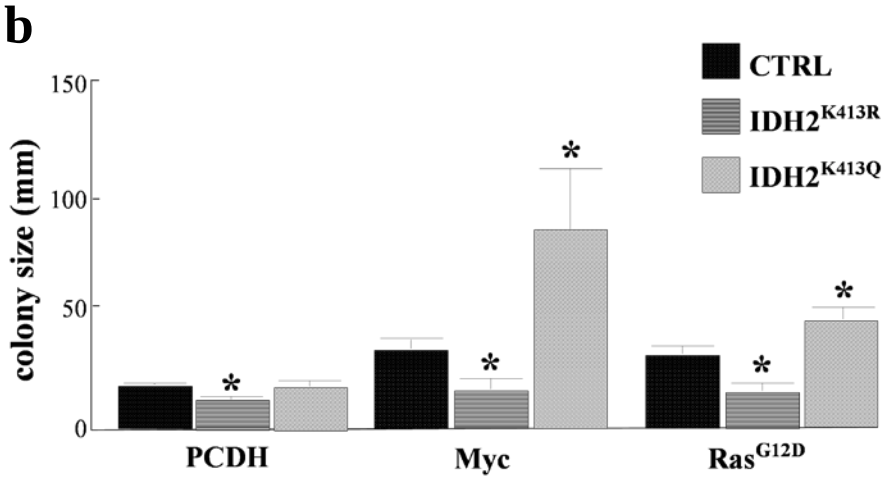
b
CTRL
IDH2K413R
IDH2K413Q
colony size (mm)
150
100
50
0
*
PCDH
Myc
RasG12D

Figure 14. Co-expression of *IDH2*^{K413Q} with *Myc* or oncogenic *Ras*^{G12D} increases the invasiveness of NIH3T3 cells in soft agar colony formation assay.

(A) NIH3T3 cells were infected with viruses expressing PCDH control plasmid, *IDH2*^{K413R}, *IDH2*^{K413Q}, *Myc*, *Myc* and *IDH2*^{K413R}, *Myc* and *IDH2*^{K413Q}, *Ras*^{G12D}, *Ras*^{G12D} and *IDH2*^{K413R}, and *Ras*^{G12D} and *IDH2*^{K413Q}. After selection in puromycin for 14 days, ten thousand cells were plated on 0.3% agar over 0.6% base agar for 21 days before colonies were observed and images were acquired. Scale bar: 20μm. **(B)** Quantification of colony sizes (n=4). Results of this figure come from the average of four separate experiments and error bars represent one standard error mean. * indicates $p<0.05$ comparing to the CTRL column by two-tailed student T test using Prism 6.0.

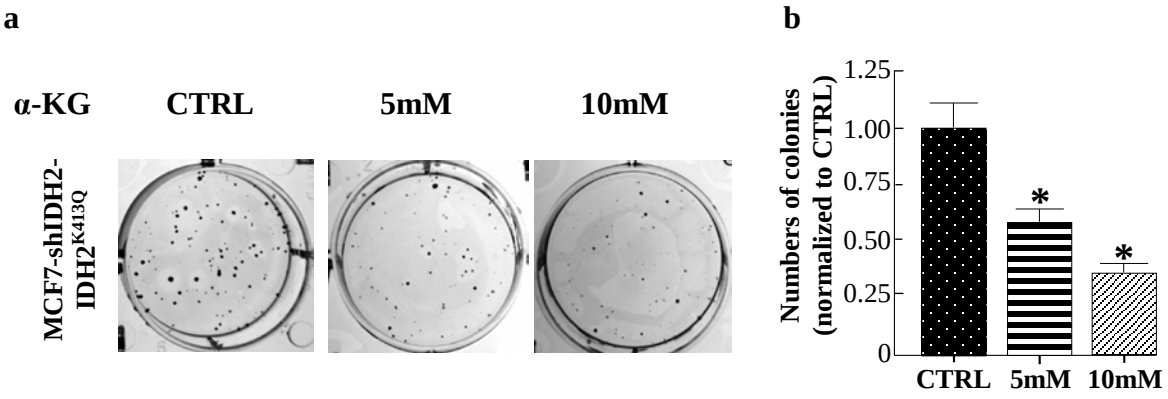
a
α-KG
CTRL
5mM
10mM
MCF7-shIDH2-IDH2K413Q
b
Numbers of colonies (normalized to CTRL)
1.25
1.00
0.75
0.50
0.25
0
*
*
CTRL
5mM
10mM

Figure 15. Exogenous alpha-ketoglutarate alters clonogenic growth and switches cancer cell metabolism *in vitro*.

(A) MCF7-shIDH2-IDH2^{K413Q} cells were grown with solvent control (CTRL), with 5mM or 10mM dimethyl-alpha-ketoglutarate (α-KG). Forty-eight hours later, 250 MCF7 cells were seeded on a 6-well plate with or without α-KG in the medium, and 14 days later, the colonies were stained with crystal violet and counted under a Zeiss Stemi DV4 dissecting microscope. **(B)** Quantification of colony numbers under a stereoscope (n=3).

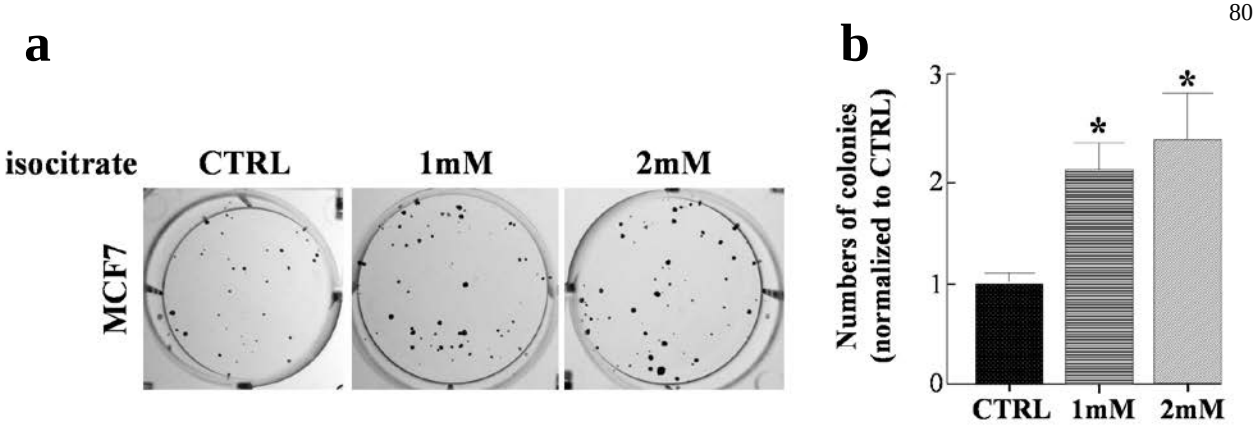
a
isocitrate
CTRL
1mM
2mM
MCF7
b
Numbers of colonies
(normalized to CTRL)
3
2
1
0
*
*
CTRL
1mM
2mM

Figure. 16 Exogenous alpha-ketoglutarate or isocitrate alters clonogenic growth and switches cancer cell metabolism *in vitro*

(A) Wild-type MCF7 cells were grown with solvent control, with 1mM or 2mM isocitrate. Forty-eight hours later, 100 MCF7 cells were seeded on a 6-well plate with or without isocitrate in the medium, and 14 days later, the colonies were stained with crystal violet and counted under a Zeiss Stemi DV4 dissecting microscope. **(B)** Quantification of colony numbers under a stereoscope (n=3).

MCF7-sh*IDH2*-IDH2^{WT}

MCF7-sh*IDH2*-IDH2^{K413R}

MCF7-sh*IDH2*-IDH2^{K413Q}

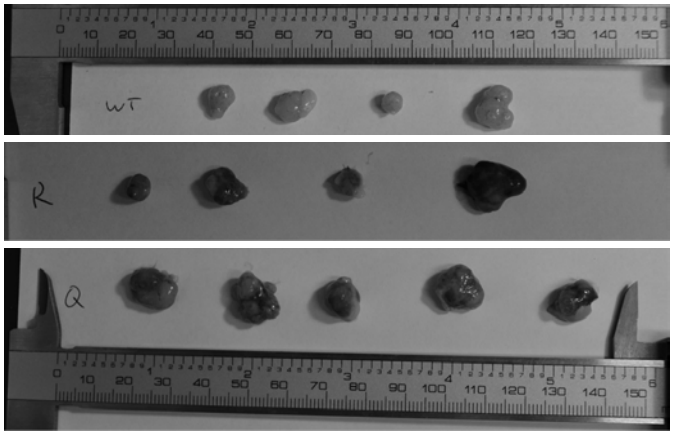

Figure. 17 Expression of IDH2 acetyl mimetics results in larger tumors in nude mice

The image of all harvested tumors from immunodeficient mice injected with MCF-shIDH2-IDH2^{WT}, MCF7-shIDH2-IDH2^{K413R} and MCF7-shIDH2-IDH2^{K413Q} cells were presented. Five million cells were injected into the immunodeficient mice and tumor sizes were measured starting from day 6 of tumor incidence. Mice were sacrificed when the average of tumor sizes from mice injected with MCF7-shIDH2-IDH2^{K413Q} reached around 1000mm^3. Tumors were isolated and tumor sizes were measured under a Vernier caliper. Results of this figure come from the average of five biological replicates, and error bars represent one standard error mean. * indicates $p<0.05$ and ** indicates $p<0.01$ comparing to WT by two-tailed unpaired t-test using Prism 6.0.

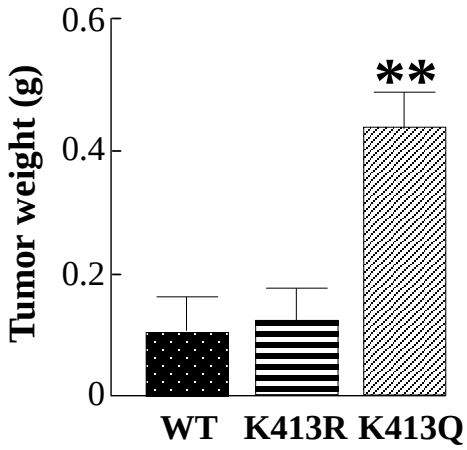
0.6
0.4
0.2
0
Tumor weight (g)
**
WT
K413R
K413Q

Figure. 18 Expression of acetyl mimetics of IDH2 results in heavier tumor formation in nude mice

Five million MCF7-shIDH2-IDH2^{WT}, MCF7-shIDH2-IDH2^{K413R}, or MCF7-shIDH2-IDH2^{K413Q} cells were injected into immunodeficient mice and tumors were harvested and weighed (n=5). Results of this figure come from the average of five biological replicates, and error bars represent one standard error mean. * indicates $p<0.05$ and ** indicates $p<0.01$ comparing to WT by two-tailed unpaired t-test using Prism 6.0.

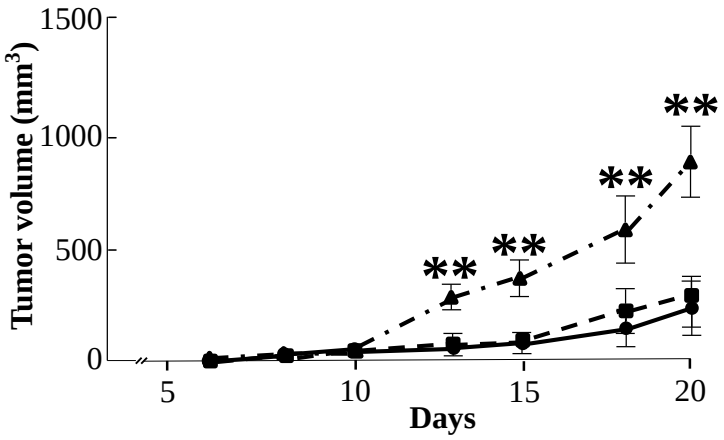
1500
1000
500
0
Tumor volume (mm3)
5
10
15
20
Days
**
**
**
**

Figure. 19 Expression of acetyl mimetics of IDH2 results in faster tumor growth in nude mice

Five million MCF7-shIDH2-IDH2^{WT}, MCF7-shIDH2-IDH2^{K413R}, or MCF7-shIDH2-IDH2^{K413Q} cells were injected into immunodeficient mice. Tumor growth was measured using a Vernier scale and calculated every other day starting from the sixth day of tumor incidence (n=5). Results of this figure come from the average of five biological replicates, and error bars represent one standard error mean. * indicates $p<0.05$ and ** indicates $p<0.01$ comparing to WT by two-tailed unpaired t-test using Prism 6.0.

Ch 3.5 Acetylation of IDH2 correlates with breast cancer malignancy risk

To establish a potential correlative clinical relationship between IDH2 acetylation and breast cancer risk, we used breast cancer patient tissue array slides consisting of different subtypes of breast malignancies and examined the levels of IDH2-K413-Ac and SIRT3 by immunohistochemistry (IHC) using an anti-IDH2-K413-Ac and anti-SIRT3 antibody. We found that the levels of IDH2-K413-Ac in Luminal B breast patient samples were significantly higher than Luminal A breast cancer patient samples (**Fig. 20**). In addition, the levels of SIRT3 in Luminal B patient samples were significantly lower than Luminal A breast cancer patient samples (**Fig. 21**). A representative staining was presented to show the difference of IDH2-K413-Ac and SIRT3 staining between luminal A and luminal B breast cancer patient samples (**Fig. 22**).

Finally, patients with low SIRT3 and high SIRT3 levels were grouped based on their IHC levels, and we found that the subgroup with lower SIRT3 levels showed higher IDH2 acetylation levels than the group with higher SIRT3 levels (**Fig. 23**). These IHC results suggested a negative correlation between acetylation of IDH2 at lysine 413 (**Fig. 24**), as a result of a loss and/or decrease in SIRT3 enzymatic activity and breast cancer malignancy risk (**Fig. 25**).

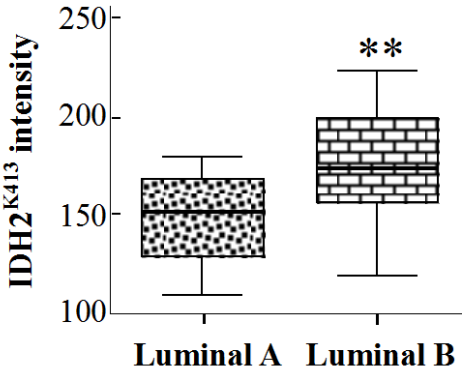
250
200
150
100
IDH2K413 intensity
**
Luminal A
Luminal B

Figure. 20 Luminal B breast cancer patient samples have a higher IDH2^{K413} staining

A breast cancer tissue array consisted of Luminal A (n=17) and Luminal B (n=38) breast cancer patient samples, were dewaxed and immunostained with anti-acetyl IDH2^{K413} antibody. The intensity of staining was quantified using HistoQuest software. The shaded boxes represent the interquartile range; whiskers represent the 10th-90th percentile range; bars represent the median. * indicates $p<0.05$ and ** indicates $p<0.01$ by two-tailed unpaired t-test using Prism 6.0.

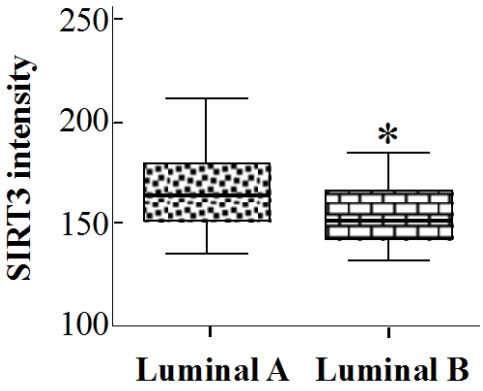
250
200
150
100
SIRT3 intensity
*
Luminal A
Luminal B

Figure. 21 Luminal B breast cancer patient samples have a lower SIRT3 staining

A breast cancer tissue array consisted of Luminal A (n=17) and Luminal B (n=38) breast cancer patient samples, were dewaxed and immunostained with anti-SIRT3 antibody. The intensity of staining was quantified using HistoQuest software. The shaded boxes represent the interquartile range; whiskers represent the 10th-90th percentile range; bars represent the median. * indicates $p<0.05$ and ** indicates $p<0.01$ by two-tailed unpaired t-test using Prism 6.0.

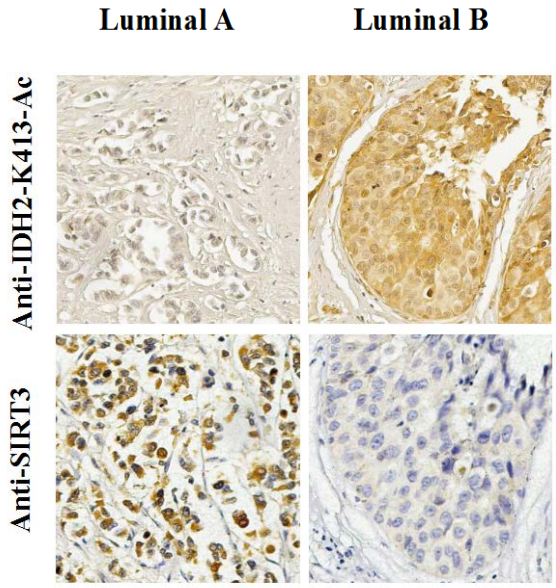
Luminal A
Luminal B
Anti-IDH2-K413-Ac
Anti-SIRT3

Fig. 22 Representative images of Luminal A vs Luminal B breast cancer staining

A representative image of the immunohistochemistry (IHC) slides demonstrating $IDH2^{K413}$ and SIRT3 staining in Luminal A and Luminal B breast cancer samples. Luminal A breast cancer sample has a higher SIRT3 staining than Luminal B breast cancer sample, whereas Luminal B breast cancer sample has a higher $IDH2^{K413}$ staining than Luminal A breast cancer sample.

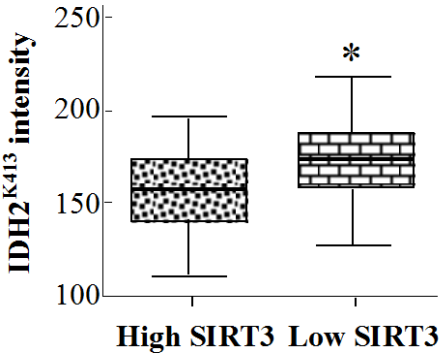
250
200
150
100
IDH2K413 intensity
*
High SIRT3
Low SIRT3

Figure. 23 The breast cancer samples with lower SIRT3 levels have a higher IDH2^{K413} staining.

The samples from the IHC slides were separated into low SIRT3 (SIRT3 staining<160, n=30) and high SIRT3 (SIRT3 staining>160, n=25) groups, and their IDH2^{K413} levels were compared. The shaded boxes represent the interquartile range; whiskers represent the 10th-90th percentile range; bars represent the median.

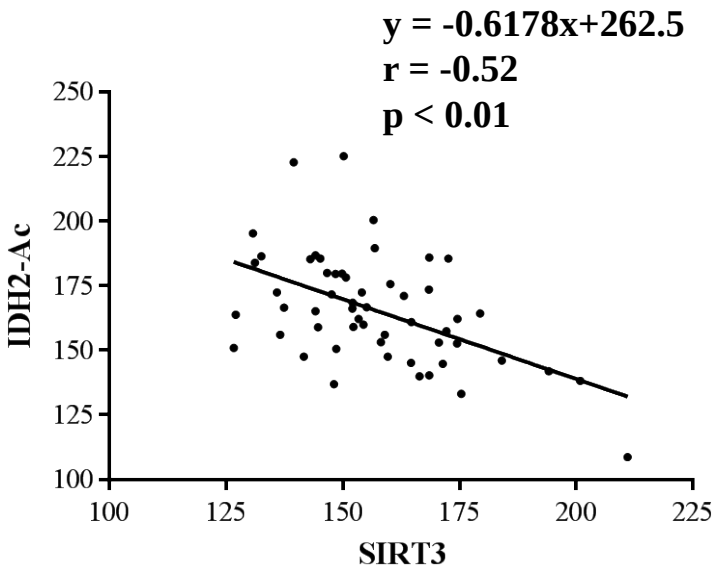
y = -0.6178x+262.5
r = -0.52
p < 0.01
IDH2-Ac
SIRT3
250
225
200
175
150
125
100
100
125
150
175
200
225

Figure 24. Acetylation of IDH2 negatively correlate with SIRT3 protein levels in breast cancer patient samples. Luminal A (n=17) and luminal B (n=38) breast cancer patient samples were stained with acetyl-IDH2^{K413} and SIRT3 antibodies. Results from these samples (n=55) were used to conduct a correlation analysis using Prism 6.0.

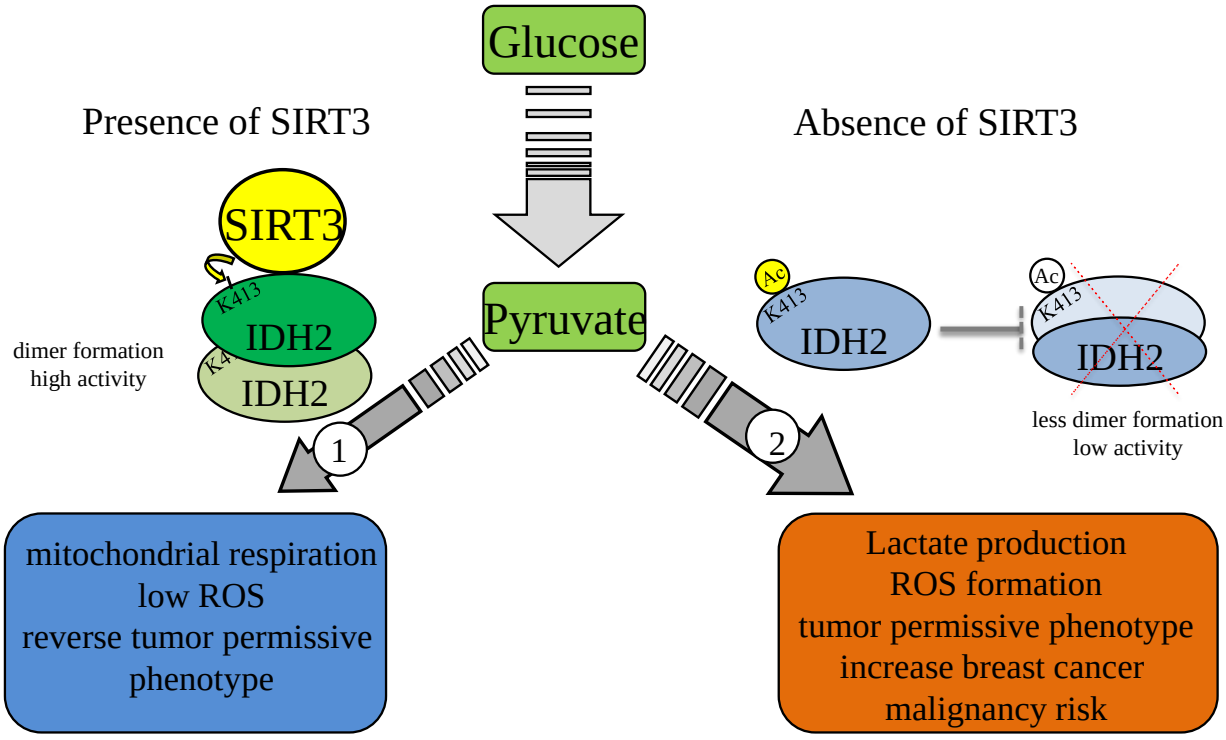
Glucose
Presence of SIRT3
Absence of SIRT3
SIRT3
K413
IDH2
IDH2
dimer formation
high activity
Pyruvate
Ac
K413
IDH2
Ac
K413
IDH2
less dimer formation
low activity
1
2
mitochondrial respiration
low ROS
reverse tumor permissive
phenotype
Lactate production
ROS formation
tumor permissive phenotype
increase breast cancer
malignancy risk

Figure. 25 Summarized mechanism.

Loss of SIRT3 decreases IDH2 dimerization and activity due to increased acetylation at lysine 413. Decreased IDH2 activity would alter mitochondrial respiration, increase ROS and promote transformation permissive phenotypes in vitro and in vivo, which correlates with breast cancer malignancy risk.

Chapter 4: Results related to MnSOD acetylation at lysine 68

Ch 4.1: MnSOD K68-Ac leads to tamoxifen resistance in breast cancer cells

Acetylation of MnSOD at lysine 68 leads to resistance to tamoxifen in vitro

Our previous studies suggest that there is a subgroup of ER+ luminal B human breast malignancies exhibiting a loss of SIRT3-MnSOD-Ac axis signaling, which confers a significantly increased risk of developing resistance to endocrine therapy (Kim et al., 2010). Thus, there may be a mechanistic link between the SIRT3-MnSOD-Ac axis and the development of Tam resistance (Razandi et al., 2013). To test this idea, we created MnSOD deacetylation mimetic ($MnSOD^{K68R}$) and MnSOD acetylation mimetic at lysine 68 ($MnSOD^{K68Q}$). MCF7, MCF7-$MnSOD^{K68R}$, MCF-$MnSOD^{K68Q}$ cells were treated with 1 μM Tam for 5 days, and clonogenic survival assays were performed. These experiments showed that MCF7 cells constitutively expressing $MnSOD^{K68Q}$ exhibited significant resistance to the cytotoxicity of Tam exposure (**Fig. 26**), suggesting a potential link between the acetylation of K68 and a Tam resistance phenotype.

Tam resistance in vitro results in a loss of SIRT3-MnSOD-Ac signature

Since breast cancer cells expressing $MnSOD^{K68Q}$ exhibited Tam resistance, it is possible that MCF7 cells selected for resistance to Tam might also display a MnSOD-K68Ac and/or loss of SIRT3 enzymatic activity signature. As such, MCF7 Tam-resistant cell lines were established by culturing cells in the presence of 1 μM Tam for three months. Both MCF7-HTR and MCF7 cells exposed to Tam for 120h showed an increase in MnSOD-K68-Ac and other SIRT3 deacetylation protein targets, including MnSOD-K122-Ac, IDH2-K413-Ac, and OSCP-K139-Ac (**Figs. 27 a-b**), all of which are a proxy and indirect method to determine SIRT3 activity. All

these results suggest that the loss of the SIRT3-MnSOD-Ac axis signature could be a marker for Tam resistance.

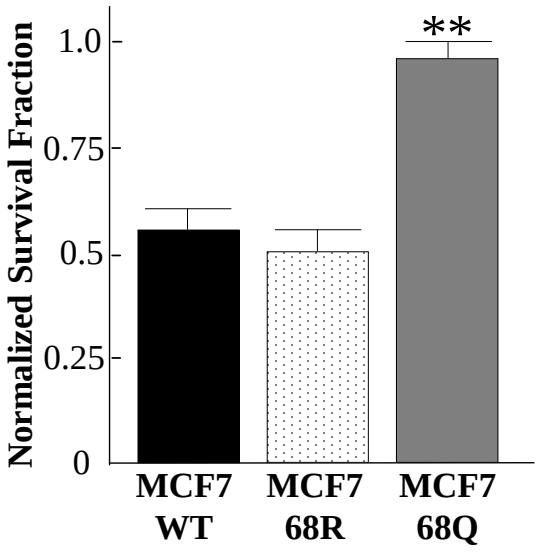
Normalized Survival Fraction
1.0
0.75
0.5
0.25
0
**
MCF7 WT
MCF7 68R
MCF7 68Q

Figure 26. MnSOD-K68-Ac leads to Tam resistance in human breast cancer cells.

MCF7-MnSOD^{WT}, MCF7-MnSOD^{K68R}, MCF7-MnSOD^{K68Q} permanent cell lines were treated with 1 μM of Tam for 24 hours and 100 cells were seeded on a 6-well plate to analyze clonogenic cell survival. All experiments were done in triplicate. Errors represent ± 1 SEM. *$p < 0.05$, **$p < 0.01$, and ***$p < 0.001$.

a

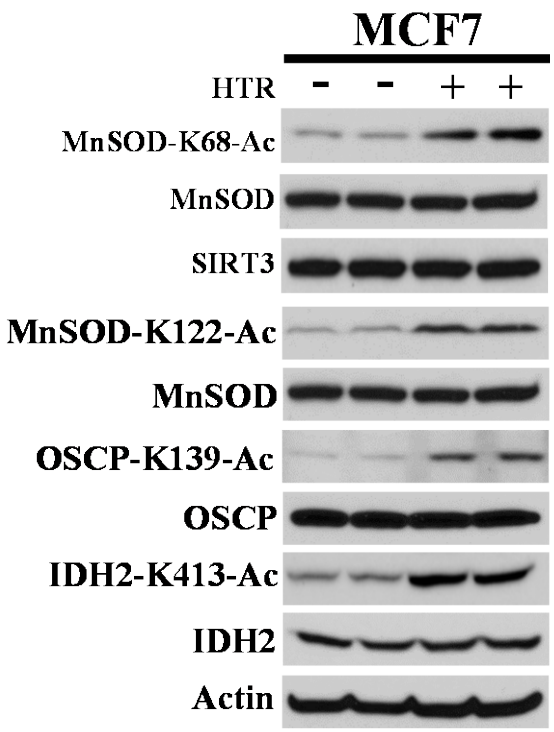
MCF7
HTR - - + +
MnSOD-K68-Ac
MnSOD
SIRT3
MnSOD-K122-Ac
MnSOD
OSCP-K139-Ac
OSCP
IDH2-K413-Ac
IDH2
Actin

b

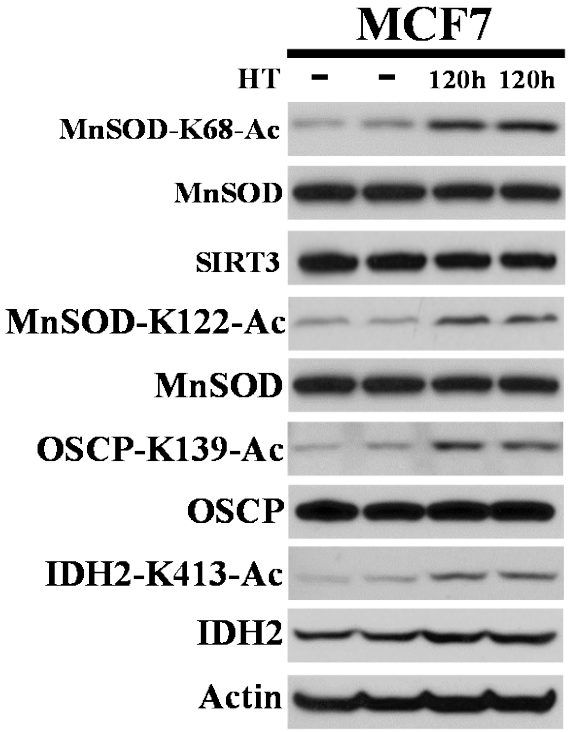
MCF7
HT - - 120h 120h
MnSOD-K68-Ac
MnSOD
SIRT3
MnSOD-K122-Ac
MnSOD
OSCP-K139-Ac
OSCP
IDH2-K413-Ac
IDH2
Actin

Figure 27. Resistance to tamoxifen in human breast cancer cells leads to a loss of SIRT3-MnSOD-Ac signature.

(A) MCF7-4HTR cell line, which were selected in Tam for 3 months, and **(B)** MCF7 cells treated with Tam for 120 hrs were harvested, separated by SDS-PAGE, and immunoblotted with anti-MnSOD-K68-Ac, MnSOD, SIRT3, MnSOD-K122-Ac, IDH2-K413-Ac, IDH2, OSCP-K139-Ac, OSCP and actin antibodies.

Ch 4.2 MnSOD-Ac increases oxidative stress in cells

MnSOD acetyl mimetic increased oxidative stress in cancer cells

It has been shown that acetylation of MnSOD at lysine 68, due to loss of SIRT3 enzymatic activity, decreases MnSOD activity (Chen et al., 2011). Since the primary function of MnSOD is to detoxify mitochondrial $O_2^{\bullet -}$, therefore, we measured the mitochondrial oxidation/reduction status in MCF7 and T47D cells expressing the various MnSOD-Ac mutants. We found an increase of the GSSG/GSH ratio in cells expressing $MnSOD^{K68Q}$, a measure of cellular oxidative stress (**Figs. 28 a-b**). This suggests that the acetyl mimetic of MnSOD at lysine 68 increased oxidative stress in MCF7 and T47D cancer cells.

Resistance to tamoxifen increased oxidative stress in cancer cells

Since MnSOD is tightly correlated with mitochondrial metabolism, and Tam exposure decreases SIRT3 activity, which increases MnSOD-K68-Ac, we also measured the GSSG/GSH ratio in MCF7 and T47D cells that became resistant to tamoxifen. We found that treatment with Tam for 120 hrs or Tam resistance increased oxidative stress in MCF7 and T47D cells, a phenotype similar to cells expressing $MnSOD^{K68Q}$ (**Fig. 29 a-b**). Therefore, inactivation of MnSOD, due to loss of SIRT3 enzymatic activity, increased oxidative stresses and may potentially result in tumor permissive phenotypes caused by mitochondrial redox imbalance.

a

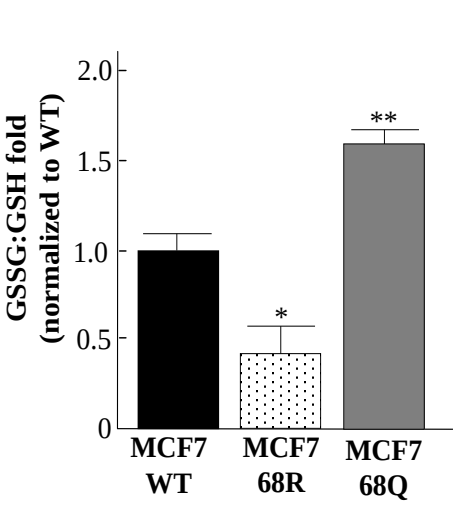
GSSG:GSH fold
(normalized to WT)
2.0
1.5
1.0
0.5
0
*
**
MCF7
WT
MCF7
68R
MCF7
68Q

b

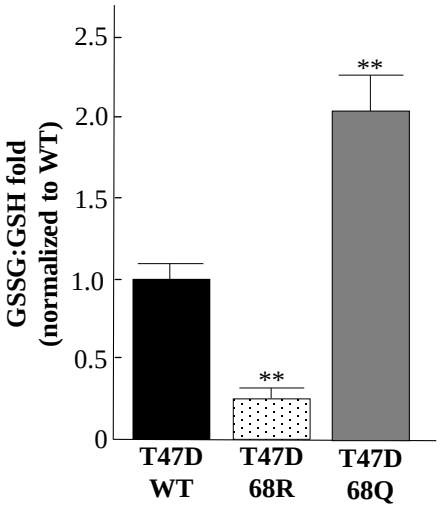
GSSG:GSH fold
(normalized to WT)
2.5
2.0
1.5
1.0
0.5
0
**
**
T47D
WT
T47D
68R
T47D
68Q

Figure 28. MnSOD-K68-Ac leads to increased oxidative stress in human breast cells.

(A) MCF7-MnSOD^{WT}, MCF7-MnSOD^{K68R}, and MCF7-MnSOD^{K68Q} and **(B)** T47D-MnSOD^{WT}, T47D-MnSOD^{K68R} , and T47D-MnSOD^{K68Q} cells were lysed and the levels of total glutathione (GSH) and oxidized glutathione (GSSG) were measured. The ratio of GSSG to GSH was compared between different samples. All experiments were done in triplicate. Errors represent ± 1 SEM. *$p < 0.05$, **$p < 0.01$, and ***$p < 0.001$.

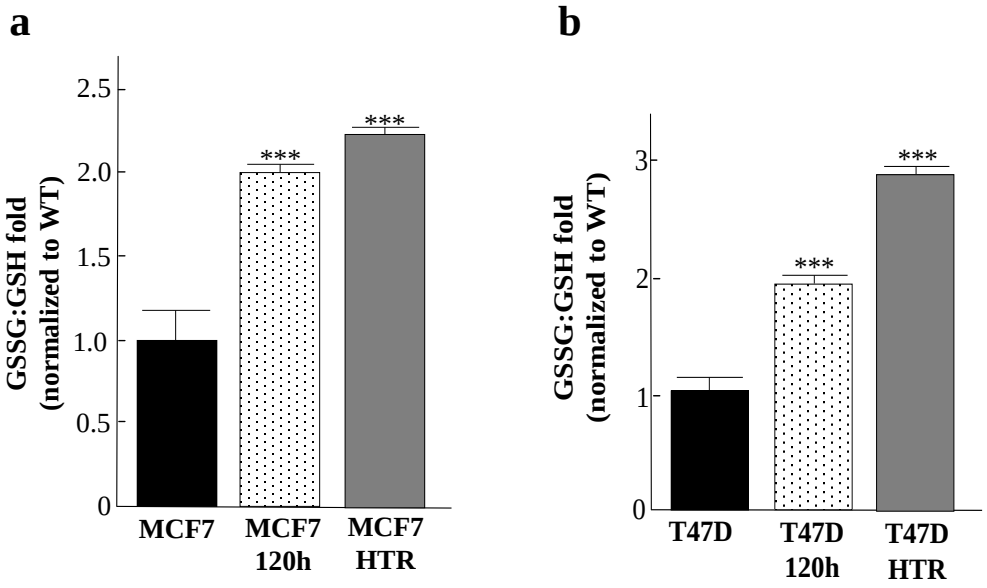
a
GSSG:GSH fold
(normalized to WT)
2.5
2.0
1.5
1.0
0.5
0
***
***
MCF7
MCF7
120h
MCF7
HTR
b
GSSG:GSH fold
(normalized to WT)
3
2
1
0
***
***
T47D
T47D
120h
T47D
HTR

Figure 29. Tamoxifen exposure increases oxidative stress in cancer cells.

(A) MCF7, MCF7 cells selected in Tam for 120 hours, and MCF7-HTR cells and **(B)** T47D, T47D cells selected in Tam for 120 hours, and T47D-HTR cells were harvested and the levels of total glutathione (GSH) and oxidized glutathione (GSSG) were measured. The ratio of GSSG to GSH was compared between different samples. All experiments were done in triplicate. Errors represent ± 1 SEM. *$p < 0.05$, **$p < 0.01$, and ***$p < 0.001$.

Ch 4.3: Acetylation of MnSOD at lysine 68 increased breast cancer malignancy risk

It has been shown that mice lacking *Sirt3* develop mammary tumors with luminal B-like phenotype that are ER^+, poorly differentiated, and display high levels of Ki-67 (Desouki et al., 2014; Kim et al., 2010; Zou et al., 2016). To determine if there is a subgroup of human ER^+ tumors that display a loss of SIRT3-MnSOD-Ac axis signature, we analyzed breast cancer patient tissue array slides consisting of different subtypes of breast malignancies. IHC staining revealed that MnSOD-K68-Ac levels are significantly higher (**Fig. 30**) and SIRT3 protein levels are markedly lower (**Fig. 31**) in the luminal B, as compared to luminal A tumor samples (**Fig. 32**). These results suggest that SIRT3-MnSOD-Ac axis signature may be a useful marker to identify a specific subgroup of women with luminal B breast cancer.

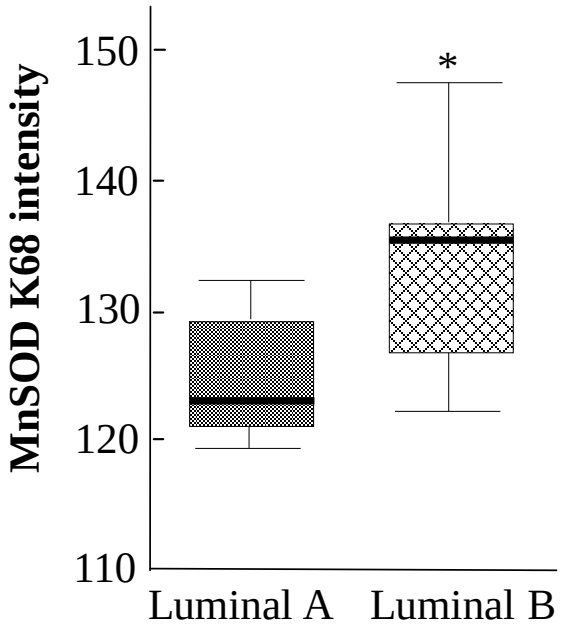
MnSOD K68 intensity
150
140
130
120
110
*
Luminal A
Luminal B

Figure 30. Luminal B breast cancer exhibited a higher MnSOD-K68-Ac staining by IHC.

A breast cancer tissue array, consisted of Luminal A (n=14) and Luminal B (n=39) breast cancer patient samples, were dewaxed and immunostained with anti-MnSOD-K68-Ac. The intensity of staining was quantified using HistoQuest software. The shaded boxes represent the interquartile range; whiskers represent the 10th-90th percentile range; bars represent the median. *$p< 0.05$ compared to Luminal A group.

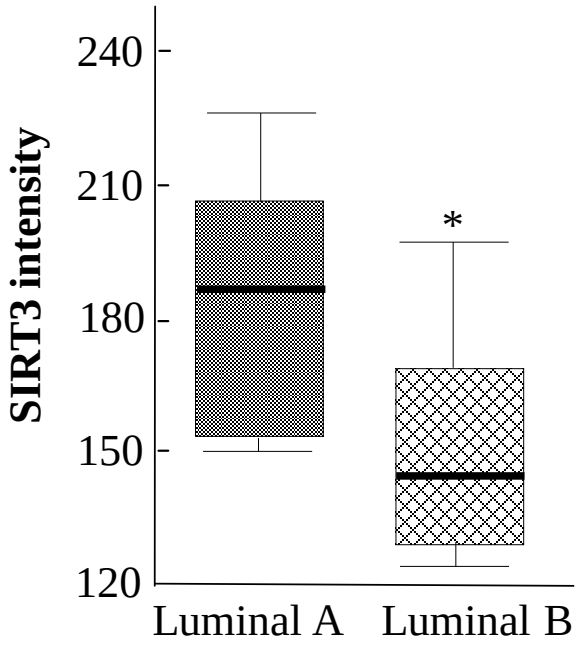
SIRT3 intensity
240
210
180
150
120
*
Luminal A
Luminal B

Figure 31. Luminal B breast cancer exhibited a lower SIRT3 staining by IHC.

A breast cancer tissue array, consisted of Luminal A (n=14) and Luminal B (n=39) breast cancer patient samples, were dewaxed and immunostained with SIRT3. The intensity of staining was quantified using HistoQuest software. The shaded boxes represent the interquartile range; whiskers represent the 10th-90th percentile range; bars represent the median. *$p< 0.05$ compared to Luminal A group.

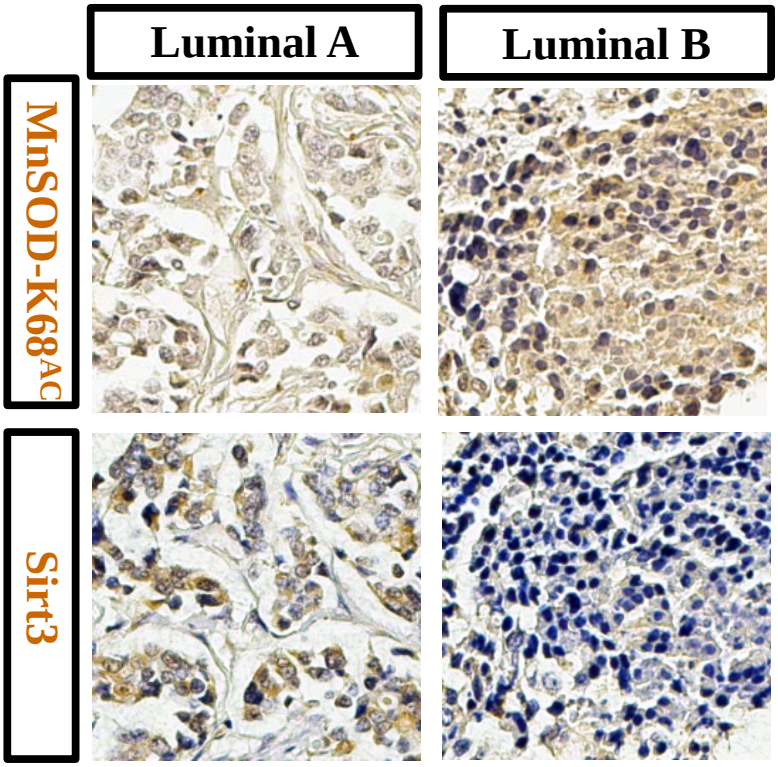
Luminal A
Luminal B
MnSOD-K68AC
Sirt3

Fig. 32 Representative images of Luminal A vs Luminal B breast cancer staining

A representative image of the immunohistochemistry (IHC) slides demonstrating $MnSOD^{K68}$ and SIRT3 staining in Luminal A and Luminal B breast cancer samples. Luminal A breast cancer sample has a higher SIRT3 staining than Luminal B breast cancer sample, whereas Luminal B breast cancer sample has a higher $IDH2^{K413}$ staining than Luminal A breast cancer sample.

Ch 4.4 Acetylation of IDH2 at lysine 413 may be related to MnSOD enzymatic activity

MnSOD consists of four subunits that form a homotetramer, which is stabilized around a manganese ion (~88 kDa), and importantly, K68 is located directly in the MnSOD tetramer interface (Borgstahl et al., 1992; Zhu et al., 2012). Our studies of IDH2 and MnSOD have shown very similar phenotypes, as acetylation of IDH2 at lysine 413 and acetylation of MnSOD at lysine 68, due to loss of SIRT3, can result in very similar tumor permissive phenotypes, i.e. decreased active dimer/tetramer formation, decreased enzymatic activity, increased oxidative stress, and increased breast cancer malignancy risk.

Therefore, we hypothesize that acetylation of IDH2, an enzyme in the TCA cycle that regulates the redox homeostasis in the mitochondria by impacting the overall NADPH and GSH levels in the mitochondria, could potentially affect MnSOD enzymatic activity. We used MCF7-shIDH2-IDH2^{WT}, MCF7-shIDH2-IDH2^{K413R}, and MCF7-shIDH2-IDH2^{K413Q} cells and we measured MnSOD acetylation at lysine 68 and MnSOD tetramerization by western blot. We found a significant increase of MnSOD acetylation at lysine 68 and a decrease of MnSOD tetramerization levels (**Fig. 33**) when IDH2 acetyl mimetic was expressed in MCF7 cells, suggesting that acetylation of IDH2 may affect MnSOD enzymatic activity, and therefore, affect MnSOD tetramerization levels.

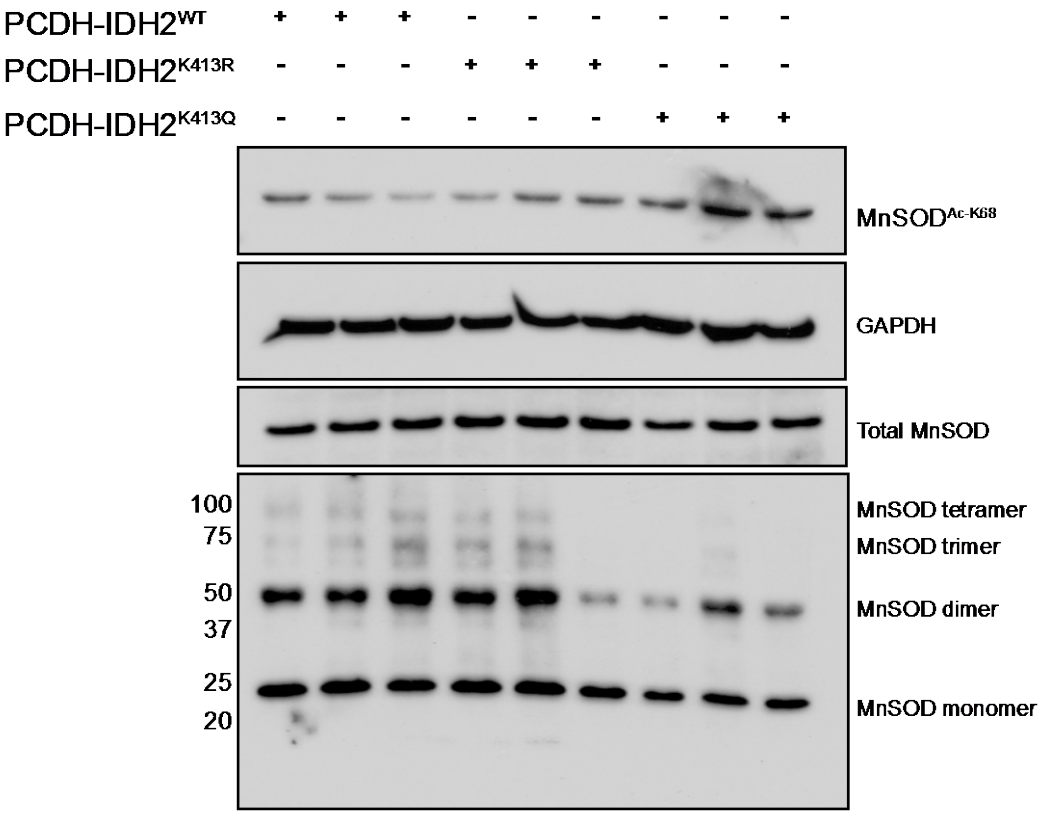
PCDH-IDH2WT + + + - - - - - -
PCDH-IDH2K413R - - - + + + - - -
PCDH-IDH2K413Q - - - - - - + + +
MnSODAc-K68
GAPDH
Total MnSOD
100
75
50
37
25
20
MnSOD tetramer
MnSOD trimer
MnSOD dimer
MnSOD monomer

Figure 33. Acetylation of IDH2 at lysine 413 might affect MnSOD tetramerization

MCF7-shIDH2-IDH2^{WT}, MCF7-shIDH2-IDH2^{K413R}, and MCF7-shIDH2-IDH2^{K413Q} cells were lysed with IP buffer before samples were immunoblotted with MnSOD-Ac-K68, MnSOD, and GAPDH antibodies. For MnSOD tetramerization immunoblotting, samples were lysed with IP buffer and crosslinked with 0.05% glutaraldehyde for 10 min before separated by SDS-PAGE and immunoblotted with MnSOD antibody. Samples were run in triplicates.

Chapter 5: Discussion

Ch 5.1: Conclusion of thesis project

Mammalian SIRT3 is regarded as the primary mitochondrial protein deacetylase that directs the acetylation status of mitochondrial Acetylome. Loss of SIRT3 enzymatic activity results in aberrant hyperacetylation of multiple mitochondrial proteins (Lombard et al., 2007), including ATP synthase F1 (Vassilopoulos et al., 2014), pyruvate dehydrogenase (Ozden et al., 2014), MnSOD (Tao et al., 2010), and IDH2 (Yu et al., 2012), resulting in abnormal mitochondrial homeostasis, aberrantly elevated ROS levels, and metabolic reprogramming in tumor cells that exhibit a preferential use of glucose consumption (Ozden et al., 2014) that is similar to that observed in the Warburg effect (Warburg, 1925, 1956; Warburg et al., 1927). Therefore, SIRT3 has been regarded as a protein that functions to maintain the mitochondrial energy metabolic homeostasis and redox balance in order to protect mammalian cells from damages caused by waste products produced during metabolism and the miss-activation of certain signaling pathways.

In this regard, the alteration of acetylation stoichiometry, due to loss of sirtuin enzymatic activity, ranges from less than 1% to about 98%, suggesting that changes in mitochondrial acetylation status can have significant effects in cellular metabolism and signaling pathways (Baeza et al., 2014). Therefore, it seems likely that the overall dysregulation of mitochondrial metabolism, due to an increase in protein acetylation, contribute to the tumor permissive phenotype observed in cells lacking *SIRT3*. As such, SIRT3 is proposed to be a tumor suppressor protein that connects mitochondrial energy generation, metabolism, and carcinogenesis (Kim et al., 2010; Zhu et al., 2014; Zou et al., 2016).

Loss of SIRT3 enzymatic activity and/or genetic loss of *Sirt3*, on the other hand, can result in different types of aging-related diseases and pathogenesis related to different organs, as sirtuins have been regarded as a longevity protein that functions to increase the life span of *C. elegans*, drosophila, and metazoans (Wood et al., 2004). For example, loss of SIRT3 results in coronary vascular dysfunction and post-myocardial infarction cardiac failure (He et al., 2016). SIRT3 also functions to maintain bone homeostasis, as loss of SIRT3 can lead to osteoclastogenesis (Huh et al., 2016). By deacetylating LCAD, SIRT3 protects liver from lipid accumulation (Chen et al., 2015). SIRT3 and IDH2 also function together to protect mice from hearing loss (Brown et al., 2014; Someya et al., 2010). All these results suggest that SIRT3 has beneficial roles in protecting mammals from a variety of diseases.

More importantly, loss of SIRT3 has been shown to be associated with many different types of cancer, and therefore, SIRT3 has been regarded as a tumor suppressor protein. The first discovery showing SIRT3 as a tumor suppressor protein suggests that loss of *Sirt3* results in luminal B like breast carcinogenesis in *Sirt3*$^{-/-}$ mice (Kim et al., 2010). Decreased SIRT3 expression results in a worse clinical outcome in breast cancer (Desouki et al., 2014). Clinically, loss of *SIRT3* is associated with a worse clinical outcome of head and neck squamous cell carcinoma (Mahjabeen and Kayani, 2016). By repressing iron metabolism and inhibiting iron regulatory protein, SIRT3 inhibits pancreatic cancer cell proliferation (Jeong et al., 2015). In human lung adenocarcinoma, *SIRT3* mRNA expression level was downregulated, and overexpression of *SIRT3* inhibited the growth of lung adenocarcinoma cell lines *in vitro* (Xiao et al., 2013). In addition, loss of *SIRT3* results in B cell malignancy, which is associated with a

phenotype of increased ROS production caused by the acetylation of IDH2 and MnSOD (Yu et al., 2016a). Therefore, studying dysregulated acetylation of mitochondrial proteins, due to loss of SIRT3 enzymatic activity, and the deleterious effects caused by hyperacetylation of these SIRT3 deacetylation target proteins in the mitochondria, has become the focus of my thesis research.

The $NADP^+$-dependent, dimeric form of IDH2 oxidizes isocitrate into α-ketoglutarate and is a key enzyme in the Krebs Cycle. It has been shown that inhibiting IDH2 enzymatic activity by acetylation or knocking it down negatively affects mitochondrial redox balance (Yu et al., 2012). One potential mechanism is that acetylation of IDH2 affects the $NADP^+$ binding site and therefore significantly increased the V_m for isocitrate binding and decreased the V_{max} for the production of α-ketoglutarate and NADPH. Decreased production of NADPH results in a decreased regeneration of total glutathione, and therefore, cells are under oxidative stress due to elevated GSSG:GSH ratio and increased mitochondrial ROS.

It has been shown that increased ROS levels and decreased total glutathione can provide growth advantage for different types of cancer. For example, increased ROS levels in breast cancer cells, due to loss of SIRT3 enzymatic activity, can activate HIF1α pathway and upregulate HIF-activated gene expression, for example, *GLUT1* and *LDHA*, both of which are involved in glycolysis and Warburg effects (Finley et al., 2011). In addition, increased MnSOD acetylation at lysine 122, due to loss of SIRT3 enzymatic activity, increased mitochondrial ROS levels and resulted in genetic instability (Tao et al., 2010). Furthermore, the acetyl-$MnSOD^{K122}$ mimetic functions similarly as an oncogene, as it has the ability to transform *Sirt3*$^{-/-}$ MEFs *in vitro*. Recently, it has been shown that B cell malignancy caused by loss of SIRT3 enzymatic

activity has an increased IDH2 acetylation at lysine 413 and MnSOD acetylation at lysine 68 and 122 (Yu et al., 2016a). All these discoveries suggest that increased ROS production caused by acetylation of mitochondrial proteins, due to loss of SIRT3 enzymatic activity, poses risks for carcinogenesis.

In my thesis research, we suggest an additional mechanism linking IDH2 acetylation at K413, due to loss of SIRT3 activity, a protein regarded as a mitochondrial tumor suppressor, to this enzymatic function by altering its homodimeric protein-protein interaction. Previously, it has been shown that binding of $NADP^+$ is negatively affected when IDH2 is acetylated at lysine 413 or IDH2 is expressed as an acetyl mimetic (K413Q) (Yu et al., 2012). The formation of IDH2 dimer depends on the conformational change of the catalytic site, where one monomeric IDH2 binds to $NADP^+$ and isocitrate and forms a dimer with the other monomeric IDH2. Therefore, it is reasonable to propose that when IDH2 is acetylated at lysine 413, due to a decreased ability to bind to NADP+, its ability to form an active, homodimeric complex, also decreases, and therefore, IDH2 enzymatic activity decreases as well. To mimic the acetylation/deacetylation status of IDH2, we created $IDH2^{K413R}$ as the deacetyl mimetic and $IDH2^{K413Q}$ as the acetyl mimetic.

Based on what we have observed in this project and in other unpublished projects, we found that when we measure parameters like ROS production and glycolytic capacity, the difference between wild-type and de-acetyl mimetic (the R form) of different mitochondrial SIRT3 deacetylation target proteins was not always significant. In contrast, it seems that the acetyl mimetic (the Q form) of SIRT3 downstream targets tend to decrease activity. In this

regard, we speculate that de-acetylated IDH2 is already present in significant amounts within cells of our model systems and hence, depending on the cell type, adding additional IDH2 de-acetyl mimetic (the R form) will not always significantly alter either the phenotype or biochemical biology. However, the overexpression of *IDH2*^{K413R} in aerobically glycolytic (Warburg) cancer cells has the ability to alter the aberrant metabolic biochemical phenotype. Therefore, while no perfect system substituting the actual acetylation exists, using R and Q as lysine mimetics have been considered as an appropriate substitution in the field of sirtuin research.

Currently, several new metabolic properties related to IDHs have been discovered. First, mutations of IDH1 and IDH2 caused neomorphic enzymatic activity, resulting in the production of an onco-metabolite named 2-hydroxyglutarate (2HG) (Ward et al., 2010). It has also been shown that 2HG can impair histone demethylation and switch cell differentiation pathways (Lu et al., 2012). In addition, a reversible reduction of α-KG to isocitrate has also been discovered under hypoxic conditions with wild-type IDH1 and IDH2, and an elevation of 2HG levels was also detected in this process (Wise et al., 2011). While the specific role of IDH2 acetylation at lysine 413 and the relationship between IDH2 acetylation and 2HG production remains unknown, it does shed light to a possible future direction whether acetyl-IDH2 provides functions of IDH2 by either reversing the TCA cycle or producing 2HG through a neomorphic enzymatic activity.

The NAD^+-dependent IDH3 has long been regarded as the main enzyme for the conversion from isocitrate to α-KG (Schiaffino et al., 2015). However, simultaneous loss of IDH2 and IDH3 inhibits ATP formation in pancreatic β-cells, suggesting that $NADP^+$-dependent

IDH2 is also involved in mitochondrial metabolism (MacDonald et al., 2013). In addition, knocking down *IDH2* results in a 25% decrease of NADPH levels in cells, suggesting that IDH2 plays a significant role in mitochondrial NADPH production (Yu et al., 2012). Furthermore, the main function of IDH2 includes producing NADPH in the mitochondria, regenerating reduced glutathione and defending against elevated ROS levels, suggesting its potential role as an anti-oxidant enzyme by protecting cells against oxidative damage.

Previous discoveries have shown that loss of SIRT3 activity increases ROS and HIF levels, as well as up regulating several oncogenic pathways (Haigis et al., 2012). It has also been shown that expression of active IDH2 and SIRT3 prevents hearing loss in mice by production of NADPH. This regenerates reduced glutathione, decreases GSSG:GSH ratio and inhibits ROS production. Furthermore, both IDH2 and SIRT3 have potential effects in protecting against acute hemorrhagic leukoencephalitis (AHL), suggesting the beneficial roles of IDH2 and SIRT3 in providing a redox homeostasis environment for cells (Someya et al., 2010). Therefore, it is reasonable to believe that acetylation of IDH2 at K413, due to loss of SIRT3 enzymatic activity, poses risks that lead to pro-oncogenic properties in cells.

Our data suggests that MCF7 cells expressing $IDH2^{K413Q}$ exhibited altered metabolism and elevated oxidative stress. These cells exhibit a similar shift to glycolysis and a decreased oxidative phosphorylation, known as the Warburg effect. Furthermore, these cells showed a decreased total glutathione level and an increased mitochondrial ROS levels, suggesting that expressing IDH2 acetyl mimetic increased oxidative stress. On the other hand, adding mitoTEMPO, a chemical that inhibits ROS production, partially reversed tumor growth in low

density, suggesting that inhibition of ROS can be a therapeutic strategy for specific cancers with redox imbalance and oxidative stresses.

More importantly, the expression of IDH2 acetyl mimetic results in tumor permissive phenotypes *in vitro* and *in vivo*. Expression of IDH2 acetyl mimetic results in an increase of tumor cell proliferation when grown in low density, and together with oncogenic *Kras* or c-*Myc*, it transforms immortalized NIH3T3 cells in soft agar. On the other hand, expression of IDH2 deacetyl mimetic not only reverse tumor cell proliferation in MCF7-sh*SIRT3* cells and *Sirt3* knockout MMTs but also reverses the transformation permissive phenotypes observed in NIH3T3 cells transfected with oncogenic *Kras* or *c-Myc*. When these cells were injected into nude mice, the subsequent tumors also exhibited similar dysregulated biochemical properties (increased oxidative stress) (Kim et al., 2010). In addition, our previous discovery in *Sirt3* knock-out mammary tumors and our observations in human Luminal A and Luminal B breast cancer patient samples have provided a correlative explanation between IDH2 acetylation, SIRT3 expression and breast cancer malignancy risk (Desouki et al., 2014). Furthermore, studies by the Denu group have also discovered that decreased *SIRT3* mRNA levels, decreased SIRT3 enzymatic activity, and hyper-acetylation of SIRT3 target proteins (IDH2 and MnSOD) can result in B cell malignancies due to increased ROS levels, suggesting that acetylation of IDH2 can promote malignancy risks in different types of cancers (Yu et al., 2016a).

The metabolic switch caused by IDH2 acetylation/deacetylation is another interesting observation in our study. The Warburg effect, also known as the preferential aerobic glycolysis in cancer cells, has been regarded as one significant metabolic property of cancer cells. Earlier,

different studies have found that loss of SIRT3 results in a metabolic switch in cancer cells, as they have an increased glycolysis and glucose uptake (Finley et al., 2011; Kim et al., 2010; Ozden et al., 2014). The metabolic switch can at least be partially explained by the acetylation of different mitochondrial proteins that are SIRT3 deacetylation targets, for example, pyruvate dehydrogenase (PDH), the first enzyme of the TCA cycle that links glycolysis to oxidative phosphorylation. Specifically, deacetyl mimitic of PDH at lysine 321 (PDH^{K321R}) increased PDH enzymatic activity, increased oxygen consumption rate, and decreased lactate production, glucose uptake and glycolysis, suggesting that active TCA cycle enzymes are responsible for a complete utilization of glucose to generate ATP efficiently (Ozden et al., 2014). Chemical inhibition of pyruvate dehydrogenase kinase (PDK), an enzyme that phosphorylates and inactivates PDH, using dichloroacetate (DCA), can partially reverse tumor proliferation *in vitro* (Ozden et al., 2014; Ruggieri et al., 2015). All these data have provided evidence that inhibiting aerobic glycolysis and activating oxidative phosphorylation can inhibit tumor growth and therefore can be a potential therapeutic strategy for certain types of cancer.

Interestingly, we have observed a very similar phenotype in our cells, as expressing $IDH2^{K413Q}$, the acetyl mimetic of IDH2, decreased oxidative phosphorylation and increased glycolysis *in vitro*. Adding dimethyl-α-ketoglutarate (DKG), a metabolite that mimics an increase of IDH2 activity, not only increased maximal respiration capacity in MCF7 cells expressing $IDH2^{K413Q}$, but also partially reversed the tumor cell proliferation when grown in low density. On the other hand, adding isocitrate, a metabolite that mimics a decrease of IDH2 activity, increased glycolysis and tumor cell proliferation in low density. All these data suggest that IDH2 activity switch not only affects mitochondrial metabolism, but also provides at least a

partial explanation of tumor permissive phenotypes *in vitro*, linking metabolism to tumor cell growth and proliferation.

Overall, our data has also provided an additional mechanistic explanation of how IHD2-K413-Ac negatively alters its enzymatic activity and promotes transformation-permissive phenotypes *in vitro* and *in vivo*. Therefore, it seems reasonable to propose that activators of SIRT3 and/or inhibition of mitochondrial ROS production may be used to protect cells from mitochondrial redox imbalance and transformation (Pillai et al., 2015; Zou et al., 2016).

Ch 5.2: Future directions

While our study has provided enough details regarding to the acetylation of IDH2 at lysine 413, due to loss of SIRT3 enzymatic activity, there are several questions that remain unanswered. First of all, how does chemical activation of SIRT3 affect IDH2 acetylation and whether chemical activation of SIRT3 can partially reverse tumor permissive phenotypes *in vitro* and *in vivo*. Answering these questions will provide a scientific explanation for a potential therapeutic use of SIRT3 activators in a subgroup of breast cancer patients with *SIRT3* genetic deletion and/or low SIRT3 enzymatic activity. Secondly, how does direct chemical inhibition of ROS caused by hyperacetylation of IDH2reverse tumor permissive phenotypes *in vitro* and *in vivo*. Specifically, because both enzymes are SIRT3 deacetylation target proteins in the mitochondria that function to fight against oxidative stress in the cells and provide a redox homeostasis, it is reasonable to propose that there are potential interactions between IDH2 and MnSOD and altering the activity of one enzyme may affect the activity of the other enzyme.

There are several candidates that function to either active SIRT3 or inhibit mitochondrial ROS production. One candidate is named honokiol, which functions as a SIRT3 activator. One study has shown that honokiol reverses cardiac hypertrophy in mice through activation of SIRT3 (Pillai et al., 2015). Treatment of honokiol results in decreased pan-acetylation levels of mitochondrial lysates, decreased ROS levels and inhibition of cardiac hypertrophy in *Sirt3* wild-type mice. Interestingly, honokiol failed to block cardiac hypertrophy in *Sirt3* knock-out mice, suggesting its potential role as a SIRT3 activator. In addition, there are several studies pointing out the potential role of honokiol as an anti-cancer reagent. For example, a combination therapy using paclitaxel (PTX) and honokiol (HK) has been shown to be a potential strategy for breast

cancer therapy, as the combination of PTX and HK inhibits tumor cell growth *in vitro* and *in vivo* (Wang et al., 2017). In this regard, another combination therapy using honokiol has been shown to decrease triple negative MDA-MB-231 cellular growth *in vivo* when injected into nude mice (Godugu et al., 2017). Furthermore, honokiol has been shown to inhibit DNA polymerase in multiple types of human-derived cancer cells, resulting in increased sensitivity to bleomycin, suggesting another potential role of honokiol in combination therapy of cancer (Gowda et al., 2017). Despite all these numerous publications related to honokiol and anti-cancer combination therapy, there is no publication suggesting the mechanism how sirtuins, specifically SIRT3, is involved in honokiol-induced anti-cancer therapy. It would be very interesting to see whether honokiol treatment results in a decrease of tumor cell proliferation when grown in low density, whether honokiol could decrease mitochondrial protein acetylation, specifically IDH2 and MnSOD, as both are considered as anti-oxidant proteins that protect cells from oxidative damages, and whether honokiol could partially reverse tumor permissive phenotypes in nude mice when injected with mammalian tumor cells with genetic deletion of *SIRT3*.

Another candidate of sirtuin activator is resveratrol. There are several publications showing that that resveratrol can activate sirtuins, including SIRT1 and SIRT3 (Deus et al., 2017; Fu et al., 2017; Mathieu et al., 2016; Xu et al., 2016). While no direct evidence of resveratrol has been linked to anti-cancer effects, the majority of the publications have suggested that resveratrol functions to decrease oxidative stress, ameliorate injury of kidney cells, and improve cardiac function (Mathieu et al., 2016; Xu et al., 2016), suggesting that resveratrol can be used as another chemical to maintain redox balance in the mitochondria by activating sirtuin enzymatic activity. Specifically, resveratrol functions to activate SIRT3 and increase the expression levels

of FOXO3, PGC-1α, and SOD2 (Fu et al., 2017). It has also been shown that exercise and/or caloric starvation results in phosphorylation of AMPK, which results in activation of SIRT3, and this in turn activates PGC-1α (Palacios et al., 2009). It is proposed that loss of PGC-1α can result in aging-related diseases, for example, telomere dysfunction and Parkinson's disease (Austin and St-Pierre, 2012). Therefore, while no direct evidence suggesting the resveratrol-SIRT3-antitumor effect exists, it is safe to assume that one function of resveratrol is to provide an activation signal for sirtuins to activate PGC-1α, which functions as a transcription factor that serves as an anti-aging reagent by decreasing oxidative stress and potentially providing a mitochondrial redox homeostasis (Austin and St-Pierre, 2012).

One particular ROS scavenger has become the focus of future research in our laboratory, namely GC4419. There is only one publication regarding the role of GC4419, a pharmacological mimetic of MnSOD, suggesting that adding GC4419 to HEK-293T cells with MnSOD CRSIPR knock-out reverses the aberrant redox state (Cramer-Morales et al., 2015). Since the main function of GC4419 is to mimic MnSOD function by removing superoxide molecules, its potential role as an anti-cancer therapeutic drug is being investigated. Currently, there are several clinical trials investigating the role of GC4419 in combination with chemo-radiation in head/neck cancer patients, and it seems that cancer patients treated with GC4419 have a positive response to radiation therapy. The side effects of GC4419 include oral mucositis in patients with oral cavities (Anderson et al.). With these ongoing studies related to GC4419, mitochondrial metabolism, and anti-cancer therapy, it seems reasonable to regard GC4419 as a potential candidate for *in vivo* studies in order to elucidate the mechanism between GC4419, ROS scavenging, SIRT3 activation, and anti-cancer therapy.

Our laboratory has provided the first piece of evidence linking SIRT3 and MnSOD acetylation with carcinogenesis and suggested that acetylated MnSOD could potentially function similarly as an oncogene, as expression of acetyl mimetic of MnSOD at lysine 122 ($MnSOD^{K122Q}$) can transform *Sirt3*$^{-/-}$ MEFs, whereas expression of deacetyl mimetic of MnSOD at lysine 122 ($MnSOD^{K122R}$) cannot transform *Sirt3*$^{-/-}$ MEFs (Kim et al., 2010; Tao et al., 2010). In my thesis research, we showed that co-expression of acetyl mimetic of IDH2 at lysine 413 ($IDH2^{K413Q}$), with either *c-Myc* or *Kras*^{G12D}, successfully transformed NIH3T3 cells, whereas co-expression of deacetyl mimetic of IDH2 at lysine 413 ($IDH2^{K413R}$), with either *c-Myc* or *Kras*^{G12D}, could reverse the transformation permissive phenotypes. Together with the study of IDH2 acetylation, MnSOD acetylation and PDH acetylation, it is reasonable to propose that SIRT3 deacetylation target proteins share a similar function, as acetyl mimetics can either result in *in vitro* transformation or result in tumor permissive phenotypes.

MnSOD and IDH2 are both SIRT3 deacetylation target proteins that share very similar functions to provide mitochondrial redox homeostasis. Our analysis of tamoxifen resistance cancer cells, a group of cells with a loss of SIRT3 signature, exhibited increased MnSOD and IDH2 acetylation. This observation is very similar to our discovery that genetic deletion of *Sirt3* in mice resulted in receptor positive breast cancer that resembles human Luminal B breast cancer (Kim et al., 2010). In addition, acetylation of MnSOD at lysine 68 and acetylation of IDH2 at lysine 413 both decreased total glutathione levels in cancer cells, increasing the oxidative stress and may promote tumor permissive phenotypes. In addition, both proteins are more acetylated in Luminal B breast cancer staining compared to Luminal A samples. Furthermore, acetylation of

IDH2 affects MnSOD acetylation at lysine 68 and decreased MnSOD tetramerization. Therefore, we expect that the activity of one enzyme would affect the other enzyme as well, and therefore treatment of GC4419 for tumors lacking SIRT3, IDH2 or MnSOD enzymatic activity will possibly reverse tumor growth *in vivo*. Furthermore, if treatment of GC4419 inhibits tumor growth *in vivo*, it would be very useful to study the biochemistry of tumors treated with or without GC4419 by measuring the levels of total glutathione and/or mitochondrial superoxide levels to elucidate the mechanism how GC4419 can inhibit tumor growth.

It has already been shown that knocking down *IDH2* significantly decreased *MnSOD* expression levels, whereas treatment of Mito-TEMPO could increase *MnSOD* expression caused by *IDH2* knockdown. Therefore, it would be interesting to see whether expression of IDH2 deacetyl/acetyl mimetic ($IDH2^{K413R/Q}$) could result in MnSOD acetylation change at lysine 68 and 122. More importantly, whether expression of $IDH2^{K413R/Q}$ would affect SIRT3 enzymatic activity and expression levels would also be an interesting direction to pursue, as no direct evidence suggesting how SIRT3 expression is regulated exists up until now. Successfully answering this question by elucidating the relationship between SIRT3 deacetylation targets and SIRT3 can provide a novel aspect whether the feedback loop exists between sirtuins and their mitochondrial deacetylation targets.

Another potential ROS scavenger that has been intensively used is Mito-TEMPO. While my study has provided some evidence suggesting that Mito-TEMPO inhibits tumor cell growth *in vitro*, it would be interesting to examine whether inhibition of ROS would affect IDH2 acetylation and mitochondrial metabolism. It has been shown that Mito-TEMPO would increase

MnSOD expression levels. Therefore, removing ROS molecules (Park et al., 2016a) and increasing MnSOD enzymatic activity would potentially increase IDH2 activity and NADPH levels. Specifically, we can express MnSOD deacetyl/acetyl mimetic (*MnSOD*$^{K68R/Q}$ and *MnSOD*$^{K122R/Q}$) and study how acetylation status change of MnSOD potentially affects IDH2 acetylation. Successfully answering these questions will allow us to further understand how different mitochondrial anti-oxidant proteins regulate and interact with each other in order to provide a redox balanced environment for cells to fight against oxidative stress. These studies will also shed light for future cancer research.

Anderson, C.M., Allen, B.G., Sun, W., Lee, C.M., Agarwala, S., Venigalla, M., Greenberg, L., Adkins, D., Chen, Y., Zhen, W., *et al.* Phase 1b/2a Trial of Superoxide (SO) Dismutase (SOD) Mimetic GC4419 to Reduce Chemoradiation Therapy–Induced Oral Mucositis (OM) in Patients With Oral Cavity or Oropharyngeal Carcinoma (OCC). International Journal of Radiation Oncology • Biology • Physics *94*, 869-870.

Austin, S., and St-Pierre, J. (2012). PGC1alpha and mitochondrial metabolism--emerging concepts and relevance in ageing and neurodegenerative disorders. J Cell Sci *125*, 4963-4971.

Baeza, J., Dowell, J.A., Smallegan, M.J., Fan, J., Amador-Noguez, D., Khan, Z., and Denu, J.M. (2014). Stoichiometry of site-specific lysine acetylation in an entire proteome. J Biol Chem *289*, 21326-21338.

Brown, K.D., Maqsood, S., Huang, J.Y., Pan, Y., Harkcom, W., Li, W., Sauve, A., Verdin, E., and Jaffrey, S.R. (2014). Activation of SIRT3 by the NAD(+) precursor nicotinamide riboside protects from noise-induced hearing loss. Cell metabolism *20*, 1059-1068.

Chen, T., Liu, J., Li, N., Wang, S., Liu, H., Li, J., Zhang, Y., and Bu, P. (2015). Mouse SIRT3 attenuates hypertrophy-related lipid accumulation in the heart through the deacetylation of LCAD. PLoS One *10*, e0118909.

Cramer-Morales, K., Heer, C.D., Mapuskar, K.A., and Domann, F.E. (2015). SOD2 targeted gene editing by CRISPR/Cas9 yields Human cells devoid of MnSOD. Free Radic Biol Med *89*, 379-386.

Desouki, M.M., Doubinskaia, I., Gius, D., and Abdulkadir, S.A. (2014). Decreased mitochondrial SIRT3 expression is a potential molecular biomarker associated with poor outcome in breast cancer. Human pathology *45*, 1071-1077.

Deus, C.M., Serafim, T.L., Magalhaes-Novais, S., Vilaca, A., Moreira, A.C., Sardao, V.A., Cardoso, S.M., and Oliveira, P.J. (2017). Sirtuin 1-dependent resveratrol cytotoxicity and pro-differentiation activity on breast cancer cells. Arch Toxicol *91*, 1261-1278.

Finley, L.W., Carracedo, A., Lee, J., Souza, A., Egia, A., Zhang, J., Teruya-Feldstein, J., Moreira, P.I., Cardoso, S.M., Clish, C.B., *et al.* (2011). SIRT3 opposes reprogramming of cancer cell metabolism through HIF1alpha destabilization. Cancer cell *19*, 416-428.

Fu, B., Zhao, J., Peng, W., Wu, H., and Zhang, Y. (2017). Resveratrol rescues cadmium-induced mitochondrial injury by enhancing transcriptional regulation of PGC-1alpha and SOD2 via the Sirt3/FoxO3a pathway in TCMK-1 cells. Biochem Biophys Res Commun.

Godugu, C., Doddapaneni, R., and Singh, M. (2017). Honokiol nanomicellar formulation produced increased oral bioavailability and anticancer effects in triple negative breast cancer (TNBC). Colloids Surf B Biointerfaces *153*, 208-219.

Gowda, A.S., Suo, Z., and Spratt, T.E. (2017). Honokiol Inhibits DNA Polymerases beta and lambda and Increases Bleomycin Sensitivity of Human Cancer Cells. Chem Res Toxicol *30*, 715-725.

Haigis, M.C., Deng, C.X., Finley, L.W., Kim, H.S., and Gius, D. (2012). SIRT3 is a mitochondrial tumor suppressor: a scientific tale that connects aberrant cellular ROS, the Warburg effect, and carcinogenesis. Cancer Res *72*, 2468-2472.

He, X., Zeng, H., and Chen, J.X. (2016). Ablation of SIRT3 causes coronary microvascular dysfunction and impairs cardiac recovery post myocardial ischemia. Int J Cardiol *215*, 349-357.

Huh, J.E., Shin, J.H., Jang, E.S., Park, S.J., Park, D.R., Ko, R., Seo, D.H., Kim, H.S., Lee, S.H., Choi, Y., *et al.* (2016). Sirtuin 3 (SIRT3) maintains bone homeostasis by regulating AMPK-PGC-1beta axis in mice. Sci Rep *6*, 22511.

Jeong, S.M., Lee, J., Finley, L.W., Schmidt, P.J., Fleming, M.D., and Haigis, M.C. (2015). SIRT3 regulates cellular iron metabolism and cancer growth by repressing iron regulatory protein 1. Oncogene *34*, 2115-2124.
Kim, H.S., Patel, K., Muldoon-Jacobs, K., Bisht, K.S., Aykin-Burns, N., Pennington, J.D., van der Meer, R., Nguyen, P., Savage, J., Owens, K.M., *et al.* (2010). SIRT3 is a mitochondria-localized tumor suppressor required for maintenance of mitochondrial integrity and metabolism during stress. Cancer Cell *17*, 41-52.
Lombard, D.B., Alt, F.W., Cheng, H.L., Bunkenborg, J., Streeper, R.S., Mostoslavsky, R., Kim, J., Yancopoulos, G., Valenzuela, D., Murphy, A., *et al.* (2007). Mammalian Sir2 homolog SIRT3 regulates global mitochondrial lysine acetylation. Molecular and cellular biology *27*, 8807-8814.
Lu, C., Ward, P.S., Kapoor, G.S., Rohle, D., Turcan, S., Abdel-Wahab, O., Edwards, C.R., Khanin, R., Figueroa, M.E., Melnick, A., *et al.* (2012). IDH mutation impairs histone demethylation and results in a block to cell differentiation. Nature *483*, 474-478.
MacDonald, M.J., Brown, L.J., Longacre, M.J., Stoker, S.W., Kendrick, M.A., and Hasan, N.M. (2013). Knockdown of both mitochondrial isocitrate dehydrogenase enzymes in pancreatic beta cells inhibits insulin secretion. Biochim Biophys Acta *1830*, 5104-5111.
Mahjabeen, I., and Kayani, M.A. (2016). Loss of Mitochondrial Tumor Suppressor Genes Expression Is Associated with Unfavorable Clinical Outcome in Head and Neck Squamous Cell Carcinoma: Data from Retrospective Study. PLoS One *11*, e0146948.
Mathieu, L., Costa, A.L., Le Bachelier, C., Slama, A., Lebre, A.S., Taylor, R.W., Bastin, J., and Djouadi, F. (2016). Resveratrol attenuates oxidative stress in mitochondrial Complex I deficiency: Involvement of SIRT3. Free Radic Biol Med *96*, 190-198.
Ozden, O., Park, S.H., Wagner, B.A., Yong Song, H., Zhu, Y., Vassilopoulos, A., Jung, B., Buettner, G.R., and Gius, D. (2014). SIRT3 deacetylates and increases pyruvate dehydrogenase activity in cancer cells. Free Radic Biol Med *76*, 163-172.
Palacios, O.M., Carmona, J.J., Michan, S., Chen, K.Y., Manabe, Y., Ward, J.L., 3rd, Goodyear, L.J., and Tong, Q. (2009). Diet and exercise signals regulate SIRT3 and activate AMPK and PGC-1alpha in skeletal muscle. Aging (Albany NY) *1*, 771-783.
Park, J.B., Nagar, H., Choi, S., Jung, S.B., Kim, H.W., Kang, S.K., Lee, J.W., Lee, J.H., Park, J.W., Irani, K., *et al.* (2016). IDH2 deficiency impairs mitochondrial function in endothelial cells and endothelium-dependent vasomotor function. Free Radic Biol Med *94*, 36-46.
Pillai, V.B., Samant, S., Sundaresan, N.R., Raghuraman, H., Kim, G., Bonner, M.Y., Arbiser, J.L., Walker, D.I., Jones, D.P., Gius, D., *et al.* (2015). Honokiol blocks and reverses cardiac hypertrophy in mice by activating mitochondrial Sirt3. Nat Commun *6*, 6656.
Ruggieri, V., Agriesti, F., Scrima, R., Laurenzana, I., Perrone, D., Tataranni, T., Mazzoccoli, C., Lo Muzio, L., Capitanio, N., and Piccoli, C. (2015). Dichloroacetate, a selective mitochondria-targeting drug for oral squamous cell carcinoma: a metabolic perspective of treatment. Oncotarget *6*, 1217-1230.
Schiaffino, S., Reggiani, C., Kostrominova, T.Y., Mann, M., and Murgia, M. (2015). Mitochondrial specialization revealed by single muscle fiber proteomics: focus on the Krebs cycle. Scand J Med Sci Sports *25 Suppl 4*, 41-48.
Someya, S., Yu, W., Hallows, W.C., Xu, J., Vann, J.M., Leeuwenburgh, C., Tanokura, M., Denu, J.M., and Prolla, T.A. (2010). Sirt3 mediates reduction of oxidative damage and prevention of age-related hearing loss under caloric restriction. Cell *143*, 802-812.
Tao, R., Coleman, M.C., Pennington, J.D., Ozden, O., Park, S.H., Jiang, H., Kim, H.S., Flynn, C.R., Hill, S., Hayes McDonald, W., *et al.* (2010). Sirt3-mediated deacetylation of evolutionarily

conserved lysine 122 regulates MnSOD activity in response to stress. Molecular cell *40*, 893-904.
Vassilopoulos, A., Pennington, J.D., Andresson, T., Rees, D.M., Bosley, A.D., Fearnley, I.M., Ham, A., Flynn, C.R., Hill, S., Rose, K.L., *et al.* (2014). SIRT3 deacetylates ATP synthase F1 complex proteins in response to nutrient- and exercise-induced stress. Antioxid Redox Signal *21*, 551-564.
Wang, N., Wang, Z., Nie, S., Song, L., He, T., Yang, S., Yang, X., Yi, C., Wu, Q., and Gong, C. (2017). Biodegradable polymeric micelles coencapsulating paclitaxel and honokiol: a strategy for breast cancer therapy in vitro and in vivo. Int J Nanomedicine *12*, 1499-1514.
Warburg, O. (1925). Iron, the Oxygen-Carrier of Respiration-Ferment. Science *61*, 575-582.
Warburg, O. (1956). On the origin of cancer cells. Science *123*, 309-314.
Warburg, O., Wind, F., and Negelein, E. (1927). The Metabolism of Tumors in the Body. The Journal of general physiology *8*, 519-530.
Ward, P.S., Patel, J., Wise, D.R., Abdel-Wahab, O., Bennett, B.D., Coller, H.A., Cross, J.R., Fantin, V.R., Hedvat, C.V., Perl, A.E., *et al.* (2010). The common feature of leukemia-associated IDH1 and IDH2 mutations is a neomorphic enzyme activity converting alpha-ketoglutarate to 2-hydroxyglutarate. Cancer Cell *17*, 225-234.
Wise, D.R., Ward, P.S., Shay, J.E., Cross, J.R., Gruber, J.J., Sachdeva, U.M., Platt, J.M., DeMatteo, R.G., Simon, M.C., and Thompson, C.B. (2011). Hypoxia promotes isocitrate dehydrogenase-dependent carboxylation of alpha-ketoglutarate to citrate to support cell growth and viability. Proc Natl Acad Sci U S A *108*, 19611-19616.
Wood, J.G., Rogina, B., Lavu, S., Howitz, K., Helfand, S.L., Tatar, M., and Sinclair, D. (2004). Sirtuin activators mimic caloric restriction and delay ageing in metazoans. Nature *430*, 686-689.
Xiao, K., Jiang, J., Wang, W., Cao, S., Zhu, L., Zeng, H., Ouyang, R., Zhou, R., and Chen, P. (2013). Sirt3 is a tumor suppressor in lung adenocarcinoma cells. Oncol Rep *30*, 1323-1328.
Xu, S., Gao, Y., Zhang, Q., Wei, S., Chen, Z., Dai, X., Zeng, Z., and Zhao, K.S. (2016). SIRT1/3 Activation by Resveratrol Attenuates Acute Kidney Injury in a Septic Rat Model. Oxid Med Cell Longev *2016*, 7296092.
Yu, W., Denu, R.A., Krautkramer, K.A., Grindle, K.M., Yang, D.T., Asimakopoulos, F., Hematti, P., and Denu, J.M. (2016). Loss of SIRT3 Provides Growth Advantage for B Cell Malignancies. J Biol Chem *291*, 3268-3279.
Yu, W., Dittenhafer-Reed, K.E., and Denu, J.M. (2012). SIRT3 protein deacetylates isocitrate dehydrogenase 2 (IDH2) and regulates mitochondrial redox status. J Biol Chem *287*, 14078-14086.
Zhu, Y., Yan, Y., Principe, D.R., Zou, X., Vassilopoulos, A., and Gius, D. (2014). SIRT3 and SIRT4 are mitochondrial tumor suppressor proteins that connect mitochondrial metabolism and carcinogenesis. Cancer Metab *2*, 15.
Zou, X., Santa-Maria, C.A., O'Brien, J., Gius, D., and Zhu, Y. (2016). Manganese Superoxide Dismutase Acetylation and Dysregulation, Due to Loss of SIRT3 Activity, Promote a Luminal B-Like Breast Carcinogenic-Permissive Phenotype. Antioxid Redox Signal.

References:

Ahn, B.H., Kim, H.S., Song, S., Lee, I.H., Liu, J., Vassilopoulos, A., Deng, C.X., and Finkel, T. (2008). A role for the mitochondrial deacetylase Sirt3 in regulating energy homeostasis. Proc Natl Acad Sci U S A *105*, 14447-14452.

Allred, D.C., Brown, P., and Medina, D. (2004). The origins of estrogen receptor alpha-positive and estrogen receptor alpha-negative human breast cancer. Breast Cancer Res *6*, 240-245.

Anderson, C.M., Allen, B.G., Sun, W., Lee, C.M., Agarwala, S., Venigalla, M., Greenberg, L., Adkins, D., Chen, Y., Zhen, W., *et al.* Phase 1b/2a Trial of Superoxide (SO) Dismutase (SOD) Mimetic GC4419 to Reduce Chemoradiation Therapy–Induced Oral Mucositis (OM) in Patients With Oral Cavity or Oropharyngeal Carcinoma (OCC). International Journal of Radiation Oncology • Biology • Physics *94*, 869-870.

Austin, S., and St-Pierre, J. (2012). PGC1alpha and mitochondrial metabolism--emerging concepts and relevance in ageing and neurodegenerative disorders. J Cell Sci *125*, 4963-4971.

Baeza, J., Dowell, J.A., Smallegan, M.J., Fan, J., Amador-Noguez, D., Khan, Z., and Denu, J.M. (2014). Stoichiometry of site-specific lysine acetylation in an entire proteome. J Biol Chem *289*, 21326-21338.

Barginear, M.F., Muss, H., Kimmick, G., Owusu, C., Mrozek, E., Shahrokni, A., Ballman, K., and Hurria, A. (2014). Breast cancer and aging: results of the U13 conference breast cancer panel. Breast Cancer Res Treat *146*, 1-6.

Becuwe, P., Ennen, M., Klotz, R., Barbieux, C., and Grandemange, S. (2014). Manganese superoxide dismutase in breast cancer: from molecular mechanisms of gene regulation to biological and clinical significance. Free Radic Biol Med *77*, 139-151.

Bell, E.L., Emerling, B.M., Ricoult, S.J., and Guarente, L. (2011). SirT3 suppresses hypoxia inducible factor 1alpha and tumor growth by inhibiting mitochondrial ROS production. Oncogene *30*, 2986-2996.

Benovic, J., Tillman, T., Cudd, A., and Fridovich, I. (1983). Electrostatic facilitation of the reaction catalyzed by the manganese-containing and the iron-containing superoxide dismutases. Archives of biochemistry and biophysics *221*, 329-332.

Bisht, K.S., Bradbury, C.M., Mattson, D., Kaushal, A., Sowers, A., Markovina, S., Ortiz, K.L., Sieck, L.K., Isaacs, J.S., Brechbiel, M.W., *et al.* (2003). Geldanamycin and 17-allylamino-17-demethoxygeldanamycin potentiate the in vitro and in vivo radiation response of cervical tumor cells via the heat shock protein 90-mediated intracellular signaling and cytotoxicity. Cancer Res *63*, 8984-8995.

Borgstahl, G.E., Parge, H.E., Hickey, M.J., Beyer, W.F., Jr., Hallewell, R.A., and Tainer, J.A. (1992). The structure of human mitochondrial manganese superoxide dismutase reveals a novel tetrameric interface of two 4-helix bundles. Cell *71*, 107-118.

Boulton, S.J., and Jackson, S.P. (1998). Components of the Ku-dependent non-homologous end-joining pathway are involved in telomeric length maintenance and telomeric silencing. EMBO J *17*, 1819-1828.

Brown, K.D., Maqsood, S., Huang, J.Y., Pan, Y., Harkcom, W., Li, W., Sauve, A., Verdin, E., and Jaffrey, S.R. (2014). Activation of SIRT3 by the NAD(+) precursor nicotinamide riboside protects from noise-induced hearing loss. Cell metabolism *20*, 1059-1068.

Brunet, A., Sweeney, L.B., Sturgill, J.F., Chua, K.F., Greer, P.L., Lin, Y., Tran, H., Ross, S.E., Mostoslavsky, R., Cohen, H.Y., *et al.* (2004). Stress-dependent regulation of FOXO transcription factors by the SIRT1 deacetylase. Science *303*, 2011-2015.

Carey, L.A., Perou, C.M., Livasy, C.A., Dressler, L.G., Cowan, D., Conway, K., Karaca, G., Troester, M.A., Tse, C.K., Edmiston, S., *et al.* (2006). Race, breast cancer subtypes, and survival in the Carolina Breast Cancer Study. JAMA *295*, 2492-2502.
Chen, H.Y., Cheng, H.L., Lee, Y.H., Yuan, T.M., Chen, S.W., Lin, Y.Y., and Chueh, P.J. (2017). Tumor-associated NADH oxidase (tNOX)-NAD+-sirtuin 1 axis contributes to oxaliplatin-induced apoptosis of gastric cancer cells. Oncotarget.
Chen, T., Liu, J., Li, N., Wang, S., Liu, H., Li, J., Zhang, Y., and Bu, P. (2015). Mouse SIRT3 attenuates hypertrophy-related lipid accumulation in the heart through the deacetylation of LCAD. PLoS One *10*, e0118909.
Chen, W.Y., Wang, D.H., Yen, R.C., Luo, J., Gu, W., and Baylin, S.B. (2005). Tumor suppressor HIC1 directly regulates SIRT1 to modulate p53-dependent DNA-damage responses. Cell *123*, 437-448.
Chen, Y., Zhang, J., Lin, Y., Lei, Q., Guan, K.L., Zhao, S., and Xiong, Y. (2011). Tumour suppressor SIRT3 deacetylates and activates manganese superoxide dismutase to scavenge ROS. EMBO reports *12*, 534-541.
Choudhary, C., Kumar, C., Gnad, F., Nielsen, M.L., Rehman, M., Walther, T.C., Olsen, J.V., and Mann, M. (2009). Lysine acetylation targets protein complexes and co-regulates major cellular functions. Science *325*, 834-840.
Cramer-Morales, K., Heer, C.D., Mapuskar, K.A., and Domann, F.E. (2015). SOD2 targeted gene editing by CRISPR/Cas9 yields Human cells devoid of MnSOD. Free Radic Biol Med *89*, 379-386.
Creighton, C.J. (2012). The molecular profile of luminal B breast cancer. Biologics *6*, 289-297.
Croxtall, J.D., and McKeage, K. (2011). Fulvestrant: a review of its use in the management of hormone receptor-positive metastatic breast cancer in postmenopausal women. Drugs *71*, 363-380.
Cui, Y., Qin, L., Wu, J., Qu, X., Hou, C., Sun, W., Li, S., Vaughan, A.T., Li, J.J., and Liu, J. (2015). SIRT3 Enhances Glycolysis and Proliferation in SIRT3-Expressing Gastric Cancer Cells. PLoS One *10*, e0129834.
Das, D., Smith, N., Wang, X., and Morgan, I.M. (2017). The deacetylase SIRT1 regulates the replication properties of human papillomavirus 16 E1 and E2. J Virol.
Dauvois, S., White, R., and Parker, M.G. (1993). The antiestrogen ICI 182780 disrupts estrogen receptor nucleocytoplasmic shuttling. J Cell Sci *106 (Pt 4)*, 1377-1388.
Desouki, M.M., Doubinskaia, I., Gius, D., and Abdulkadir, S.A. (2014). Decreased mitochondrial SIRT3 expression is a potential molecular biomarker associated with poor outcome in breast cancer. Human pathology *45*, 1071-1077.
Deus, C.M., Serafim, T.L., Magalhaes-Novais, S., Vilaca, A., Moreira, A.C., Sardao, V.A., Cardoso, S.M., and Oliveira, P.J. (2017). Sirtuin 1-dependent resveratrol cytotoxicity and pro-differentiation activity on breast cancer cells. Arch Toxicol *91*, 1261-1278.
Dhar, S.K., and St Clair, D.K. (2012). Manganese superoxide dismutase regulation and cancer. Free Radic Biol Med *52*, 2209-2222.
Donmez, G., and Guarente, L. (2010). Aging and disease: connections to sirtuins. Aging Cell *9*, 285-290.
Du, Y., Wu, J., Zhang, H., Li, S., and Sun, H. (2017). Reduced expression of SIRT2 in serous ovarian carcinoma promotes cell proliferation through disinhibition of CDK4 expression. Mol Med Rep.

Early Breast Cancer Trialists' Collaborative, G., Davies, C., Godwin, J., Gray, R., Clarke, M., Cutter, D., Darby, S., McGale, P., Pan, H.C., Taylor, C., *et al.* (2011). Relevance of breast cancer hormone receptors and other factors to the efficacy of adjuvant tamoxifen: patient-level meta-analysis of randomised trials. Lancet *378*, 771-784.
Ellis, M.J., Tao, Y., Luo, J., A'Hern, R., Evans, D.B., Bhatnagar, A.S., Chaudri Ross, H.A., von Kameke, A., Miller, W.R., Smith, I., *et al.* (2008). Outcome prediction for estrogen receptor-positive breast cancer based on postneoadjuvant endocrine therapy tumor characteristics. J Natl Cancer Inst *100*, 1380-1388.
Ershler, W.B., and Longo, D.L. (1997a). Aging and cancer: issues of basic and clinical science. J Natl Cancer Inst *89*, 1489-1497.
Ershler, W.B., and Longo, D.L. (1997b). The biology of aging: the current research agenda. Cancer *80*, 1284-1293.
Fadoukhair, Z., Zardavas, D., Chad, M.A., Goulioti, T., Aftimos, P., and Piccart, M. (2015). Evaluation of targeted therapies in advanced breast cancer: the need for large-scale molecular screening and transformative clinical trial designs. Oncogene.
Finkel, T., Deng, C.X., and Mostoslavsky, R. (2009). Recent progress in the biology and physiology of sirtuins. Nature *460*, 587-591.
Finley, L.W., Carracedo, A., Lee, J., Souza, A., Egia, A., Zhang, J., Teruya-Feldstein, J., Moreira, P.I., Cardoso, S.M., Clish, C.B., *et al.* (2011). SIRT3 opposes reprogramming of cancer cell metabolism through HIF1alpha destabilization. Cancer cell *19*, 416-428.
Fiskus, W., Coothankandaswamy, V., Chen, J., Ma, H., Ha, K., Saenz, D.T., Krieger, S.S., Mill, C.P., Sun, B., Huang, P., *et al.* (2016). SIRT2 Deacetylates and Inhibits the Peroxidase Activity of Peroxiredoxin-1 to Sensitize Breast Cancer Cells to Oxidant Stress-Inducing Agents. Cancer Res *76*, 5467-5478.
Fritz, K.S., Galligan, J.J., Hirschey, M.D., Verdin, E., and Petersen, D.R. (2012). Mitochondrial Acetylome Analysis in a Mouse Model of Alcohol-Induced Liver Injury Utilizing SIRT3 Knockout Mice. Journal of proteome research *11*, 1633-1643.
Fu, B., Zhao, J., Peng, W., Wu, H., and Zhang, Y. (2017). Resveratrol rescues cadmium-induced mitochondrial injury by enhancing transcriptional regulation of PGC-1alpha and SOD2 via the Sirt3/FoxO3a pathway in TCMK-1 cells. Biochem Biophys Res Commun.
Gius, D., Botero, A., Shah, S., and Curry, H.A. (1999a). Intracellular oxidation/reduction status in the regulation of transcription factors NF-kappaB and AP-1. Toxicol Lett *106*, 93-106.
Gius, D.R., Ezhevsky, S.A., Becker-Hapak, M., Nagahara, H., Wei, M.C., and Dowdy, S.F. (1999b). Transduced p16INK4a peptides inhibit hypophosphorylation of the retinoblastoma protein and cell cycle progression prior to activation of Cdk2 complexes in late G1. Cancer Res *59*, 2577-2580.
Godugu, C., Doddapaneni, R., and Singh, M. (2017). Honokiol nanomicellar formulation produced increased oral bioavailability and anticancer effects in triple negative breast cancer (TNBC). Colloids Surf B Biointerfaces *153*, 208-219.
Goldhirsch, A., Wood, W.C., Coates, A.S., Gelber, R.D., Thurlimann, B., Senn, H.J., and Panel, m. (2011). Strategies for subtypes--dealing with the diversity of breast cancer: highlights of the St. Gallen International Expert Consensus on the Primary Therapy of Early Breast Cancer 2011. Ann Oncol *22*, 1736-1747.
Gowda, A.S., Suo, Z., and Spratt, T.E. (2017). Honokiol Inhibits DNA Polymerases beta and lambda and Increases Bleomycin Sensitivity of Human Cancer Cells. Chem Res Toxicol *30*, 715-725.

Guarente, L. (2007). Sirtuins in aging and disease. Cold Spring Harbor symposia on quantitative biology *72*, 483-488.
Guarente, L. (2008). Mitochondria--a nexus for aging, calorie restriction, and sirtuins? Cell *132*, 171-176.
Guarente, L., and Kenyon, C. (2000). Genetic pathways that regulate ageing in model organisms. Nature *408*, 255-262.
Haigis, M.C., Deng, C.X., Finley, L.W., Kim, H.S., and Gius, D. (2012). SIRT3 is a mitochondrial tumor suppressor: a scientific tale that connects aberrant cellular ROS, the Warburg effect, and carcinogenesis. Cancer Res *72*, 2468-2472.
Hallahan, D.E., Gius, D., Kuchibhotla, J., Sukhatme, V., Kufe, D.W., and Weichselbaum, R.R. (1993). Radiation signaling mediated by Jun activation following dissociation from a cell type-specific repressor. J Biol Chem *268*, 4903-4907.
Haque, R., Ahmed, S.A., Inzhakova, G., Shi, J., Avila, C., Polikoff, J., Bernstein, L., Enger, S.M., and Press, M.F. (2012). Impact of breast cancer subtypes and treatment on survival: an analysis spanning two decades. Cancer Epidemiol Biomarkers Prev *21*, 1848-1855.
He, X., Zeng, H., and Chen, J.X. (2016). Ablation of SIRT3 causes coronary microvascular dysfunction and impairs cardiac recovery post myocardial ischemia. Int J Cardiol *215*, 349-357.
Hirschey, M.D., Shimazu, T., Goetzman, E., Jing, E., Schwer, B., Lombard, D.B., Grueter, C.A., Harris, C., Biddinger, S., Ilkayeva, O.R., *et al.* (2010). SIRT3 regulates mitochondrial fatty-acid oxidation by reversible enzyme deacetylation. Nature *464*, 121-125.
Hitchler, M.J., Oberley, L.W., and Domann, F.E. (2008). Epigenetic silencing of SOD2 by histone modifications in human breast cancer cells. Free Radic Biol Med *45*, 1573-1580.
Huang, Y., He, T., and Domann, F.E. (1999). Decreased expression of manganese superoxide dismutase in transformed cells is associated with increased cytosine methylation of the SOD2 gene. DNA Cell Biol *18*, 643-652.
Huh, J.E., Shin, J.H., Jang, E.S., Park, S.J., Park, D.R., Ko, R., Seo, D.H., Kim, H.S., Lee, S.H., Choi, Y., *et al.* (2016). Sirtuin 3 (SIRT3) maintains bone homeostasis by regulating AMPK-PGC-1beta axis in mice. Sci Rep *6*, 22511.
Jenkins, E.O., Deal, A.M., Anders, C.K., Prat, A., Perou, C.M., Carey, L.A., and Muss, H.B. (2014). Age-specific changes in intrinsic breast cancer subtypes: a focus on older women. Oncologist *19*, 1076-1083.
Jeong, S.M., Lee, J., Finley, L.W., Schmidt, P.J., Fleming, M.D., and Haigis, M.C. (2015). SIRT3 regulates cellular iron metabolism and cancer growth by repressing iron regulatory protein 1. Oncogene *34*, 2115-2124.
Jing, E., Emanuelli, B., Hirschey, M.D., Boucher, J., Lee, K.Y., Lombard, D., Verdin, E.M., and Kahn, C.R. (2011). Sirtuin-3 (Sirt3) regulates skeletal muscle metabolism and insulin signaling via altered mitochondrial oxidation and reactive oxygen species production. Proc Natl Acad Sci U S A *108*, 14608-14613.
Kaewpila, S., Venkataraman, S., Buettner, G.R., and Oberley, L.W. (2008). Manganese superoxide dismutase modulates hypoxia-inducible factor-1 alpha induction via superoxide. Cancer Res *68*, 2781-2788.
Kattan, Z., Minig, V., Leroy, P., Dauca, M., and Becuwe, P. (2008). Role of manganese superoxide dismutase on growth and invasive properties of human estrogen-independent breast cancer cells. Breast Cancer Res Treat *108*, 203-215.

Kim, H., Kim, S.H., Cha, H., Kim, S.R., Lee, J.H., and Park, J.W. (2016). IDH2 deficiency promotes mitochondrial dysfunction and dopaminergic neurotoxicity: implications for Parkinson's disease. Free Radic Res *50*, 853-860.
Kim, H.S., Patel, K., Muldoon-Jacobs, K., Bisht, K.S., Aykin-Burns, N., Pennington, J.D., van der Meer, R., Nguyen, P., Savage, J., Owens, K.M., *et al.* (2010). SIRT3 is a mitochondria-localized tumor suppressor required for maintenance of mitochondrial integrity and metabolism during stress. Cancer Cell *17*, 41-52.
Kim, H.S., Vassilopoulos, A., Wang, R.H., Lahusen, T., Xiao, Z., Xu, X., Li, C., Veenstra, T.D., Li, B., Yu, H., *et al.* (2011). SIRT2 maintains genome integrity and suppresses tumorigenesis through regulating APC/C activity. Cancer Cell *20*, 487-499.
Kim, S.C., Sprung, R., Chen, Y., Xu, Y., Ball, H., Pei, J., Cheng, T., Kho, Y., Xiao, H., Xiao, L., *et al.* (2006). Substrate and functional diversity of lysine acetylation revealed by a proteomics survey. Molecular cell *23*, 607-618.
Kouzarides, T. (2000). Acetylation: a regulatory modification to rival phosphorylation? Embo J *19*, 1176-1179.
Ku, H.J., Ahn, Y., Lee, J.H., Park, K.M., and Park, J.W. (2015). IDH2 deficiency promotes mitochondrial dysfunction and cardiac hypertrophy in mice. Free Radic Biol Med *80*, 84-92.
Land, H., Chen, A.C., Morgenstern, J.P., Parada, L.F., and Weinberg, R.A. (1986). Behavior of myc and ras oncogenes in transformation of rat embryo fibroblasts. Molecular and cellular biology *6*, 1917-1925.
Land, H., Parada, L.F., and Weinberg, R.A. (1983). Tumorigenic conversion of primary embryo fibroblasts requires at least two cooperating oncogenes. Nature *304*, 596-602.
Li, J.J., Oberley, L.W., St Clair, D.K., Ridnour, L.A., and Oberley, T.D. (1995). Phenotypic changes induced in human breast cancer cells by overexpression of manganese-containing superoxide dismutase. Oncogene *10*, 1989-2000.
Li, M., Chiu, J.F., Mossman, B.T., and Fukagawa, N.K. (2006). Down-regulation of manganese-superoxide dismutase through phosphorylation of FOXO3a by Akt in explanted vascular smooth muscle cells from old rats. J Biol Chem *281*, 40429-40439.
Liu, G., Park, S.H., Imbesi, M., Nathan, W.J., Zou, X., Zhu, Y., Jiang, H., Parisiadou, L., and Gius, D. (2016). Loss of NAD-Dependent Protein Deacetylase Sirtuin-2 Alters Mitochondrial Protein Acetylation and Dysregulates Mitophagy. Antioxid Redox Signal.
Lombard, D.B., Alt, F.W., Cheng, H.L., Bunkenborg, J., Streeper, R.S., Mostoslavsky, R., Kim, J., Yancopoulos, G., Valenzuela, D., Murphy, A., *et al.* (2007). Mammalian Sir2 homolog SIRT3 regulates global mitochondrial lysine acetylation. Molecular and cellular biology *27*, 8807-8814.
Love, R.R., Laudico, A.V., Van Dinh, N., Allred, D.C., Uy, G.B., Quang le, H., Salvador, J.D., Siguan, S.S., Mirasol-Lumague, M.R., Tung, N.D., *et al.* (2015). Timing of adjuvant surgical oophorectomy in the menstrual cycle and disease-free and overall survival in premenopausal women with operable breast cancer. J Natl Cancer Inst *107*, djv064.
Lu, C., Ward, P.S., Kapoor, G.S., Rohle, D., Turcan, S., Abdel-Wahab, O., Edwards, C.R., Khanin, R., Figueroa, M.E., Melnick, A., *et al.* (2012). IDH mutation impairs histone demethylation and results in a block to cell differentiation. Nature *483*, 474-478.
Lumachi, F., Brunello, A., Maruzzo, M., Basso, U., and Basso, S.M. (2013). Treatment of estrogen receptor-positive breast cancer. Curr Med Chem *20*, 596-604.
Lumachi, F., Santeufemia, D.A., and Basso, S.M. (2015). Current medical treatment of estrogen receptor-positive breast cancer. World J Biol Chem *6*, 231-239.

Luo, J., Bao, Y.C., Ji, X.X., Chen, B., Deng, Q.F., and Zhou, S.W. (2017). SPOP promotes SIRT2 degradation and suppresses non-small cell lung cancer cell growth. Biochem Biophys Res Commun *483*, 880-884.
MacDonald, M.J., Brown, L.J., Longacre, M.J., Stoker, S.W., Kendrick, M.A., and Hasan, N.M. (2013). Knockdown of both mitochondrial isocitrate dehydrogenase enzymes in pancreatic beta cells inhibits insulin secretion. Biochim Biophys Acta *1830*, 5104-5111.
Mahjabeen, I., and Kayani, M.A. (2016). Loss of Mitochondrial Tumor Suppressor Genes Expression Is Associated with Unfavorable Clinical Outcome in Head and Neck Squamous Cell Carcinoma: Data from Retrospective Study. PLoS One *11*, e0146948.
Martin, A.M., Cagney, D.N., Catalano, P.J., Warren, L.E., Bellon, J.R., Punglia, R.S., Claus, E.B., Lee, E.Q., Wen, P.Y., Haas-Kogan, D.A., *et al.* (2017). Brain Metastases in Newly Diagnosed Breast Cancer: A Population-Based Study. JAMA Oncol.
Mathieu, L., Costa, A.L., Le Bachelier, C., Slama, A., Lebre, A.S., Taylor, R.W., Bastin, J., and Djouadi, F. (2016). Resveratrol attenuates oxidative stress in mitochondrial Complex I deficiency: Involvement of SIRT3. Free Radic Biol Med *96*, 190-198.
Mitri, Z., Constantine, T., and O'Regan, R. (2012). The HER2 Receptor in Breast Cancer: Pathophysiology, Clinical Use, and New Advances in Therapy. Chemother Res Pract *2012*, 743193.
Mokbel, K. (2002). The evolving role of aromatase inhibitors in breast cancer. Int J Clin Oncol *7*, 279-283.
Ozden, O., Park, S.H., Wagner, B.A., Yong Song, H., Zhu, Y., Vassilopoulos, A., Jung, B., Buettner, G.R., and Gius, D. (2014). SIRT3 deacetylates and increases pyruvate dehydrogenase activity in cancer cells. Free Radic Biol Med *76*, 163-172.
Palacios, O.M., Carmona, J.J., Michan, S., Chen, K.Y., Manabe, Y., Ward, J.L., 3rd, Goodyear, L.J., and Tong, Q. (2009). Diet and exercise signals regulate SIRT3 and activate AMPK and PGC-1alpha in skeletal muscle. Aging (Albany NY) *1*, 771-783.
Park, J.B., Nagar, H., Choi, S., Jung, S.B., Kim, H.W., Kang, S.K., Lee, J.W., Lee, J.H., Park, J.W., Irani, K., *et al.* (2016a). IDH2 deficiency impairs mitochondrial function in endothelial cells and endothelium-dependent vasomotor function. Free Radic Biol Med *94*, 36-46.
Park, S.H., Ozden, O., Liu, G., Song, H.Y., Zhu, Y., Yan, Y., Zou, X., Kang, H.J., Jiang, H., Principe, D.R., *et al.* (2016b). SIRT2-Mediated Deacetylation and Tetramerization of Pyruvate Kinase Directs Glycolysis and Tumor Growth. Cancer Res *76*, 3802-3812.
Park, S.H., Zhu, Y., Ozden, O., Kim, H.S., Jiang, H., Deng, C.X., Gius, D., and Vassilopoulos, A. (2012). SIRT2 is a tumor suppressor that connects aging, acetylome, cell cycle signaling, and carcinogenesis. Transl Cancer Res *1*, 15-21.
Parker, J.S., Mullins, M., Cheang, M.C., Leung, S., Voduc, D., Vickery, T., Davies, S., Fauron, C., He, X., Hu, Z., *et al.* (2009). Supervised risk predictor of breast cancer based on intrinsic subtypes. J Clin Oncol *27*, 1160-1167.
Perez, A.A., Balabram, D., Rocha, R.M., da Silva Souza, A., and Gobbi, H. (2015). Co-Expression of p16, Ki67 and COX-2 Is Associated with Basal Phenotype in High-Grade Ductal Carcinoma In Situ of the Breast. J Histochem Cytochem *63*, 408-416.
Perou, C.M., Sorlie, T., Eisen, M.B., van de Rijn, M., Jeffrey, S.S., Rees, C.A., Pollack, J.R., Ross, D.T., Johnsen, H., Akslen, L.A., *et al.* (2000). Molecular portraits of human breast tumours. Nature *406*, 747-752.

Pillai, V.B., Samant, S., Sundaresan, N.R., Raghuraman, H., Kim, G., Bonner, M.Y., Arbiser, J.L., Walker, D.I., Jones, D.P., Gius, D., *et al.* (2015). Honokiol blocks and reverses cardiac hypertrophy in mice by activating mitochondrial Sirt3. Nat Commun *6*, 6656.
Qiu, G., Li, X., Wei, C., Che, X., He, S., Lu, J., Wang, S., Pang, K., and Fan, L. (2016). The Prognostic Role of SIRT1-Autophagy Axis in Gastric Cancer. Dis Markers *2016*, 6869415.
Qiu, X., Brown, K., Hirschey, M.D., Verdin, E., and Chen, D. (2010). Calorie restriction reduces oxidative stress by SIRT3-mediated SOD2 activation. Cell metabolism *12*, 662-667.
Razandi, M., Pedram, A., Jordan, V.C., Fuqua, S., and Levin, E.R. (2013). Tamoxifen regulates cell fate through mitochondrial estrogen receptor beta in breast cancer. Oncogene *32*, 3274-3285.
Ren, N.S., Ji, M., Tokar, E.J., Busch, E.L., Xu, X., Lewis, D., Li, X., Jin, A., Zhang, Y., Wu, W.K., *et al.* (2017). Haploinsufficiency of SIRT1 Enhances Glutamine Metabolism and Promotes Cancer Development. Curr Biol *27*, 483-494.
Ruggieri, V., Agriesti, F., Scrima, R., Laurenzana, I., Perrone, D., Tataranni, T., Mazzoccoli, C., Lo Muzio, L., Capitanio, N., and Piccoli, C. (2015). Dichloroacetate, a selective mitochondria-targeting drug for oral squamous cell carcinoma: a metabolic perspective of treatment. Oncotarget *6*, 1217-1230.
Rush, G.F., Gorski, J.R., Ripple, M.G., Sowinski, J., Bugelski, P., and Hewitt, W.R. (1985). Organic hydroperoxide-induced lipid peroxidation and cell death in isolated hepatocytes. Toxicol Appl Pharmacol *78*, 473-483.
Sarsour, E.H., Kalen, A.L., Xiao, Z., Veenstra, T.D., Chaudhuri, L., Venkataraman, S., Reigan, P., Buettner, G.R., and Goswami, P.C. (2012). Manganese superoxide dismutase regulates a metabolic switch during the mammalian cell cycle. Cancer Res *72*, 3807-3816.
Saunders, L.R., and Verdin, E. (2009). Cell biology. Stress response and aging. Science *323*, 1021-1022.
Schiaffino, S., Reggiani, C., Kostrominova, T.Y., Mann, M., and Murgia, M. (2015). Mitochondrial specialization revealed by single muscle fiber proteomics: focus on the Krebs cycle. Scand J Med Sci Sports *25 Suppl 4*, 41-48.
Siegel, R., DeSantis, C., Virgo, K., Stein, K., Mariotto, A., Smith, T., Cooper, D., Gansler, T., Lerro, C., Fedewa, S., *et al.* (2012). Cancer treatment and survivorship statistics, 2012. CA Cancer J Clin *62*, 220-241.
Someya, S., Yu, W., Hallows, W.C., Xu, J., Vann, J.M., Leeuwenburgh, C., Tanokura, M., Denu, J.M., and Prolla, T.A. (2010). Sirt3 mediates reduction of oxidative damage and prevention of age-related hearing loss under caloric restriction. Cell *143*, 802-812.
Spitz, D.R., Azzam, E.I., Li, J.J., and Gius, D. (2004). Metabolic oxidation/reduction reactions and cellular responses to ionizing radiation: a unifying concept in stress response biology. Cancer metastasis reviews *23*, 311-322.
Takata, T., and Ishikawa, F. (2003). Human Sir2-related protein SIRT1 associates with the bHLH repressors HES1 and HEY2 and is involved in HES1- and HEY2-mediated transcriptional repression. Biochem Biophys Res Commun *301*, 250-257.
Tao, R., Coleman, M.C., Pennington, J.D., Ozden, O., Park, S.H., Jiang, H., Kim, H.S., Flynn, C.R., Hill, S., Hayes McDonald, W., *et al.* (2010). Sirt3-mediated deacetylation of evolutionarily conserved lysine 122 regulates MnSOD activity in response to stress. Molecular cell *40*, 893-904.
Tao, R., Vassilopoulos, A., Parisiadou, L., Yan, Y., and Gius, D. (2014). Regulation of MnSOD enzymatic activity by Sirt3 connects the mitochondrial acetylome signaling networks to aging and carcinogenesis. Antioxid Redox Signal *20*, 1646-1654.

Tomayko, M.M., and Reynolds, C.P. (1989). Determination of subcutaneous tumor size in athymic (nude) mice. Cancer Chemother Pharmacol *24*, 148-154.
Vassilopoulos, A., Pennington, J.D., Andresson, T., Rees, D.M., Bosley, A.D., Fearnley, I.M., Ham, A., Flynn, C.R., Hill, S., Rose, K.L., *et al.* (2014). SIRT3 deacetylates ATP synthase F1 complex proteins in response to nutrient- and exercise-induced stress. Antioxid Redox Signal *21*, 551-564.
Vaziri, H., Dessain, S.K., Ng Eaton, E., Imai, S.I., Frye, R.A., Pandita, T.K., Guarente, L., and Weinberg, R.A. (2001). hSIR2(SIRT1) functions as an NAD-dependent p53 deacetylase. Cell *107*, 149-159.
Vera-Ramirez, L., Sanchez-Rovira, P., Ramirez-Tortosa, M.C., Ramirez-Tortosa, C.L., Granados-Principal, S., Lorente, J.A., and Quiles, J.L. (2011). Free radicals in breast carcinogenesis, breast cancer progression and cancer stem cells. Biological bases to develop oxidative-based therapies. Crit Rev Oncol Hematol *80*, 347-368.
Vitek, W.S., Shayne, M., Hoeger, K., Han, Y., Messing, S., and Fung, C. (2014). Gonadotropin-releasing hormone agonists for the preservation of ovarian function among women with breast cancer who did not use tamoxifen after chemotherapy: a systematic review and meta-analysis. Fertil Steril *102*, 808-815 e801.
Wang, M., Kirk, J.S., Venkataraman, S., Domann, F.E., Zhang, H.J., Schafer, F.Q., Flanagan, S.W., Weydert, C.J., Spitz, D.R., Buettner, G.R., *et al.* (2005). Manganese superoxide dismutase suppresses hypoxic induction of hypoxia-inducible factor-1alpha and vascular endothelial growth factor. Oncogene *24*, 8154-8166.
Wang, N., Wang, Z., Nie, S., Song, L., He, T., Yang, S., Yang, X., Yi, C., Wu, Q., and Gong, C. (2017). Biodegradable polymeric micelles coencapsulating paclitaxel and honokiol: a strategy for breast cancer therapy in vitro and in vivo. Int J Nanomedicine *12*, 1499-1514.
Warburg, O. (1925). Iron, the Oxygen-Carrier of Respiration-Ferment. Science *61*, 575-582.
Warburg, O. (1956). On the origin of cancer cells. Science *123*, 309-314.
Warburg, O., Wind, F., and Negelein, E. (1927). The Metabolism of Tumors in the Body. The Journal of general physiology *8*, 519-530.
Ward, P.S., Patel, J., Wise, D.R., Abdel-Wahab, O., Bennett, B.D., Coller, H.A., Cross, J.R., Fantin, V.R., Hedvat, C.V., Perl, A.E., *et al.* (2010). The common feature of leukemia-associated IDH1 and IDH2 mutations is a neomorphic enzyme activity converting alpha-ketoglutarate to 2-hydroxyglutarate. Cancer Cell *17*, 225-234.
Wilking-Busch, M.J., Ndiaye, M.A., Huang, W., and Ahmad, N. (2017). Expression profile of SIRT2 in human melanoma and implications for sirtuin-based chemotherapy. Cell Cycle *16*, 574-577.
Wise, D.R., Ward, P.S., Shay, J.E., Cross, J.R., Gruber, J.J., Sachdeva, U.M., Platt, J.M., DeMatteo, R.G., Simon, M.C., and Thompson, C.B. (2011). Hypoxia promotes isocitrate dehydrogenase-dependent carboxylation of alpha-ketoglutarate to citrate to support cell growth and viability. Proc Natl Acad Sci U S A *108*, 19611-19616.
Wood, J.G., Rogina, B., Lavu, S., Howitz, K., Helfand, S.L., Tatar, M., and Sinclair, D. (2004). Sirtuin activators mimic caloric restriction and delay ageing in metazoans. Nature *430*, 686-689.
Xiao, K., Jiang, J., Wang, W., Cao, S., Zhu, L., Zeng, H., Ouyang, R., Zhou, R., and Chen, P. (2013). Sirt3 is a tumor suppressor in lung adenocarcinoma cells. Oncol Rep *30*, 1323-1328.
Xiong, Y., Wang, M., Zhao, J., Wang, L., Li, X., Zhang, Z., Jia, L., and Han, Y. (2017). SIRT3 is correlated with the malignancy of non-small cell lung cancer. Int J Oncol *50*, 903-910.

Xu, S., Gao, Y., Zhang, Q., Wei, S., Chen, Z., Dai, X., Zeng, Z., and Zhao, K.S. (2016). SIRT1/3 Activation by Resveratrol Attenuates Acute Kidney Injury in a Septic Rat Model. Oxid Med Cell Longev *2016*, 7296092.

Yu, W., Denu, R.A., Krautkramer, K.A., Grindle, K.M., Yang, D.T., Asimakopoulos, F., Hematti, P., and Denu, J.M. (2016a). Loss of SIRT3 Provides Growth Advantage for B Cell Malignancies. J Biol Chem *291*, 3268-3279.

Yu, W., Dittenhafer-Reed, K.E., and Denu, J.M. (2012). SIRT3 protein deacetylates isocitrate dehydrogenase 2 (IDH2) and regulates mitochondrial redox status. J Biol Chem *287*, 14078-14086.

Yu, Y., Liu, Y., Zong, C., Yu, Q., Yang, X., Liang, L., Ye, F., Nong, L., Jia, Y., Lu, Y., *et al.* (2016b). Mesenchymal stem cells with Sirt1 overexpression suppress breast tumor growth via chemokine-dependent natural killer cells recruitment. Sci Rep *6*, 35998.

Yu, Y., Zhang, Q., Meng, Q., Zong, C., Liang, L., Yang, X., Lin, R., Liu, Y., Zhou, Y., Zhang, H., *et al.* (2016c). Mesenchymal stem cells overexpressing Sirt1 inhibit prostate cancer growth by recruiting natural killer cells and macrophages. Oncotarget *7*, 71112-71122.

Zhou, W., Ni, T.K., Wronski, A., Glass, B., Skibinski, A., Beck, A., and Kuperwasser, C. (2016). The SIRT2 Deacetylase Stabilizes Slug to Control Malignancy of Basal-like Breast Cancer. Cell Rep *17*, 1302-1317.

Zhu, Y., Park, S.H., Ozden, O., Kim, H.S., Jiang, H., Vassilopoulos, A., Spitz, D.R., and Gius, D. (2012). Exploring the electrostatic repulsion model in the role of Sirt3 in directing MnSOD acetylation status and enzymatic activity. Free Radic Biol Med *53*, 828-833.

Zhu, Y., Yan, Y., Principe, D.R., Zou, X., Vassilopoulos, A., and Gius, D. (2014). SIRT3 and SIRT4 are mitochondrial tumor suppressor proteins that connect mitochondrial metabolism and carcinogenesis. Cancer Metab *2*, 15.

Zou, X., Santa-Maria, C.A., O'Brien, J., Gius, D., and Zhu, Y. (2016). Manganese Superoxide Dismutase Acetylation and Dysregulation, Due to Loss of SIRT3 Activity, Promote a Luminal B-Like Breast Carcinogenic-Permissive Phenotype. Antioxid Redox Signal.